Identification of proteins involved in neutral lipid metabolism in hepatic stellate cells:

potential therapeutic targets for liver fibrosis

Maidina Tuohetahuntila

Identification of proteins involved in neutral lipid metabolism in hepatic stellate cells:

potential therapeutic targets for liver fibrosis

Identificatie van eiwitten die betrokken zijn bij de vetstofwisseling in hepatische stellaat cellen:

mogelijke therapeutische aangrijpingspunten voor leverfibrose

(met een samenvatting in het Nederlands)

Proefschrift

ter verkrijging van de graad van doctor aan de Universiteit Utrecht op gezag van de rector magnificus, prof.dr. G.J. van der Zwaan, ingevolge het besluit van het college voor promoties in het openbaar te verdedigen op dinsdag 11 oktober 2016 des ochtends te 10.30 uur

door

Maidina Tuohetahuntila

geboren op 2 juli 1979 te Ghulja, Xinjiang, China

Promotor: Prof.dr. J.B. Helms

Copromotor: Dr. A.B. Vaandrager

TABLE OF CONTENTS

Introduction

Chapter

1

ROLE OF HEPATIC STELLATE CELLS IN LIVER FIBROSIS

Liver fibrosis

Liver fibrosis or scarring is characterized by the excessive accumulation of extracellular matrix (ECM) components, especially collagens, in response to chronic liver injury[1,2]. Liver fibrosis and liver cirrhosis are significant health problems with high worldwide mortality. The main causes of liver injury and subsequent fibrosis and cirrhosis in developed countries are viral hepatitis, metabolic disorders such as Wilson's disease, alcohol and drug abuse and autoimmune diseases. In addition, obesity is also recognized as an important risk factor for the development of steato-hepatitis leading to liver fibrosis[3].

In normal liver, the subendothelial space of Disse contains non-fibril forming collagens IV and VI[4]. Normal ECM is critical for maintaining the differentiated functions of resident liver cells, including hepatocytes, stellate cells and sinusoidal endothelial cells[4]. Under these physiological conditions, the rate of ECM production equals its degradation, resulting in no net accumulation of matrix. Inflammation represents the driving force for the progressive accumulation of ECM components[5]. As the liver becomes fibrotic, an imbalance occurs between ECM degradation and production. Significant changes occur in quality, quantity and distribution of ECM components in the periportal and perisinusoidal space[4]. Low density ECM is replaced by high-density collagen matrix and the amount of ECM is increased up to 10-fold over normal liver[6]. This is associated with a loss of hepatocyte microvilli, sinusoidal capillarization, and impaired liver function[4]. Although synthesis of ECM initially serves as a repair mechanism to allow proper healing of the damaged tissue, it may eventually lead to fibrosis and can develop into liver cirrhosis[7]. Reversibility of hepatic fibrosis varies depending on the duration of injury, the degree of angiogenesis, composition and distribution of the scarred tissue. Changes in ECM distort the hepatic architecture and form regenerative nodules caused by the disturbance of flow of metabolites between the hepatocytes and the perfusing plasma. This leads to intrahepatic vascular resistance and sinusoidal remodeling, inducing portal hypertension and to cirrhosis as the final stage[8]. Advanced fibrotic changes decrease survival rates as they are strongly associated with hepatocellular carcinoma[9].

Activation of hepatic stellate cells (HSCs) is a central event in the pathogenesis of liver fibrosis. HSCs are resident perisinusoidal cells in the subendothelial space between hepatocytes and sinusoidal endothelial cells and are the primary source of ECM in normal and fibrotic liver. As a result of liver injury, HSCs undergo a process of activation that is mediated by the concerted action of resident hepatic cell types such as Kupffer cells, liver endothelial cells and hepatocytes. Furthermore, the activated HSCs also produce a number of cytokines and active peptides that promote the development of liver fibrosis by stimulating the constrictive, proliferative, and transformative properties of the HSCs in an autocrine manner[10-12]. In particular, the contractile

features of activated HSCs form the basis for their pivotal role in portal hypertension, a major clinical characteristic of liver cirrhosis[13]. Therefore, inhibiting the proliferation and/or activation of HSCs seems a relevant strategy to inhibit liver fibrosis. We will describe the function of HSCs and the processes involved in HSC activation in more detail below.

Functions of the HSC

In normal liver, HSCs represent about 5–8% of all resident cells and are located in the subendo-thelial space of Disse[14]. In their normal quiescent state they are the principal storage site of retinol (vitamin A metabolites) as precursor for retinoids[15,16]. Approximately 70% of all dietary retinol is stored in the liver and 80-90% of this amount is stored in HSC lipid droplets (LDs) as retinyl esters (REs)[17,18]. Retinoids are important mediators of many physiological processes in the body. The storage and metabolism of retinoids is important for the overall health of the body as the body cannot synthesize them by itself. Retinoids regulate important cellular processes including cellu-lar proliferation, differentiation and apoptosis, and hence they have roles in many essential physi-ological processes including reproduction, embryonic development, bone growth, immunity and vision[19]. Most of these essential processes are thought to be mediated by all-*trans*-retinoic acid and 9-*cis*-retinoic acid, which regulate transcription by serving as ligands for nuclear hormone re-ceptors[20]. Over 500 genes are reported to be responsive to either all-*trans*- or 9-*cis*-retinoic acid[21]. It has been reported that retinol binding protein 4 (RBP4) is associated with the development of metabolic diseases like insulin resistance, liver disease and cardiovascular disease[22-24]. Thus, the storage and metabolism of retinoids in the body has immediate implications for the overall health and metabolic homeostasis of mammals. Another important function of HSCs in healthy liver is the secretion of basal levels of ECM required for support and normal development of liver tissue.

Upon liver injury, all resident cells contribute to HSC activation. During this activation process, HSCs trans-differentiate from quiescent vitamin A-rich cells into proliferative, fibrogenic, and con-tractile myofibroblasts[25]. Several mediators are central to the fibrotic process, including platelet-derived growth factor (PDGF) and transforming growth factor-β1 (TGF-β1), as shown in figure 1.

PDGF is a potent mitogen for cells of mesenchymal origin, including myofibroblasts, while TGF-β1 primarily functions in fibrogenesis to stimulate collagen deposition[26]. Increased levels of TGF-β have been described in chronic liver diseases, and activated HSCs represent a major cellular source of TGF-*β* in injured liver. In HSCs, TGF-β promotes transformation into myofibroblasts, thus simulating the synthesis of extracellular matrix proteins and inhibiting their degradation. The composition of the ECM changes upon HSC activation and consists of large amounts of fibrillar collagens I and III. The switch in the amount and types of collagens is accompanied by an increased expression of matrix metalloproteinases (MMPs), which induce three-dimensional alterations in the ECM[27]. MMPs degrade the normal basement membrane matrix, while having
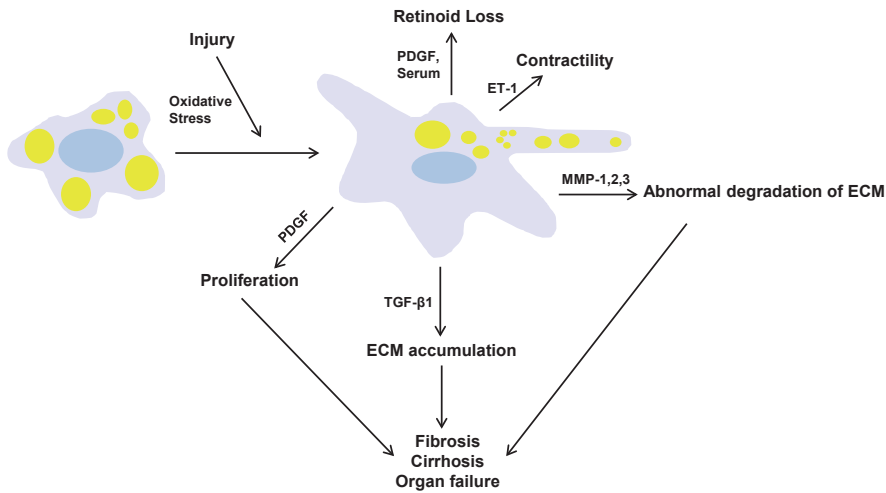
Figure 1. HSC activation during liver injury. In response to liver injury, HSCs undergo activation and release growth factors and inflammatory cytokines and secrete large amounts of type I collagen and other extracellular matrix (ECM) components which leads to fibrosis and eventually liver failure. PDGF: platelet derived growth factor; ET-1: endothelin-1; MMP: matrix metalloproteinase protein; TGFβ: transforming growth factor β; ECM: extracellular matrix.

a mild effect on the matrix rich in fibrillar collagen. At the same time, the production of tissue inhibitors of metalloproteinases (TIMPs) by HSCs also increase, promoting ECM accumulation by inhibiting matrix degradation[28,29]. Excess deposition of ECM in the space of Disse disrupts the normal architecture of the liver, leading to a decrease in function. Another typical feature of HSC activation is the increased expression of the cytoskeletal protein α-smooth muscle actin (αSMA), which is involved in the contractile phenotype of activated HSCs. The disturbed liver architecture, caused by the ECM deposition, together with the increased contractile state of the HSCs lead to portal hypertension (PH), an early and important consequence of fibrosis[30]. Furthermore, αSMA up-regulation is widely used as a marker of activated HSCs[31].

Finally, upon activation HSC lose their quiescent retinoid-storing phenotype as the large RE containing LDs gradually disappear from HSCs. One of the unresolved issue in the field of HSC research is whether the change in lipid metabolism is causally related to the activation process. In other words, is the loss of LDs required for the activation process? If this is the case, treatments aiming to interfere with lipid metabolism in HSCs would be therapeutically interesting. There is evidence supporting the proposal that inhibition of the breakdown of the accumulated lipids inhibits the activation of HSCs. Mouse HSC lipid breakdown was shown to be partially mediated by a lipophagic pathway, as inhibition of autophagy increased the amount of LDs[32,33]. Because

inhibition of autophagy was shown to impair HSC activation in mice and this effect could be partially reversed by addition of exogenous fatty acids, it was suggested that LD breakdown is required to fulfill the energy demands of HSCs during activation[33]. On the other hand, HSC activation was shown to be relatively undisturbed in the absence of LDs in Lecithin:retinol acyl transferase (LRAT) knockout mice[34]. The current knowledge on neutral lipid metabolism with a focus on HSCs will be described below.

LD AND NEUTRAL LIPID METABOLISM IN HSCs

Lipids are essential in life as the building blocks of bio-membranes and as a major source of energy for the organism. In eukaryotic cells, excess of hydrophobic molecules (mainly neutral lipids) are stored in LDs. The hydrophobic core of LDs is separated from the aqueous cytosol by a monolayer of surface phospholipids. In times of insufficient uptake of nutrients, LDs serve as a source of these hydrophobic compounds linked to many cellular functions, including energy generation, membrane synthesis, protein degradation as well as viral replication[35]. The number of LDs and their size in a cell depend on the type of cell, but also differs between individual cells of a population. Some cell types are specialized in lipid storing, like adipocytes, adrenal cortex cells and quiescent HSCs. Non-specialized cells usually contain small LDs of less than 1 µm, while LDs in adipocytes can be up to 200 µm[36]. The LD core in mammals mainly contains triacylglycerols (TAGs) and cholesterol esters (CEs), but may also contain REs as in case of HSCs.

In eukaryotes, LDs form from the endoplasmic reticulum (ER) where the enzymes that synthesize neutral lipids reside[37]. LDs appear to remain in contact with the ER once formed, and proteins that associate with both compartments move between them[38]. The surface of LDs is decorated with proteins which regulate their growth or utilization. Since the identification of perilipins as lipid droplet marker proteins that are important for the regulation of lipid metabolism[39,40], proteomic and cell biological analyses have revealed hundreds of LD resident protein candidates in various cell types. However, methodological issues confounded the interpretation of some of these studies. The consistently increasing sensitivity of mass spectrometry for proteomics however now leads to ever-longer growing lists of proteins that are identified in lipid droplet fractions. The overlap among these studies serves to identify a core set of LD proteins, although it is often difficult to determine which identified proteins are genuine LD proteins and which are low level contaminants of the analyzed LD fraction. Recent advances in quantitative proteomics that measure the abundance and enrichment of proteins in the LD fraction, rather than just their presence (such as protein correlation profiling) are likely to overcome the limitations of mass spectrometry, especially for low abundance proteins or proteins expressed in a specific tissue cell type[41].

TAG metabolism

The main function of TAG is to provide energy in times of limited food intake. In mammals, TAGs are concentrated primarily in adipocytes. Excessive accumulation of TAG has been reported in obesity in adipose tissue[42]. In HSCs, the amount of TAG in LDs was estimated to be 50-80% of all neutral lipids[43]. Upon activation of HSCs, not only the amount of TAG decreases, but also the fatty acid (FA) composition of TAG was shown to change prior to degradation[44]. During the first phase of activation a specific increase in TAG species containing long chain poly-unsaturated fatty acids (PUFA-TAGs), like arachidonic acid (AA), were observed[44]. The mechanism of this specific enrichment is as yet unknown, but involves the incorporation of exogenous PUFAs during TAG synthesis[44].

TAG synthesis

There are two major biochemical pathways for *de-novo* TAG synthesis. The so-called monoacylglycerol acyltransferase (MGAT) and glycerol-3-phosphate (G-3-*P*) pathways (see Figure 2). In the monoacylglycerol pathway, diacylglycerol (DAG) is formed directly from monoacylglycerol (MAG) and fatty acyl-CoA by a MGAT. In higher organisms, a family of three related genes (Mogat1, 2, and 3) with MGAT activity, which are localized in the ER, has been identified. Mogat1 and Mogat2 have sequence homology with acyl-Co-A:diacylglycerol acyltransferase 2 (DGAT2). Mogat1 is expressed in the stomach, kidney, white and brown adipose tissues, and liver but not in the small intestine[45]. Mogat2 is highly expressed in the small intestine, liver, stomach, kidney, colon, and white adipose tissue[46,47]. Recently, it was reported that mice lacking Mogat2 are unsusceptible to
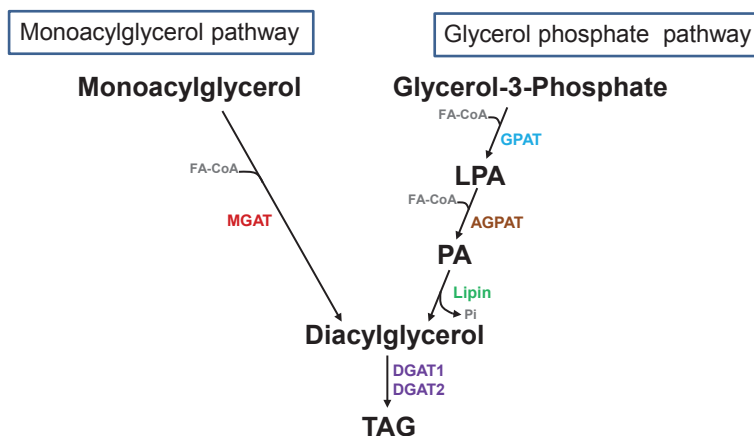

Figure 2. Monoacylglycerol (MAG) and Glycerol phosphate pathways for de novo triacylglycerol (TAG) synthesis. GPAT, glycerol-3-phosphate acyltransferase; LPA, lysophosphatidic acid; AGPAT, 1-acylglycerol-3-phosphate acyltransferase; PA, phosphatidic acid; DGAT, diacylglycerol acyltransferase; TAG, triacylglycerol.

developing obesity, glucose intolerance, or fatty liver even when fed on a high-fat diet[48]. These findings suggest that Mogat2 plays an important role in dietary fat absorption in mouse intestine and consequently is a therapeutic target for treating obesity and other metabolic diseases associated with excessive fat intake. Mogat3, the third MGAT gene, which is highly homologous to Mogat1 and Mogat2, is an intestinal specific enzyme implicated in dietary fat absorption[49].

MGAT preferentially acylates MAG that contain a polyunsaturated fatty acyl moiety at the *sn*-2 position[50]. Recent work suggested that human liver exhibits significant MGAT activity and MGAT expression is strikingly increased in NAFLD[51]. In general, MGATs are reported to play a significant role in tissues that have high TAG synthesizing activity such as small intestine, liver, and adipose tissue while the G-3-*P* pathway is ubiquitously present in all tissues. However, how MGAT and G-3-*P* pathways contribute to total TAG synthesis in HSCs remain unclear.

In the G-3-*P* pathway, DAG is synthesized by subsequent acylation's of glycerol-3-phosphate to phosphatidic acid (PA) by an acyl-CoA:glycerol-3-phosphate acyltransferase (GPAT) and an acyl-CoA: 1-acyl-glycerol-3-phosphate acyltransferase (AGPAT), respectively. This is followed by dephosphorylation of phosphatidic acid by a member of the lipin gene family in mammals. The *G-3-*P and MGAT pathways share the final step, which convert DAG to TAG, a reaction catalyzed by DGATs[52,53]. Two mammalian DGATs have been identified, DGAT1 and DGAT2. Both enzymes are ubiquitously expressed with the highest expression in tissues involved in TAG metabolism, such as liver, adipose tissue and small intestine and mammary gland. Concerning the differential roles of DGAT1 and 2 in HSCs, it was reported that DGAT2 is expressed in mouse stellate cells at low levels compared to hepatocytes, whereas expression of DGAT1 in stellate cells was found to be higher than in hepatocytes. However, expression of DGAT2 was not compared directly to DGAT1 in HSCs[54].

TAG lipolysis

When energy is required, free fatty acids (FFAs) are liberated from TAG stores and either used by the cells or secreted and carried by serum albumin in the plasma for delivery to tissues for utilization. Accumulation of FFAs in a cell can be toxic, therefore it is essential to maintain a tight regulation of TAG synthesis and breakdown. There is a constant cycle and balance of TAG lipolysis/esterification in response to the hormonal or nutritional state[55]. TAG hydrolysis takes place sequentially. First DAG is formed via liberation of the first FA from the glycerol backbone. This is then followed by hydrolysis of the second FA to form MAG and finally the process is completed by hydrolysis of MAG to release the final FA and the glycerol backbone[56]. Breakdown of LDs is best characterized in adipose cells, in which key roles were assigned to adipose triglyceride lipase (ATGL)[57] and hormone-sensitive lipase (HSL). ATGL specifically removes the first FA from the TAG molecule generating FFA and DAG[58]. The drastic impairment of adipocyte lipolysis in ATGL inhibition stud-

ies *in vitro* indicates that the enzyme is responsible for most of the HSL-independent lipolytic activity. An essential role of ATGL in lipolysis became evident from studies in ATGL knockout (ko) mice[59]. ATGL ko mice exhibited enlarged fat deposits and TAG accumulation in multiple tissues. ATGL is mainly expressed in white adipose tissue and brown adipose tissue, however detectable levels can be found in all tissues[58]. ATGL has a high substrate specificity for TAG and its activity is significantly enhanced by its co-activator, comparative gene identification-58 (CGI-58)[60]. Interactions of CGI-58 and ATGL together with LDs are essential to activate lipolysis[61] (see Figure 3). The N-terminal region of the patatin domain of ATGL is responsible for the activation of the enzyme by CGI-58, whereas the C-terminal region is critical for inhibition of activity via G0/G1 switch protein 2 (G0S2)[62]. CGI-58 is required for the translocation of ATGL to the lipid droplet surface by removing G0S2. ATGL is an important enzyme involved in intracellular degradation of TAGs as it has six to tenfold higher TAG lipase activity than DAG lipase. HSL, a cytoplasmic protein, is activated by the hormone glucagon, and shows significant DAG lipase activity that is 10-fold higher than its TAG
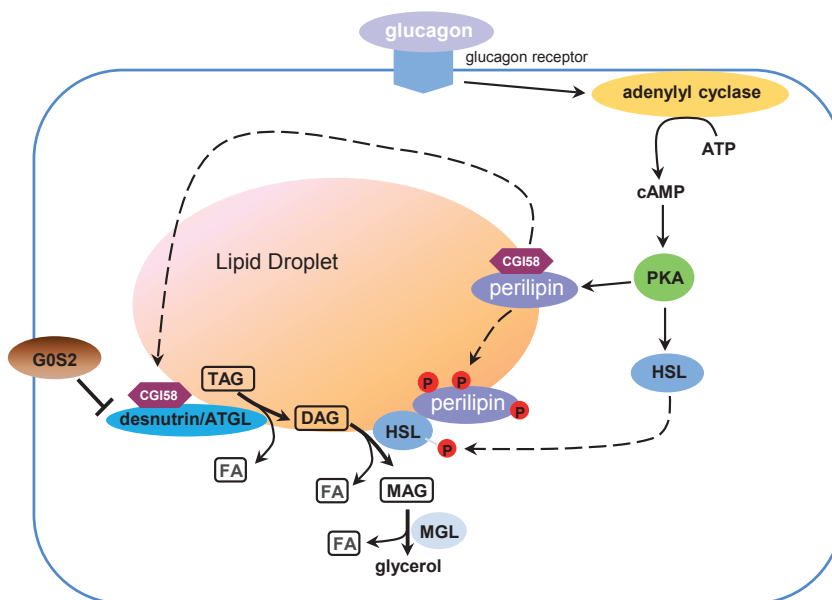
Figure 3. Hormone-mediated regulation of adipocyte lipolysis: Glucagon stimulates FA release from triglycerides stored in adipocyte fat droplets. Glucagon binding to their respective receptors triggers activation of adenylate cylcase (AC) and subsequently PKA. Activated PKA phosphorylates both perilipin-1 and HSL. The phosphorylation of perilipin-1 leads to the release of the ATGL co-activator CGI-58. CGI-58 then increases the activity of ATGL, thereby providing more DAG substrates for PKA-activated HSL. HSL hydrolyzes DAG to a FFA and MAG. Glycerol is released through the action of monoacylglycerol lipase (MGL). ATGL, adipose triglyceride lipase; CGI-58, comparative gene identification-58; HSL, hormone-sensitive lipase; MGL, monoglyceride lipase; PLIN-1, perilipin-1; cAMP, Cyclic adenosine monophosphate; PKA, Protein kinase A.

lipase activity in adipose tissue. HSL is diffusively distributed throughout the fat cell cytosol in unstimulated conditions, but translocates to the LD after phosphorylation by protein kinase A. Both phosphorylation of HSL and that of perilipin seem to be essential for the fragmentation and dispersion of the LDs and full lipolytic stimulation[63-65]. The molecular mechanisms and identity of the enzymes involved in lipid remodeling and breakdown of the lipid droplets during HSC activation are unknown. Rat HSCs were shown to express ATGL, although it was down regulated upon activation[66]. In activated mouse and human HSCs a role of autophagy in lipid breakdown (lipophagy) was demonstrated.

Lipophagy

Until recently, the breakdown of TAGs and CEs in LDs was attributed exclusively to the actions of cytosolic hydrolytic enzymes or lipases. The role of lysosomes in lipid metabolism was previously thought to be confined to the breakdown of lipoproteins after endocytosis. However, recently, the lysosomal degradative pathway was also shown to play a role in the in the breakdown of intracellular LD stores by the process of macroautophagy[67]. During autophagy of LDs, called lipophagy, cells mobilize fat in response to cellular needs and external stimuli[68]. Lipophagy is a specific form of autophagy, the process by which macromolecules are surrounded by the formation of an autophagosome (AP) and subsequently degraded by fusion of the AP with the lysosome. This process depends on a set of autophagy related genes (ATGs), which are responsible for the production of the double membrane AP structure. Lipophagy is now recognized as an alternative method of lipid hydrolysis[67,69]. Lipophagy was first described in hepatocytes[67], which have a much lower activity of cytosolic lipases as compared to adipocytes. In liver, lipophagy makes a quantitatively significant contribution to overall TAG degradation[70,71].The lipase responsible for TAG breakdown in lysosomes is thought to be lysosomal acidic lipase (LAL), also known as acidic lipase (Lipa). This enzyme also degrades CE and will be described in more detail in 2.2.2.

A role of lipophagy was also demonstrated in activated HSCs. HSCs activated *in vitro* or isolated in the activated state from fibrotic mouse livers have increased levels of autophagy as compared quiescent cells[32,33]. Furthermore, deletion of *atg7* (autophagy gene essential for AP formation) in mouse HSCs or treatment with autophagy inhibitors, such as bafilomycin A1, hydroxychloroquine and 3-methyladenine, led to an increase in LD size and TAG content[32,33]. Interestingly, pharmacological or genetic inhibition of autophagy also blocked trans-differentiation of HSCs into myofibroblasts[32,33]. The inhibition of HSC activation in by blocking lipophagy was suggested to be the result of decreased ATP levels. This was presumably a consequence of a shortage of FFAs, normally generated by the lipophagic process, as supplementation with oleic acid partially reversed the effect of autophagy inhibitors on HSC activation[32]. These findings suggest that HSCs increase autophagy in order to break down lipids to meet their increased energy demands during activation.

Cholesterol ester (CE)

Apart from TAG breakdown, lipophagy is also involved in CE metabolism. Cholesterol is the most abundant sterol in animal tissue and can be esterified to CE for storage. Sterols are structural components of membranes, modulating its fluidity. Furthermore, they serve as precursors for bile acids, vitamin D and various steroid hormones. Deregulation of their metabolism results in numerous pathological processes. Nearly all cells in the body take up unesterified cholesterol (UC) and/or CE by receptor-mediated endocytosis of various lipoproteins present in the surrounding pericellular fluid[72,73]. The sterol in these particles is processed in the late endosomal/lysosomal compartment by the sequential action of at least three proteins, (LAL/Lipa)[74], Niemann-Pick C1 (NPC1)[75], and Niemann-Pick C2 (NPC2)[76], before being exported into the cytosolic compartment. Mutations in any one of these three proteins cause accumulation of CE (LAL, Wolman disease) or UC (NPC1 or NPC2, Niemann-Pick C disease) in every tissue, which leads to cell dysfunction and to a variety of clinical syndromes including disease of the liver, lungs and the central nervous system. LAL is an acidic hydrolase, its deficiency results in either Wolman disease or its milder variant, Cholesteryl Ester Storage Disease (CESD)[77]. The difference in the severity of the phenotype between CESD and Wolman disease originates primarily from the level of residual enzymatic activity of LAL, which depends on the molecular nature of the mutation[78]. NPC disease, a rare hereditary lysosomal storage disorder is marked by accumulation of free cholesterol and other lipids in cells of a variety of organs, including brain, liver, and lung[79-81]. The majority (95%) of cases of NPC disease are caused by a mutation in NPC1, while the remaining cases (5%) are due to mutations in NPC2[82]. After export from the lysosomal system, UC is added to a metabolically active pool together with newly synthesized UC from acetyl-CoA. Because UC is potentially toxic to cells, the size of this metabolically active pool is tightly monitored by sterol regulatory element binding proteins (SREBPs) [83] and liver X receptors (LXRs)[84], which in turn regulate the expression of genes controlling the uptake, synthesis, degradation, and export of UC.

CE biosynthesis

Excess cellular cholesterol is stored as CEs in LDs. Steroidogenic tissues such as adrenals contain a relatively large amount of CEs that serves as a cholesterol reservoir for producing steroid hormones. In atherosclerosis, chronic accumulation of CE in macrophages causes these cells to appear foamy and is a hallmark of early stages in atherosclerosis. In most cell types, however, CEs are present only in low levels, mainly in cytoplasmic lipid droplets. Likewise, HSCs are known to contain small amounts of CEs in their LDs and the amount of CEs were shown to increase in the first phase of activation *in vitro*[44].

The conversion of cholesterol to CE is catalyzed by an acyl-coenzyme A:cholesterol acyltransferase (ACAT). ACATs are membrane-bound proteins that utilize long-chain fatty acyl-CoA and cholesterol as substrates to form cholesteryl esters. Esterification of cholesterol by ACAT is one
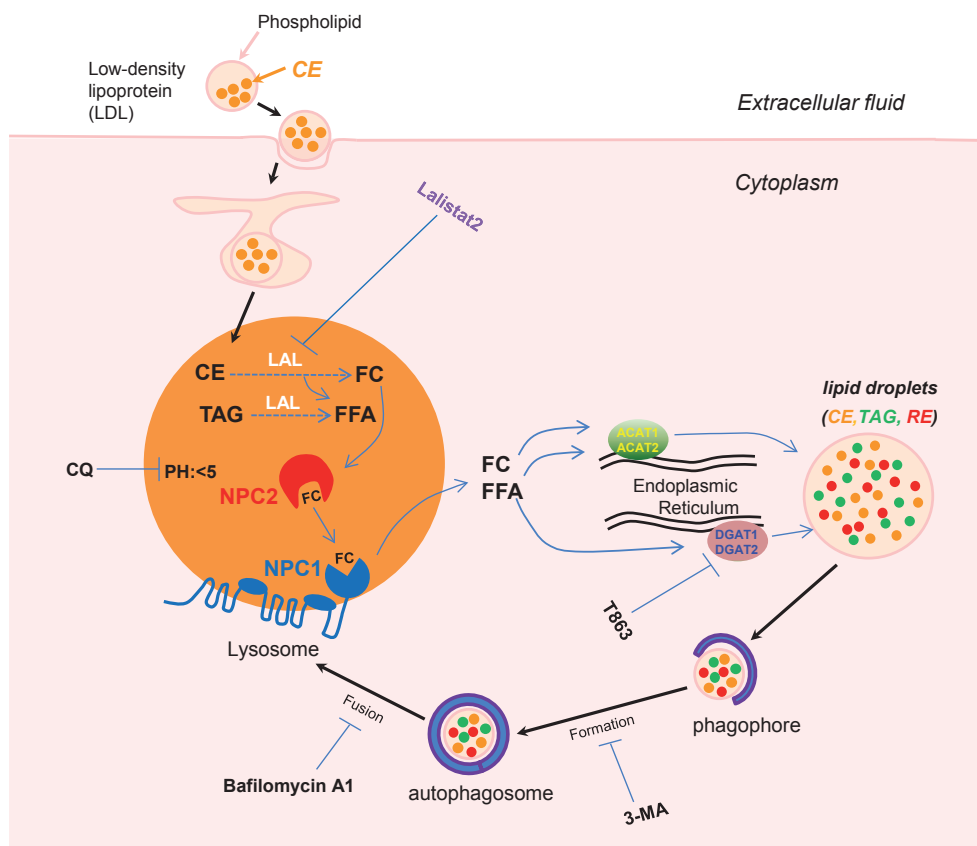
Figure 4. Lipophagy and the role of the lysosome in CE metabolism. Cells take up circulating low-density lipoproteins (LDL) by receptor-mediated endocytosis, directing them to lysosomes. Intracellular neutral lipids can also be directed to lysosomes by autophagy of LDs (lipophagy). The first step in lipophagy is the formation of double membrane structures (phagophores) which sequester (portions of the) LDs to be degraded. Phagophores mature into autophagosomes, which fuse with lysosomes to form autolysosomes. Autophagy can be inhibited by drugs like 3-methyl adenine (3-MA) at early stages or by bafilomycin A1 at the fusion stage between autophagosome and lysosome. In endosome-lysosomes, CEs are cleaved by LAL to yield free cholesterol, which is then bound by NPC2, transferred to NPC1, and exported. Cholesterol can be re-esterified by ACAT and stored in LDs as CEs. Lalistat 2 is an inhibitor of LAL. T863 is an orally active, selective and potent DGAT1 inhibitor. CQ block autophagy by inhibiting lysosomal proteases and autophagosome-lysosomal fusion events.

of the critical upregulated homeostatic responses upon elevated FA or cholesterol levels. High cholesterol levels cause allosteric activation of ACAT and the resulting cholesterol esters are stored along with triglycerides in the cytosolic lipid droplets[85]. In mammals, two isoenzymes (ACAT1 and ACAT2) exist that are encoded by two different genes[37,86,87] Together with DGAT1 they belong to the so-called membrane-bound O-acyltransferase (MBOAT) enzyme family[88]. ACAT1 is ubiquitously expressed whereas ACAT2 is mainly expressed in small intestine and liver[37,87]. In general ACAT1 is involved in CE deposition into cytoplasmic lipid droplets, while ACAT2 has been linked to lipoprotein-mediated secretion of CE. In human liver ACAT1 is the predominant enzyme, whereas in mice hepatocytes ACAT2 is the major enzyme. The relative distribution of ACAT1 and ACAT2 in HSCs is unknown.

CE breakdown

Net breakdown of CEs in LDs takes place when cellular cholesterol levels fall. A number of neutral CE hydrolases, like CEH (CES1), Nceh1 /KIAA1363 and HSL are implicated in the breakdown of CE from cytosolic LDs[89]. But similar to TAG, also an autophagic/lipophagic pathway, involving LAL/ Lipa was found to be capable of CE hydrolysis in LDs of macrophages[89]. This would implicate a role for LAL/Lipa in both in the uptake of cholesterol from lipoproteins and in the release from cytosolic LDs (see Figure 4).

Retinyl esters (REs)

The most distinguishing feature of HSCs is the presence of RE containing LDs in the cytoplasm[17,18]. REs consist of retinol esterified with a fatty acid, primarily palmitic acid. Retinol is also known as vitamin A and its metabolites are essential in the visual process and play an important role in the regulation of gene transcription during e.g. differentiation, embryogenesis and the immune response. Within the body, excess retinoids are stored as REs mainly in the liver and to a lesser extent in adipose tissue[90-94]. Mammals take up retinoids mostly from plants as pro-vitamin *beta*-carotene and from animal tissues as REs. Esterified retinol is packaged into chylomicrons together with other dietary lipids and secreted into the lymphatic system[92]. In the bloodstream chylomicrons are converted into chylomicron remnants by lipoprotein lipase. After uptake of the chylomicron remnants by hepatocytes in the liver, the REs are hydrolyzed presumably in a endosomal compartment, and free retinol will be transferred to a cellular retinol binding protein (CRBP)[95]. Retinol will then either be transported to the HSCs for storage as REs or can be converted into other metabolites such as retinoic acids or retinal[96].

Retinol esterification

Lecithin:retinol acyltransferase (LRAT) in the liver is responsible for almost all RE synthesis. LRAT is required for HSC LD formation, since *Lrat*-deficient mice lack of LDs[97]. It has long been established that the predominant REs present in the intact liver are those containing saturated FAs, predomi-

nantly palmitic and stearic acid[98]. The RE composition in HSC LDs faithfully reflects the hepatic RE composition. It is believed that this RE composition arises from the substrate specificity of LRAT, transferring a fatty acyl group from the sn-1 position of phosphatidyl choline to retinol.

In the HSC, retinol is bound by CRBPI and transferred to LRAT for esterification[99]. The binding of retinol to CRBPI is necessary for its transport in the aqueous environment of the cytosol and has been proposed to prevent acyl CoA-dependent enzymes in the liver from catalyzing retinyl ester formation[99]. Both LRAT and CRBPI are enriched in HSCs[100] and both proteins are required to assure optimal HSC accumulation of retinoid stores. Earlier *in vitro* studies suggested that ARAT may work in conjunction with LRAT to catalyze RE formation[101]. DGAT1 has been shown to participate in retinol esterification as DGAT1^{-/-} mice have reduced RE and retinol levels both *in vitro* and *in vivo* studies[102-105].

RE hydrolysis

Mobilization of REs from intracellular LDs depends on the hydrolytic actions of RE hydrolases (REHs). Early work on vitamin A metabolism demonstrated that HSC enriched fractions from rat liver contain high levels of neutral bile salt dependent REH activity[106]. Next to bile salt dependent REH activity, bile salt independent REH activities at neutral and acidic pH were identified in HSC enriched fractions, but were not preferentially enriched as compared to hepatocytes[107]. Furthermore, a REH activity was found in hepatocytes and HSC homogenates with an enzymatic pH 4.1[108]. REH was shown to be different from LAL/Lipa, although it was enriched in a lysosomal fraction. LDs are capable of fusing with primary lysosomes in HSCs suggesting that this lysosomal acidic REH may be physiologically relevant in hepatic retinol mobilization[108]. In line with the various REH activities described above, there is also various other proteins found to possess REH activity including neutral carboxy esterases ES-2, ES-3 and ES -10. It was also suggested that HSL and patatin like phospholipase domain containing 2 (PNPLA2, ATGL) acts as a REH, promoting the degradation of RE stores in addition to their established functions as TAG lipases[109]. Finally, PNPLA3 was reported to be responsible for retinyl palmitate hydrolysis in human HSCs[110,112]. This would indicate a potential novel link between HSCs, retinoid metabolism and PNPLA3 in the susceptibility to chronic liver diseases. The exact role of any of these suggested REH in RE breakdown in HSCs *in vivo* remains to be established.

LIPID DROPLETS AND EICOSANOIDS

As discussed in before, liver fibrosis is mediated by a complex interplay of both pro and anti-fibrotic factors. One class of these factors is the eicosanoids which are locally acting bioactive signaling lipids derived from arachidonic acid and related PUFAs that regulate a diverse set of homeostatic

and inflammatory processes[112,113]. Analyses of LDs in different cell types have demonstrated that LDs are particularly active sites for the metabolism of arachidonyl lipids.

The synthesis of eicosanoids depends on the availability of free AA. When tissues are exposed to diverse physiological and pathological stimuli such as growth factors, hormones or cytokines, AA is produced from membrane phospholipids by the action of phospholipase A2 (PLA2). AA can be enzymatically metabolized by three main pathways: P-450 epoxygenase, cyclooxygenases (COXs) and lipoxygenases (LOXs). The P-450 epoxygenase pathway produces hydroxyeicosatetraenoic acids (HETEs) and epoxides. The COX pathway produces PGG2 and PGH2, which are subsequently converted into prostaglandins (PGs) and thromboxanes (TXs). COX exists in two isoforms commonly referred to as COX1 (constitutively expressed in most cells) and COX2 (generally absent in resting cells and rapidly induced by hormones, cytokines)[114,115]. COX2 has a role in inflammation and carcinogenesis and the COX2 pathway is associated with various liver diseases[116]. It was reported that quiescent human HSCs do not express COX2 but activated human HSCs do express COX2, suggesting that the COX2 pathway has an active role in hepatic fibrogenesis[117].

Numerous LOX enzymes convert AA into diverse hydroperoxyeicosatetraenoic acids (HPETEs) and HETEs. 5-HETE is converted into the leukotriene (LT) LTA4, which is the precursor of LTB4, cysteinyl-LTs (including LTC4, LTD4 and LTE4) and lipoxins (LXs). Synthesis of LXs is dependent on the activity of the interacting LOXs and the proximity of cells that are necessary for the metabolism of AA to the LX end products. In some instances, the metabolite is transferred to another cell that in turn converts it into another compound. Thus, biosynthesis of different eicosanoids is dependent on local production and distribution of specific precursors and enzymes in specific cells.

During inflammatory conditions, LDs may compartmentalize the entire enzymatic machinery for eicosanoid synthesis[118]. However, efficient eicosanoid production is not only determined by the availability of arachidonic acid and of eicosanoid forming enzymes but also requires sequential interactions between specific proteins and may involve very unique spatial interactions[118]. Therefore, just by detecting eicosanoid forming enzymes in lipid droplets one cannot establish these organelles as accountable for the efficient and enhanced eicosanoid synthesis observed during inflammatory responses. It has been demonstrated that there are significant correlations between lipid droplet formation and enhanced generation of both LOX and COX derived eicosanoids *in vitro*[119-121] as well as *in vivo*[122-125], suggesting that increased LD numbers in cells enhances the capacity for eicosanoid production.

Electron microscopic observations demonstrated that exogenous radiolabeled AA was incorporated prominently in LDs of eosinophils, neutrophils, mast cells, macrophages and epithelial cells[126-128]. LDs obtained by subcellular fractionation provided direct evidence that these organ-

elles are stores of esterified AA. Although negligible amounts of free AA were identified in LDs, different enzymes involved in AA metabolism as well proteins involved in AA transport were characterized in LDs, thus providing strong evidence for a major role for LDs in AA metabolism. If LDs are indeed involved in AA signaling and eicosanoid formation, then the AA present in these lipid rich organelles must be released by lipases and the free arachidonate must have access to eicosanoid forming enzymes. As yet a possible correlation between LD metabolism and eicosanoid secretion in activated HSC has not been studied, but seems plausible considering the reported increase of TAG species containing long PUFAs in activated HSCs[44].

THESIS OUTLINE

HSCs store neutral lipids (triacylglycerols, cholesterol esters and retinyl esters) in cytoplasmic lipid droplets (LDs). LDs are ubiquitous dynamic organelles found in the cytoplasm of all cells that serve as an energy depot and allow maintenance of a balanced lipid metabolism. HSC activation is a critical step in the development of chronic liver disease. During activation, HSCs transform into myofibroblasts and lose their LDs. HSC lipid metabolism in HSC activation was investigated in this thesis. In Fig.5, the outline of the thesis is represented schematically.

We previously observed that the level of triacylglycerol (TAG) species containing long polyunsaturated fatty acids (PUFAs) is increased in *in vitro* activated HSC. In **chapter 2**, we investigate the cause and consequences of the rise in PUFA-TAGs by profiling enzymes involved in PUFA incorporation.

One of the unresolved issues in the field of HSC research is, whether the change in lipid metabolism is causally related to the activation process. In **chapter 3**, we aimed to investigate which enzymes are involved in TAG/LD turnover in HSC during activation *in vitro*.

In **chapter 4**, we investigate the role of the lipophagy/autophagy path in LD homeostasis by inhibiting the lipid breakdown in the lysosomal compartment by the specific lipa/LAL inhibitor lalistat.

To assess whether HSCs can be a source of eicosanoids during liver fibrosis and the effect of COX inhibitors on prostaglandins, we analyzed the eicosanoid secretion pattern of primary mouse and rat HSCs by HPLC-MS in **chapter 5**.

Finally, in **chapter 6** the research findings are summarized and placed in a broader perspective.
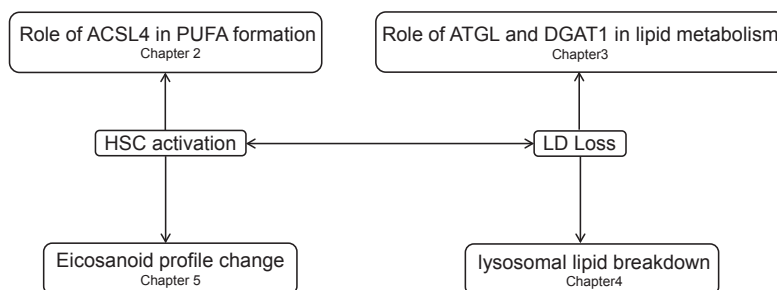

Figure 5. Schematic overview of the research topics described in this thesis

REFERENCES

1.   Alcolado, R., Arthur, M. J. & Iredale, J. P. (1997). Pathogenesis of liver fibrosis. *Clin. Sci. (Lond)* **92**, 103-112.

2.   Friedman, S. L. (2003). Liver fibrosis -- from bench to bedside. *J. Hepatol.* **38** Suppl 1, S38-53.

3.   Nair, S., Mason, A., Eason, J., Loss, G. & Perrillo, R. P. (2002). Is obesity an independent risk factor for hepatocellular carcinoma in cirrhosis? *Hepatology* **36**, 150-155.

4.   Schuppan, D., Ruehl, M., Somasundaram, R. & Hahn, E. G. (2001). Matrix as a modulator of hepatic fibrogenesis. *Semin. Liver Dis.* **21**, 351-372.

5.   Sorokin, L. (2010). The impact of the extracellular matrix on inflammation. *Nat. Rev. Immunol.* **10**, 712-723.

6.   Rojkind, M., Giambrone, M. A. & Biempica, L. (1979). Collagen types in normal and cirrhotic liver. *Gastroenterology* **76**, 710-719.

7.   Wynn, T. A. (2008). Cellular and molecular mechanisms of fibrosis. *J. Pathol.* **214**, 199-210.

8.   Thabut, D. & Shah, V. (2010). Intrahepatic angiogenesis and sinusoidal remodeling in chronic liver disease: new targets for the treatment of portal hypertension? *J. Hepatol.* **53**, 976-980.

9.   Baffy, G., Brunt, E. M. & Caldwell, S. H. (2012). Hepatocellular carcinoma in non-alcoholic fatty liver disease: an emerging menace. *J. Hepatol.* **56**, 1384-1391.

10.   Annoni, G., Weiner, F. R. & Zern, M. A. (1992). Increased transforming growth factor-beta 1 gene expression in human liver disease. *J. Hepatol.* **14**, 259-264.

11.   Bataller, R., Gines, P., Nicolas, J. M., Gorbig, M. N., Garcia-Ramallo, E., Gasull, X., Bosch, J., Arroyo, V. & Rodes, J. (2000). Angiotensin II induces contraction and proliferation of human hepatic stellate cells. *Gastroenterology* **118**, 1149-1156.

12.   Kinnman, N., Goria, O., Wendum, D., Gendron, M. C., Rey, C., Poupon, R. & Housset, C. (2001). Hepatic stellate cell proliferation is an early platelet-derived growth factor-mediated cellular event in rat cholestatic liver injury. *Lab. Invest.* **81**, 1709-1716.

13.   Shah, V. (2001). Cellular and molecular basis of portal hypertension. *Clin. Liver Dis.* **5**, 629-644.

14.   Geerts, A. (2001). History, heterogeneity, developmental biology, and functions of quiescent hepatic stellate cells. *Semin. Liver Dis.* **21**, 311-335.

15.   Wake, K. (1971). "Sternzellen" in the liver: perisinusoidal cells with special reference to storage of vitamin A. *Am. J. Anat.* **132**, 429-462.

16.   Friedman, S. L. (2008). Hepatic stellate cells: protean, multifunctional, and enigmatic cells of the liver. *Physiol. Rev.* **88**, 125-172.

17.   Bataller, R. & Brenner, D. A. (2001). Hepatic stellate cells as a target for the treatment of liver fibrosis. *Semin. Liver Dis.* **21**, 437-451.

18.   Hendriks, H. F., Verhoofstad, W. A., Brouwer, A., de Leeuw, A. M. & Knook, D. L. (1985). Perisinusoidal fat-storing cells are the main vitamin A storage sites in rat liver. *Exp. Cell Res.* **160**, 138-149.

19.   Gudas, L. J. (2012). Emerging roles for retinoids in regeneration and differentiation in normal and disease states. *Biochim. Biophys. Acta* **1821**, 213-221.

20.   Chambon, P. (1996). A decade of molecular biology of retinoic acid receptors. *FASEB J.* **10**, 940-954.

21. Balmer, J. E. & Blomhoff, R. (2002). Gene expression regulation by retinoic acid. *J. Lipid Res.* **43**, 1773-1808.

22. Graham, T. E., Yang, Q., Bluher, M., Hammarstedt, A., Ciaraldi, T. P., Henry, R. R., Wason, C. J., Oberbach, A., Jansson, P. A., Smith, U. *et al*. (2006). Retinol-binding protein 4 and insulin resistance in lean, obese, and diabetic subjects. *N. Engl. J. Med.* **354**, 2552-2563.

23. Kloting, N., Graham, T. E., Berndt, J., Kralisch, S., Kovacs, P., Wason, C. J., Fasshauer, M., Schon, M. R., Stumvoll, M., Bluher, M. *et al*. (2007). Serum retinol-binding protein is more highly expressed in visceral than in subcutaneous adipose tissue and is a marker of intra-abdominal fat mass. *Cell. Metab.* **6**, 79-87.

24. Maher, J. J. (2013). Retinol binding protein 4 and fatty liver: A direct link? *Hepatology* **58**, 477-479.

25. Geerts, A., Lazou, J. M., De Bleser, P. & Wisse, E. (1991). Tissue distribution, quantitation and proliferation kinetics of fat-storing cells in carbon tetrachloride-injured rat liver. *Hepatology* **13**, 1193-1202.

26. Friedman, S. L. (2000). Molecular regulation of hepatic fibrosis, an integrated cellular response to tissue injury. *J. Biol. Chem.* **275**, 2247-2250.

27. Yan, C., Zhou, L. & Han, Y. P. (2008). Contribution of hepatic stellate cells and matrix metalloproteinase 9 in acute liver failure. *Liver Int.* **28**, 959-971.

28. Han, Y. P. (2006). Matrix metalloproteinases, the pros and cons, in liver fibrosis. *J. Gastroenterol. Hepatol.* **21** Suppl 3, S88-91.

29. Ramachandran, P. & Iredale, J. P. (2012). Liver fibrosis: a bidirectional model of fibrogenesis and resolution. *QJM* **105**, 813-817.

30. Bataller, R. & Brenner, D. A. (2005). Liver fibrosis. *J. Clin. Invest.* **115**, 209-218.

31. Rubbia-Brandt, L., Mentha, G., Desmouliere, A., Alto Costa, A. M., Giostra, E., Molas, G., Enzan, H. & Gabbiani, G. (1997). Hepatic stellate cells reversibly express alpha-smooth muscle actin during acute hepatic ischemia. *Transplant. Proc.* **29**, 2390-2395.

32. Thoen, L. F., Guimaraes, E. L., Dolle, L., Mannaerts, I., Najimi, M., Sokal, E. & van Grunsven, L. A. (2011). A role for autophagy during hepatic stellate cell activation. *J. Hepatol.* **55**, 1353-1360.

33. Hernandez-Gea, V., Ghiassi-Nejad, Z., Rozenfeld, R., Gordon, R., Fiel, M. I., Yue, Z., Czaja, M. J. & Friedman, S. L. (2012). Autophagy releases lipid that promotes fibrogenesis by activated hepatic stellate cells in mice and in human tissues. *Gastroenterology* **142**, 938-946.

34. O'Byrne, S. M., Wongsiriroj, N., Libien, J., Vogel, S., Goldberg, I. J., Baehr, W., Palczewski, K. & Blaner, W. S. (2005). Retinoid absorption and storage is impaired in mice lacking lecithin:retinol acyltransferase (LRAT). *J. Biol. Chem.* **280**, 35647-35657.

35. Walther, T. C. & Farese, R. V.,Jr. (2012). Lipid droplets and cellular lipid metabolism. *Annu. Rev. Biochem.* **81**, 687-714.

36. Martin, S. & Parton, R. G. (2006). Lipid droplets: a unified view of a dynamic organelle. *Nat. Rev. Mol. Cell Biol.* **7**, 373-378.

37. Buhman, K. K., Chen, H. C. & Farese, R. V.,Jr. (2001). The enzymes of neutral lipid synthesis. *J. Biol. Chem.* **276**, 40369-40372.

38. Jacquier, N., Choudhary, V., Mari, M., Toulmay, A., Reggiori, F. & Schneiter, R. (2011). Lipid droplets are functionally connected to the endoplasmic reticulum in Saccharomyces cerevisiae. *J. Cell. Sci.* **124**, 2424-2437.

39.   Greenberg, A. S., Egan, J. J., Wek, S. A., Garty, N. B., Blanchette-Mackie, E. J. & Londos, C. (1991). Perilipin, a major hormonally regulated adipocyte-specific phosphoprotein associated with the periphery of lipid storage droplets. *J. Biol. Chem.* **266**, 11341-11346.

40.   Londos, C., Brasaemle, D. L., Gruia-Gray, J., Servetnick, D. A., Schultz, C. J., Levin, D. M. & Kimmel, A. R. (1995). Perilipin: unique proteins associated with intracellular neutral lipid droplets in adipocytes and steroidogenic cells. *Biochem. Soc. Trans.* **23**, 611-615.

41.   Krahmer, N., Hilger, M., Kory, N., Wilfling, F., Stoehr, G., Mann, M., Farese, R. V.,Jr & Walther, T. C. (2013). Protein correlation profiles identify lipid droplet proteins with high confidence. *Mol. Cell. Proteomics* **12**, 1115-1126.

42.   Gregoire, F. M., Smas, C. M. & Sul, H. S. (1998). Understanding adipocyte differentiation. *Physiol. Rev.* **78**, 783-809.

43.   Yamada, M., Blaner, W. S., Soprano, D. R., Dixon, J. L., Kjeldbye, H. M. & Goodman, D. S. (1987). Biochemical characteristics of isolated rat liver stellate cells. *Hepatology* **7**, 1224-1229.

44.   Testerink, N., Ajat, M., Houweling, M., Brouwers, J. F., Pully, V. V., van Manen, H. J., Otto, C., Helms, J. B. & Vaandrager, A. B. (2012). Replacement of retinyl esters by polyunsaturated triacylglycerol species in lipid droplets of hepatic stellate cells during activation. *PLoS One* **7**, e34945.

45.   Yen, C. L., Stone, S. J., Cases, S., Zhou, P. & Farese, R. V.,Jr. (2002). Identification of a gene encoding MGAT1, a monoacylglycerol acyltransferase. *Proc. Natl. Acad. Sci.* **99**, 8512-8517.

46.   Yen, C. L. & Farese, R. V.,Jr. (2003). MGAT2, a monoacylglycerol acyltransferase expressed in the small intestine. *J. Biol. Chem.* **278**, 18532-18537.

47.   Lockwood, J. F., Cao, J., Burn, P. & Shi, Y. (2003). Human intestinal monoacylglycerol acyltransferase: differential features in tissue expression and activity. *Am. J. Physiol. Endocrinol. Metab.* **285**, E927-37.

48.   Yen, C. L., Cheong, M. L., Grueter, C., Zhou, P., Moriwaki, J., Wong, J. S., Hubbard, B., Marmor, S. & Farese, R. V.,Jr. (2009). Deficiency of the intestinal enzyme acyl CoA:monoacylglycerol acyltransferase-2 protects mice from metabolic disorders induced by high-fat feeding. *Nat. Med.* **15**, 442-446.

49.   Cheng, D., Nelson, T. C., Chen, J., Walker, S. G., Wardwell-Swanson, J., Meegalla, R., Taub, R., Billheimer, J. T., Ramaker, M. & Feder, J. N. (2003). Identification of acyl coenzyme A:monoacylglycerol acyltransferase 3, an intestinal specific enzyme implicated in dietary fat absorption. *J. Biol. Chem.* **278**, 13611-13614.

50.   Xia, T., Mostafa, N., Bhat, B. G., Florant, G. L. & Coleman, R. A. (1993). Selective retention of essential fatty acids: the role of hepatic monoacylglycerol acyltransferase. *Am. J. Physiol.* **265**, R414-9.

51.   Hall, A. M., Kou, K., Chen, Z., Pietka, T. A., Kumar, M., Korenblat, K. M., Lee, K., Ahn, K., Fabbrini, E., Klein, S. *et al.* (2012). Evidence for regulated monoacylglycerol acyltransferase expression and activity in human liver. *J. Lipid Res.* **53**, 990-999.

52.   Cases, S., Smith, S. J., Zheng, Y. W., Myers, H. M., Lear, S. R., Sande, E., Novak, S., Collins, C., Welch, C. B., Lusis, A. J. *et al.* (1998). Identification of a gene encoding an acyl CoA:diacylglycerol acyltransferase, a key enzyme in triacylglycerol synthesis. *Proc. Natl. Acad. Sci. U. S. A.* **95**, 13018-13023.

53.   Coleman, R. A. & Lee, D. P. (2004). Enzymes of triacylglycerol synthesis and their regulation. *Prog. Lipid Res.* **43**, 134-176.

54.   Choi, C. S., Savage, D. B., Kulkarni, A., Yu, X. X., Liu, Z. X., Morino, K., Kim, S., Distefano, A., Samuel, V. T., Neschen, S. *et al.* (2007). Suppression of diacylglycerol acyltransferase-2 (DGAT2), but not DGAT1, with

antisense oligonucleotides reverses diet-induced hepatic steatosis and insulin resistance. *J. Biol. Chem.* **282**, 22678-22688.

55. Duncan, R. E., Ahmadian, M., Jaworski, K., Sarkadi-Nagy, E. & Sul, H. S. (2007). Regulation of lipolysis in adipocytes. *Annu. Rev. Nutr.* **27**, 79-101.

56. Coleman, R. A. & Mashek, D. G. (2011). Mammalian triacylglycerol metabolism: synthesis, lipolysis, and signaling. *Chem. Rev.* **111**, 6359-6386.

57. Zimmermann, R., Strauss, J. G., Haemmerle, G., Schoiswohl, G., Birner-Gruenberger, R., Riederer, M., Lass, A., Neuberger, G., Eisenhaber, F., Hermetter, A. *et al*. (2004). Fat mobilization in adipose tissue is promoted by adipose triglyceride lipase. *Science* **306**, 1383-1386.

58. Kershaw, E. E., Hamm, J. K., Verhagen, L. A., Peroni, O., Katic, M. & Flier, J. S. (2006). Adipose triglyceride lipase: function, regulation by insulin, and comparison with adiponutrin. *Diabetes* **55**, 148-157.

59. Haemmerle, G., Lass, A., Zimmermann, R., Gorkiewicz, G., Meyer, C., Rozman, J., Heldmaier, G., Maier, R., Theussl, C., Eder, S. *et al*. (2006). Defective lipolysis and altered energy metabolism in mice lacking adipose triglyceride lipase. *Science* **312**, 734-737.

60. Lass, A., Zimmermann, R., Haemmerle, G., Riederer, M., Schoiswohl, G., Schweiger, M., Kienesberger, P., Strauss, J. G., Gorkiewicz, G. & Zechner, R. (2006). Adipose triglyceride lipase-mediated lipolysis of cellular fat stores is activated by CGI-58 and defective in Chanarin-Dorfman Syndrome. *Cell. Metab.* **3**, 309-319.

61. Yamaguchi, T., Omatsu, N., Morimoto, E., Nakashima, H., Ueno, K., Tanaka, T., Satouchi, K., Hirose, F. & Osumi, T. (2007). CGI-58 facilitates lipolysis on lipid droplets but is not involved in the vesiculation of lipid droplets caused by hormonal stimulation. *J. Lipid Res.* 48, 1078-1089.

62. Yang, X., Lu, X., Lombes, M., Rha, G. B., Chi, Y. I., Guerin, T. M., Smart, E. J. & Liu, J. (2010). The G(0)/G(1) switch gene 2 regulates adipose lipolysis through association with adipose triglyceride lipase. *Cell. Metab.* **11**, 194-205.

63. Miyoshi, H., Perfield, J. W.,2nd, Souza, S. C., Shen, W. J., Zhang, H. H., Stancheva, Z. S., Kraemer, F. B., Obin, M. S. & Greenberg, A. S. (2007). Control of adipose triglyceride lipase action by serine 517 of perilipin A globally regulates protein kinase A-stimulated lipolysis in adipocytes. *J. Biol. Chem.* **282**, 996-1002.

64. Marcinkiewicz, A., Gauthier, D., Garcia, A. & Brasaemle, D. L. (2006). The phosphorylation of serine 492 of perilipin a directs lipid droplet fragmentation and dispersion. *J. Biol. Chem.* **281**, 11901-11909.

65. Miyoshi, H., Souza, S. C., Zhang, H. H., Strissel, K. J., Christoffolete, M. A., Kovsan, J., Rudich, A., Kraemer, F. B., Bianco, A. C., Obin, M. S. *et al*. (2006). Perilipin promotes hormone-sensitive lipase-mediated adipocyte lipolysis via phosphorylation-dependent and -independent mechanisms. *J. Biol. Chem.* **281**, 15837-15844.

66. Mello, T., Nakatsuka, A., Fears, S., Davis, W., Tsukamoto, H., Bosron, W. F. & Sanghani, S. P. (2008). Expression of carboxylesterase and lipase genes in rat liver cell-types. *Biochem. Biophys. Res. Commun.* **374**, 460-464.

67. Singh, R., Kaushik, S., Wang, Y., Xiang, Y., Novak, I., Komatsu, M., Tanaka, K., Cuervo, A. M. & Czaja, M. J. (2009). Autophagy regulates lipid metabolism. *Nature* **458**, 1131-1135.

68. Zechner, R. & Madeo, F. (2009). Cell biology: Another way to get rid of fat. *Nature* **458**, 1118-1119.

69. Singh, R. & Cuervo, A. M. (2011). Autophagy in the cellular energetic balance. *Cell. Metab.* **13**, 495-504.

70. Cahova, M., Dankova, H., Palenickova, E., Papackova, Z. & Kazdova, L. (2010). The autophagy-lysosomal pathway is involved in TAG degradation in the liver: the effect of high-sucrose and high-fat diet. *Folia Biol. (Praha)* **56**, 173-182.

71. Cahova, M., Dankova, H., Palenickova, E., Papackova, Z., Komers, R., Zdychova, J., Sticova, E. & Kazdova, L. (2012). The increased activity of liver lysosomal lipase in nonalcoholic Fatty liver disease contributes to the development of hepatic insulin resistance. *Biochem. Res. Int.* **2012**, 135723.

72. Brown, M. S. & Goldstein, J. L. (1986). A receptor-mediated pathway for cholesterol homeostasis. *Science* **232**, 34-47.

73. Liu, B., Xie, C., Richardson, J. A., Turley, S. D. & Dietschy, J. M. (2007). Receptor-mediated and bulk-phase endocytosis cause macrophage and cholesterol accumulation in Niemann-Pick C disease. *J. Lipid Res.* **48**, 1710-1723.

74. Du, H., Duanmu, M., Witte, D. & Grabowski, G. A. (1998). Targeted disruption of the mouse lysosomal acid lipase gene: long-term survival with massive cholesteryl ester and triglyceride storage. *Hum. Mol. Genet.* **7**, 1347-1354.

75. Carstea, E. D., Morris, J. A., Coleman, K. G., Loftus, S. K., Zhang, D., Cummings, C., Gu, J., Rosenfeld, M. A., Pavan, W. J., Krizman, D. B. *et al*. (1997). Niemann-Pick C1 disease gene: homology to mediators of cholesterol homeostasis. *Science* **277**, 228-231.

76. Naureckiene, S., Sleat, D. E., Lackland, H., Fensom, A., Vanier, M. T., Wattiaux, R., Jadot, M. & Lobel, P. (2000). Identification of HE1 as the second gene of Niemann-Pick C disease. *Science* **290**, 2298-2301.

77. Sloan, H. R. & Fredrickson, D. S. (1972). Enzyme deficiency in cholesteryl ester storage idisease. *J. Clin. Invest.* **51**, 1923-1926.

78. Anderson, R. A., Bryson, G. M. & Parks, J. S. (1999). Lysosomal acid lipase mutations that determine phenotype in Wolman and cholesterol ester storage disease. *Mol. Genet. Metab.* **68**, 333-345.

79. Ioannou, Y. A. (2005). Guilty until proven innocent: the case of NPC1 and cholesterol. *Trends Biochem. Sci.* **30**, 498-505.

80. Peake, K. B. & Vance, J. E. (2010). Defective cholesterol trafficking in Niemann-Pick C-deficient cells. *FEBS Lett.* **584**, 2731-2739.

81. Xie, C., Turley, S. D. & Dietschy, J. M. (1999). Cholesterol accumulation in tissues of the Niemann-pick type C mouse is determined by the rate of lipoprotein-cholesterol uptake through the coated-pit pathway in each organ. *Proc. Natl. Acad. Sci.* **96**, 11992-11997.

82. Loftus, S. K., Morris, J. A., Carstea, E. D., Gu, J. Z., Cummings, C., Brown, A., Ellison, J., Ohno, K., Rosenfeld, M. A., Tagle, D. A. *et al*. (1997). Murine model of Niemann-Pick C disease: mutation in a cholesterol homeostasis gene. *Science* **277**, 232-235.

83. Goldstein, J. L., DeBose-Boyd, R. A. & Brown, M. S. (2006). Protein sensors for membrane sterols. *Cell* **124**, 35-46.

84. Chawla, A., Repa, J. J., Evans, R. M. & Mangelsdorf, D. J. (2001). Nuclear receptors and lipid physiology: opening the X-files. *Science* 294, 1866-1870.

85. Chang, T. Y., Chang, C. C. & Cheng, D. (1997). Acyl-coenzyme A:cholesterol acyltransferase. *Annu. Rev. Biochem.* **66**, 613-638.

86. Cases, S., Novak, S., Zheng, Y. W., Myers, H. M., Lear, S. R., Sande, E., Welch, C. B., Lusis, A. J., Spencer, T. A., Krause, B. R. *et al.* (1998). ACAT-2, a second mammalian acyl-CoA:cholesterol acyltransferase. Its cloning, expression, and characterization. *J. Biol. Chem.* **273**, 26755-26764.

87. Anderson, R. A., Joyce, C., Davis, M., Reagan, J. W., Clark, M., Shelness, G. S. & Rudel, L. L. (1998). Identification of a form of acyl-CoA:cholesterol acyltransferase specific to liver and intestine in nonhuman primates. *J. Biol. Chem.* **273**, 26747-26754.

88. Hofmann, K. (2000). A superfamily of membrane-bound O-acyltransferases with implications for wnt signaling. *Trends Biochem. Sci.* **25**, 111-112.

89. Ouimet, M. & Marcel, Y. L. (2012). Regulation of lipid droplet cholesterol efflux from macrophage foam cells. *Arterioscler. Thromb. Vasc. Biol.* **32**, 575-581.

90. Blomhoff, R. & Wake, K. (1991). Perisinusoidal stellate cells of the liver: important roles in retinol metabolism and fibrosis. *FASEB J.* **5**, 271-277.

91. Blomhoff, R., Rasmussen, M., Nilsson, A., Norum, K. R., Berg, T., Blaner, W. S., Kato, M., Mertz, J. R., Goodman, D. S. & Eriksson, U. (1985). Hepatic retinol metabolism. Distribution of retinoids, enzymes, and binding proteins in isolated rat liver cells. *J. Biol. Chem.* **260**, 13560-13565.

92. Senoo, H., Kojima, N. & Sato, M. (2007). Vitamin A-storing cells (stellate cells). *Vitam. Horm.* **75**, 131-159.

93. Blomhoff, R., Berg, T. & Norum, K. R. (1988). Distribution of retinol in rat liver cells: effect of age, sex and nutritional status. *Br. J. Nutr.* **60**, 233-239.

94. Tsutsumi, C., Okuno, M., Tannous, L., Piantedosi, R., Allan, M., Goodman, D. S. & Blaner, W. S. (1992). Retinoids and retinoid-binding protein expression in rat adipocytes. *J. Biol. Chem.* **267**, 1805-1810.

95. Blomhoff, R., Green, M. H., Berg, T. & Norum, K. R. (1990). Transport and storage of vitamin A. *Science* **250**, 399-404.

96. D'Ambrosio, D. N., Clugston, R. D. & Blaner, W. S. (2011). Vitamin A metabolism: an update. *Nutrients* **3**, 63-103.

97. O'Byrne, S. M., Wongsiriroj, N., Libien, J., Vogel, S., Goldberg, I. J., Baehr, W., Palczewski, K. & Blaner, W. S. (2005). Retinoid absorption and storage is impaired in mice lacking lecithin:retinol acyltransferase (LRAT). *J. Biol. Chem.* **280**, 35647-35657.

98. HUANG, H. S. & GOODMAN, D. S. (1965). Vitamin a and Carotenoids. I. Intestinal Absorption and Metabolism of 14c-Labelled Vitamin a Alcohol and Beta-Carotene in the Rat. *J. Biol. Chem.* **240**, 2839-2844.

99. O'Byrne, S. M. & Blaner, W. S. (2013). Retinol and retinyl esters: biochemistry and physiology. *J. Lipid Res.* **54**, 1731-1743.

100. Leo, M. A. & Lieber, C. S. (1982). Hepatic vitamin A depletion in alcoholic liver injury. *N. Engl. J. Med.* **307**, 597-601.

101. Ross, A. C. (1982). Retinol esterification by rat liver microsomes. Evidence for a fatty acyl coenzyme A: retinol acyltransferase. *J. Biol. Chem.* **257**, 2453-2459.

102. O'Byrne, S. M., Wongsiriroj, N., Libien, J., Vogel, S., Goldberg, I. J., Baehr, W., Palczewski, K. & Blaner, W. S. (2005). Retinoid absorption and storage is impaired in mice lacking lecithin:retinol acyltransferase (LRAT). *J. Biol. Chem.* **280**, 35647-35657.

103. Yen, C. L., Monetti, M., Burri, B. J. & Farese, R. V.,Jr. (2005). The triacylglycerol synthesis enzyme DGAT1 also catalyzes the synthesis of diacylglycerols, waxes, and retinyl esters. *J. Lipid Res.* **46**, 1502-1511.

104. Orland, M. D., Anwar, K., Cromley, D., Chu, C. H., Chen, L., Billheimer, J. T., Hussain, M. M. & Cheng, D. (2005). Acyl coenzyme A dependent retinol esterification by acyl coenzyme A: diacylglycerol acyl-transferase 1. *Biochim. Biophys. Acta* **1737**, 76-82.

105. Shih, M. Y., Kane, M. A., Zhou, P., Yen, C. L., Streeper, R. S., Napoli, J. L. & Farese, R. V.,Jr. (2009). Retinol Esterification by DGAT1 Is Essential for Retinoid Homeostasis in Murine Skin. *J. Biol. Chem.* **284**, 4292-4299.

106. Blaner, W. S., Hendriks, H. F., Brouwer, A., de Leeuw, A. M., Knook, D. L. & Goodman, D. S. (1985). Reti-noids, retinoid-binding proteins, and retinyl palmitate hydrolase distributions in different types of rat liver cells. *J. Lipid Res.* **26**, 1241-1251.

107. Matsuura, T., Gad, M. Z., Harrison, E. H. & Ross, A. C. (1997). Lecithin:retinol acyltransferase and retinyl ester hydrolase activities are differentially regulated by retinoids and have distinct distributions be-tween hepatocyte and nonparenchymal cell fractions of rat liver. *J. Nutr.* **127**, 218-224.

108. Azais-Braesco, V., Dodeman, I., Delpal, S., Alexandre-Gouabau, M. C., Partier, A., Borel, P. & Grolier, P. (1995). Vitamin A contained in the lipid droplets of rat liver stellate cells is substrate for acid retinyl ester hydrolase. *Biochim. Biophys. Acta* **1259**, 271-276.

109. Taschler, U., Schreiber, R., Chitraju, C., Grabner, G. F., Romauch, M., Wolinski, H., Haemmerle, G., Brein-bauer, R., Zechner, R., Lass, A. *et al*. (2015). Adipose triglyceride lipase is involved in the mobilization of triglyceride and retinoid stores of hepatic stellate cells. *Biochim. Biophys. Acta* **1851**, 937-945.

110. He, S., McPhaul, C., Li, J. Z., Garuti, R., Kinch, L., Grishin, N. V., Cohen, J. C. & Hobbs, H. H. (2010). A sequence variation (I148M) in PNPLA3 associated with nonalcoholic fatty liver disease disrupts triglyc-eride hydrolysis. *J. Biol. Chem.* **285**, 6706-6715.

111. Pirazzi, C., Adiels, M., Burza, M. A., Mancina, R. M., Levin, M., Stahlman, M., Taskinen, M. R., Orho-Me-lander, M., Perman, J., Pujia, A. *et al*. (2012). Patatin-like phospholipase domain-containing 3 (PNPLA3) I148M (rs738409) affects hepatic VLDL secretion in humans and in vitro. *J. Hepatol.* **57**, 1276-1282.

112. Funk, C. D. (2001). Prostaglandins and leukotrienes: advances in eicosanoid biology. *Science* **294**, 1871-1875.

113. Buczynski, M. W., Dumlao, D. S. & Dennis, E. A. (2009). Thematic Review Series: Proteomics. An inte-grated omics analysis of eicosanoid biology. *J. Lipid Res.* **50**, 1015-1038.

114. Chang, Y. W., Putzer, K., Ren, L., Kaboord, B., Chance, T. W., Qoronfleh, M. W. & Jakobi, R. (2005). Differen-tial regulation of cyclooxygenase 2 expression by small GTPases Ras, Rac1, and RhoA. *J. Cell. Biochem.* **96**, 314-329.

115. Smith, W. L., Garavito, R. M. & DeWitt, D. L. (1996). Prostaglandin endoperoxide H synthases (cyclooxy-genases)-1 and -2. *J. Biol. Chem.* **271**, 33157-33160.

116. Piston, D., Wang, S., Feng, Y., Ye, Y. J., Zhou, J., Jiang, K. W., Xu, F., Zhao, Y. & Cui, Z. R. (2007). The role of cyclooxygenase-2/prostanoid pathway in visceral pain induced liver stress response in rats. *Chin. Med. J. (Engl)* **120**, 1813-1819.

117. Efsen, E., Bonacchi, A., Pastacaldi, S., Valente, A. J., Wenzel, U. O., Tosti-Guerra, C., Pinzani, M., Laffi, G., Abboud, H. E., Gentilini, P. *et al*. (2001). Agonist-specific regulation of monocyte chemoattractant protein-1 expression by cyclooxygenase metabolites in hepatic stellate cells. *Hepatology* **33**, 713-721.

118. Bozza, P. T., Magalhaes, K. G. & Weller, P. F. (2009). Leukocyte lipid bodies - Biogenesis and functions in inflammation. *Biochim. Biophys. Acta* **1791**, 540-551.

119.   Bozza, P. T., Yu, W., Penrose, J. F., Morgan, E. S., Dvorak, A. M. & Weller, P. F. (1997). Eosinophil lipid bodies: specific, inducible intracellular sites for enhanced eicosanoid formation. *J. Exp. Med.* **186**, 909-920.

120.   Bozza, P. T., Payne, J. L., Goulet, J. L. & Weller, P. F. (1996). Mechanisms of platelet-activating factor-induced lipid body formation: requisite roles for 5-lipoxygenase and de novo protein synthesis in the compartmentalization of neutrophil lipids. *J. Exp. Med.* **183**, 1515-1525.

121.   Weller, P. F., Bozza, P. T., Yu, W. & Dvorak, A. M. (1999). Cytoplasmic lipid bodies in eosinophils: central roles in eicosanoid generation. *Int. Arch. Allergy Immunol.* **118**, 450-452.

122.   Maya-Monteiro, C. M., Almeida, P. E., D'Avila, H., Martins, A. S., Rezende, A. P., Castro-Faria-Neto, H. & Bozza, P. T. (2008). Leptin induces macrophage lipid body formation by a phosphatidylinositol 3-kinase- and mammalian target of rapamycin-dependent mechanism. *J. Biol. Chem.* **283**, 2203-2210.

123.   Vieira-de-Abreu, A., Assis, E. F., Gomes, G. S., Castro-Faria-Neto, H. C., Weller, P. F., Bandeira-Melo, C. & Bozza, P. T. (2005). Allergic challenge-elicited lipid bodies compartmentalize in vivo leukotriene C4 synthesis within eosinophils. *Am. J. Respir. Cell Mol. Biol.* **33**, 254-261.

124.   de Assis, E. F., Silva, A. R., Caiado, L. F., Marathe, G. K., Zimmerman, G. A., Prescott, S. M., McIntyre, T. M., Bozza, P. T. & de Castro-Faria-Neto, H. C. (2003). Synergism between platelet-activating factor-like phospholipids and peroxisome proliferator-activated receptor gamma agonists generated during low density lipoprotein oxidation that induces lipid body formation in leukocytes. *J. Immunol.* **171**, 2090-2098.

125.   Melo, R. C., D'Avila, H., Fabrino, D. L., Almeida, P. E. & Bozza, P. T. (2003). Macrophage lipid body induction by Chagas disease in vivo: putative intracellular domains for eicosanoid formation during infection. *Tissue Cell* **35**, 59-67.

126.   Weller, P. F., Monahan-Earley, R. A., Dvorak, H. F. & Dvorak, A. M. (1991). Cytoplasmic lipid bodies of human eosinophils. Subcellular isolation and analysis of arachidonate incorporation. *Am. J. Pathol.* **138**, 141-148.

127.   Plotkowski, M. C., Brandao, B. A., de Assis, M. C., Feliciano, L. F., Raymond, B., Freitas, C., Saliba, A. M., Zahm, J. M., Touqui, L. & Bozza, P. T. (2008). Lipid body mobilization in the ExoU-induced release of inflammatory mediators by airway epithelial cells. *Microb. Pathog.* **45**, 30-37.

128.   Dvorak, A. M., Dvorak, H. F., Peters, S. P., Shulman, E. S., MacGlashan, D. W.,Jr, Pyne, K., Harvey, V. S., Galli, S. J. & Lichtenstein, L. M. (1983). Lipid bodies: cytoplasmic organelles important to arachidonate metabolism in macrophages and mast cells. *J. Immunol.* **131**, 2965-2976.

CHAPTER 1

Role of long-chain acyl-CoA synthetase 4 in formation of polyunsaturated lipid species in hepatic stellate cells

Maidina Tuohetahuntila[a], Bart Spee[b], Hedwig S. Kruitwagen[b], Richard Wubbolts[a], Jos F. Brouwers[a], Chris H. van de Lest[a], Martijn R. Molenaar[a], Martin Houweling[a], J. Bernd Helms[a], Arie B. Vaandrager[a]

[a] Department of Biochemistry and Cell Biology, Faculty of Veterinary Medicine & Institute of Biomembranes, Utrecht University, Yalelaan 2, 3584 CM Utrecht, The Netherlands

[b] Department of Clinical Sciences of Companion Animals, Faculty of Veterinary Medicine, Utrecht University, Yalelaan 104, 3584 CM Utrecht, The Netherlands

Chapter

2

ABSTRACT

Hepatic stellate cell (HSC) activation is a critical step in the development of chronic liver disease. We previously observed that the levels of triacylglycerol (TAG) species containing long polyunsaturated fatty acids (PUFAs) are increased in *in vitro* activated HSCs. Here we investigated the cause and consequences of the rise in PUFA-TAGs by profiling enzymes involved in PUFA incorporation. We report that acyl CoA synthetase (ACSL) type 4, which has a preference for PUFAs, is the only upregulated ACSL family member in activated HSCs. Inhibition of the activity of ACSL4 by siRNA-mediated knockdown or addition of rosiglitazone specifically inhibited the incorporation of deuterated arachidonic acid (AA-d8) into TAG in HSCs. In agreement with this, ACSL4 was found to be partially localized around lipid droplets (LDs) in HSCs. Inhibition of ACSL4 also prevented the large increase in PUFA-TAGs in HSCs upon activation and to a lesser extent the increase of arachidonate-containing phosphatidylcholine species. Inhibition of ACSL4 by rosiglitazone was associated with an inhibition of HSC activation and prostaglandin secretion. Our combined data show that upregulation of ACSL4 is responsible for the increase in PUFA-TAG species during activation of HSCs, which may serve to protect cells against a shortage of PUFAs required for eicosanoid secretion.

Keywords: prostaglandin, eicosanoid, phosphatidylcholine, lipidomics, heavy isotope labeling, arachidonic acid.

INTRODUCTION

Hepatic stellate cells (HSCs) are non-parenchymal cells which are located in the spaces of Disse, between the sinusoidal endothelial cells and the hepatocytes[1,2]. In a healthy liver, HSCs are involved in vitamin A (retinol) homeostasis as they are filled with large LDs containing retinylesters, together with triacylglycerols (TAGs) and cholesteryl esters. HSCs also play a role in the turnover of hepatic extracellular matrix (ECM) components such as collagen, glycoprotein and proteoglycan[3]. HSC proliferation and collagen synthesis are regulated by the 3D structure of the ECM[4]. Upon liver injury, quiescent HSCs can transdifferentiate into an activated myofibroblastic phenotype. Activated Kupffer cells may initiate this transition by secreting cytokines, such as transforming growth factor beta (TGF-β), which stimulate the synthesis of matrix proteins and the release of retinoids by HSCs[5]. Production of TGF-β by activated HSCs further stimulates the excess synthesis of ECM and results in liver fibrosis[6].

We previously reported that LD degradation in activated hepatic stellate cell is a highly dynamic and regulated process[7]. Upon activation of the hepatic stellate cells, the LDs reduce in size, but increase in number during the first 7 days in culture. The LDs migrate to cellular extensions in this first phase, before they disappear in a later phase. Raman and lipidomic studies showed that in the initial phase of HSC activation, the retinyl esters are disappearing more rapidly than the triacylglycerols. Interestingly, a large and specific increase in poly-unsaturated fatty acid (PUFA)-containing triacylglycerol species was observed during the first 7 days in culture, together with the decrease in retinyl esters[7]. The increase in PUFA-TAGs was caused by a large increase in the uptake of PUFAs from the medium as assessed from deuterium-labeled arachidonic acid uptake studies[7]. So far, the molecular mechanisms and identity of the enzymes involved in the lipid remodeling and breakdown of the LDs during HSC activation are unknown. In this study, we aim to identify lipid enzymes responsible for the accumulation of PUFA-TAG species in activated HSCs and their possible role in the activation or function of HSCs. Our initial targets were isoforms of the family of acyl-CoA synthetases (ACSLs). Members of this family are key enzymes in the synthesis of complex lipids like phospholipids (PLs), cholesterol esters and TAGs by converting free long-chain fatty acids into acyl-CoAs[8]. Furthermore, uptake of long chain fatty acids is tightly linked to CoA-esterification by acyl-CoA synthetases. Five isoforms of ACSL have been identified in mammals. The ACSL family members differ in their specificity for fatty acid species and in their tissue distributions. Among the ACSLs, ACSL4 is a peripheral membrane protein that was found to be selective for arachidonic acid (AA) and other longer chain polyunsaturated fatty acids and is highly expressed in adrenal gland, brain, ovary and testis[9].

The identification of the enzyme responsible for the increase in PUFA-TAGs will allow us to investigate the role of these lipids in the functioning of HSCs. Elevation of TAG-PUFA species may be

physiologically relevant as storage pools for AA, waiting to be incorporated in PLs. AA is also a precursor for eicosanoids, which are signaling lipids that play a role in a broad range of processes, such as modulation of inflammation and the immune system[10,11]. Eicosanoid synthesis typically starts with the release of AA from the sn-2 position of PLs by specific Ca^{2+}-dependent phospholipases in response to hormones/cytokines[12]. Subsequently AA is converted to various eicosanoids, like prostaglandins, thromboxanes or leukotrienes, depending on the relative activity of their respective synthases.

Here, we report that ACSL4 upregulation is critically involved in the increase in TAG-PUFA formation in activated HSCs, which may serve as a storage pool for eicosanoid production.

MATERIALS AND METHODS

Reagents

AA-d8 was purchased from Cayman Chemical (Ann Arbor, MI, USA). 15-deoxy-Δ12,14prostaglandin J2 (15-dPGJ2) was from Tocris Bioscience (United Kingdom). Dulbecco's modified Eagle medium (DMEM), fetal bovine serum (FBS), and penicillin/streptomycin were obtained from Gibco (Paisley, UK). Bovine Serum Albumin (BSA) fraction V was obtained from PAA (Pasching, Austria). Rosiglitazone was obtained from Enzo Life Sciences (Belgium). Collagenase (Clostridium histolyticum Type I) was obtained from Sigma-Aldrich (St. Louis, MO, USA). Anti-rabbit IgG ACSL4 antibody was from Santa Cruz Biotechnology (Santa Cruz, CA, USA). The antibody against alpha-smooth muscle actin (α-SMA) was from Thermo Scientific (Waltham, MA, USA), and mouse monoclonal anti-tubulin antibody from Sigma-Aldrich (St. Louis, MO, USA). Lipid droplet staining dye LD540 was kindly donated by Dr. C. Thiele, Bonn, Germany. Hoechst 33342 was obtained from Molecular Probes (Paisley, UK), paraformaldehyde (PF) (8%) was obtained from Electron Microscopy Sciences (Hatfield, PA, USA). FluorSave was obtained from Calbiochem (Billerica, MA, USA), all HPLC-MS solvents were from Biosolve (Valkenswaard, the Netherlands) with exception of chloroform (Carl Roth, Karlsruhe, Germany) and were of HPLC grade. Silica-G (0.063–0.200 mm) was purchased from Merck (Darmstadt, Germany).

Animals

Procedures of rat care and handling were in accordance with governmental and international guidelines on animal experimentation, and were approved by the Animal Experimentation Committee (Dierexperimentencommissie; DEC) of Utrecht University (DEC-numbers: 2010.III.09.110 and 2012. III.10.100).

Cell line

Human hepatic stellate cell line (LX-2) was kindly donated by Dr. Friedman (New York, NY, USA). LX-2 cells were cultured in DMEM medium supplemented with 10% FBS, 100 units/ml penicillin, and 100 μg/ml streptomycin and cells were maintained in a humidified 5% CO_2 incubator at 37 °C.

Rat HSC isolation and in vitro primary cell culture

Adult male Wistar rats (300–400 g) were used in all experiments. Stellate cells were isolated from rat liver by collagenase digestion followed by differential centrifugation[13]. After isolation, HSCs were plated in 24, 12 or 6 well plates at a density of 2×10^4, 5×10^4 or 1×10^5 cells/well, respectively. Cells were maintained in DMEM supplemented with 10% FBS, 100 units/ml penicillin, 100 μg/ml streptomycin and 4 μl/ml Fungizone and cells were maintained in a humidified 5% CO_2 incubator at 37 °C. Medium was changed every 3 days. Purity of the HSC preparation as determined by desmin staining was 80–90%.

Gene silencing of Acsl4

Gene-silencing experiments were performed using small interfering RNA (siRNA) for*Acsl4* or non-targeting siRNA as a control (ON-TARGETplus SMARTpool of 4 siRNAs, Thermo-Scientific, Rochester, NY, USA) according to the manufacturer's instructions. Briefly, two days after plating, the cells were treated with 40 nM siRNA using 5 μl/ml RNAiMAX (Invitrogen, Breda, the Netherlands) in antibiotic free complete media (with FBS). After 6 h of transfection, media was changed to standard culturing conditions up to day 7.

RNA isolation, cDNA synthesis and QPCR

Total RNA was isolated from rat HSCs grown in a 24-well plate using RNeasy Mini Kit (Qiagen, Venlo, the Netherlands) including the optional on-column DNase digestion (Qiagen RNase-free DNase kit). RNA was dissolved in 30 μl of RNase free water and was quantified spectrophotometerically using a Nanodrop ND-1000 (Isogen Life Science, IJsselstein, the Netherlands). An iScript cDNA Synthesis Kit (Bio-Rad, Veenendaal, the Netherlands) was used to synthesize cDNA. Primer design and qPCR conditions were as described previously[14]. Briefly, qPCR reactions were performed in duplicate using Bio-Rad detection system. Amplifications were carried out in a volume of 25 μl containing 12.5 μl of 2xSYBR green supermix (BioRad), 1 μl of forward and reverse primer and 1 μl cDNA. Cycling conditions were as follows: initial denaturation at 95 °C for 3-minute, followed by 45 cycles of denaturation (95 °C for 10 s), annealing temperature (see Supplementary Table S1) for 30 s, and elongation (72 °C for 30 s). A melting curve analysis was performed for every reaction. To determine relative expression of a gene, a 4-fold dilution series from a pool of all samples were used. IQ5 Real-Time PCR detection system software (BioRad) was used for data analysis. Expression levels were normalized by using the average relative amount of the housekeeping genes. Housekeeping genes used for normalization are, based on their stable expression in stellate cells,

namely, *tyrosine 3-monooxygenase/tryptophan 5-monooxygenase activation protein, zeta (Ywhaz),* *hypoxanthine phosphoribosyl transferase (Hprt),* and*hydroxylmethylbilane synthase (Hmbs)*. Primers for housekeeping genes and genes of interest are listed in Supplementary Table S1.

Western blot analysis

Cell homogenates were collected and equal amounts of proteins were heated to 95 °C for 5 min in loading buffer and then separated on 10% SDS-polyacrylamide gel and blotted onto polyvinylidene difluoride membranes (GE Healthcare Europe GmbH, Belgium). The membranes were incubated with 5% BSA in Tris-buffered saline (TBS) for 30 min at room temperature. The incubation of the primary antibody was performed at 4 °C overnight for all antibodies (see Supplementary Table S2) in TBS with 0.1% Tween-20 (Boom B.V., Meppel, the Netherlands) and 1% BSA. After washing, membranes were incubated with horseradish peroxidase-conjugated secondary antibody (Nordic Immunology, the Netherlands) at room temperature for 1 h. Blots were detected by ECL kit (Supersignal West Pico; Pierce, Rockford, IL). Blots were then stripped in stripping buffer containing 100 mM 2-mercaptoethanol, 2% (w/v) SDS, 62.5 mM Tris–HCl (pH 6.7) and then probed with anti-tubulin antibody for protein content normalization. Imaging was performed on a ChemiDoc XRS System (BioRad). Western blot was performed in at least three different experiments, and representative blots are shown.

Immunofluorescence

Freshly isolated HSCs were grown on glass coverslips in 24 well plate untill day 1 or day 7 at 37 °C. In parallel, HSCs transfected at day 2 in culture with siRNAs targeted against*Acsl4* were grown until day 7 at 37 °C. Staining of cells was performed as follows: cells were fixed in 4% (v/v) PF at room temperature for 30 min and stored in 1% (v/v) PF at 4 °C for a maximum of 1 week. HSCs were washed twice in PBS, permeabilized (0.1% (w/v) saponin (PBS-S; Riedel-de Haën, Seelze, Germany)) and blocked with 2% BSA for 1 h at room temperature. After blocking, slides were incubated 1 h with the primary antibody against ACSL4 (4 µg/ml), washed again, and incubated for 1 h with anti-rabbit antibody (15 µg/ml) supplemented with Hoechst (4 µg/ml) for nuclear counterstaining and lipid droplet dye LD540 (0.05 µg/ml). Thereafter, coverslips were mounted with FluorSave on microscopic slides and Image acquisition was performed at the Center of Cellular Imaging, Faculty of Veterinary Medicine, Utrecht University, on a Leica TCS SPE-II confocal microscope. Images were adjusted in ImageJ (freeware available at www.download-imagej.com).

Analysis of neutral and phospholipids by HPLC-MS

Lipids were extracted from a total cell homogenate of HSCs grown in a 12-well plate by the method of Bligh and Dyer[15]. Extracted lipids were separated in a neutral and phospholipid fraction by fractionation on a freshly prepared silica-G column (approximately 10 mg of 0.063–0.200 mm silica)[16]. Lipid extracts were dissolved in methanol/chloroform (1/9, v/v) and loaded on top of

the silica column. Neutral lipids were eluted with two volumes acetone, dried under nitrogen gas and stored at − 20 °C. Just before HPLC-MS analysis, the neutral lipid fraction was reconstituted in methanol/chloroform (1/1, v/v) and separated on a Kinetex/HALO C8-e column (2.6 µm, 150 × 3.00 mm; Phenomenex, the Netherlands). A gradient was generated from methanol/H_2O (5/5, v/v) and methanol/isopropanol (8/2, v/v) at a constant flow rate of 0.3 ml/min. Mass spectrometry of neutral lipids (TAGs and cholesterol) was performed using Atmospheric Pressure Chemical Ionization (APCI) interface (AB Sciex Instruments, Toronto, ON, Canada) on a Biosystems API-2000 Q-trap. The system was controled by Analyst version 1.4.2 software (MDS Sciex, Concord, ON, Canada) and operated in positive ion mode using settings described in[7]. Absolute quantitation of all the TAG species was hampered by their sheer numbers (> 1000) and the differential fragmentation of the various TAG species during ionization into DAG and MAG ions. The fragmentation depended on the saturation of the acyl chains, as almost no intact TAG ions were observed from TAGs with less than 2 double bonds, whereas some more unsaturated TAG species fragmented less than 40%. On average 40–50% of PUFA-containing TAGs were observed as intact ions. The fragmentation of specific TAG species was very reproducible between different samples, therefore we generally performed a relative quantitation of a number of abundant and representative TAG species. Typical TAG species quantitated were: non PUFA, 52:3 (m/z 859) and 54:3 (m/z 885); 1xPUFA, 56:5 (m/z 909) and 58:6 (m/z 935); 2xPUFA, 60:9 (m/z 957) and 62:11 (m/z 981). For the experiments with AA-d8 typical TAG species were: 1xPUFA-d8, 54:4 (m/z 881, 889), 56:5 (m/z 909, 917), 56:6 (m/z 907, 915), and 56:7 (m/z 905, 913); 2xPUFA-d8, 56:8 (m/z 903, 911, 919), 58:8 (m/z 931, 939, 947), 60:9 (m/z 957, 965, 973), and 3xPUFA, 60:12 (m/z 951, 959, 967, 975), and 62:12 (m/z 979, 987, 995, 1003). The quantitated TAG species were normalized to the amount of cholesterol in the same sample. Cholesterol was found to be a good marker for both recovery and cellular material, as the cholesterol/protein ratio was found to be constant during HSC culture. The phospholipid fraction was also dissolved in methanol/chloroform (1/1, v/v) and separated on a Kinetex/HALO C18-e column (2.6 µm, 150 × 3.00 mm; Phenomenex, the Netherlands).A gradient was generated from acetonitril/methanol/H_2O (6/9/5, v/v) and acetone/methanol (4/6, v/v) at a constant flow rate of 0.6 ml/min. Mass spectrometry ofphosphatidylcholine (PC) was performed using electrospray ionization (ESI) on a Biosystems API-2000 Q-trap. The system was controled by Analyst version 1.4.2 software (MDS Sciex, Concord, ON, Canada) and operated in positive mode, precursor scan of 184 m/z, using settings described in[7].

Analysis of fatty acid constitution of neutral lipids and phospholipids

Total lipids from 400 µl of HSC homogenate were extracted using the method of Bligh and Dyer[15]. Internal standard (200 pmol of tripentadecanoylglycerol) was added to each sample prior to extraction to calculate absolute concentrations and the recovery. Subsequently, lipids were separated into a neutral and a phospholipid fraction according to[16] described as above on a silica-G column. Fractions were hydrolyzed at 75 °C for 1 h with 1 ml of MeOH:3 M NaOH (9:1, v/v) The

released free fatty acids were obtained with extraction with hexane after subsequent acidification of the methanol phase according to[17], and evaporated under nitrogen and stored at − 20 °C until analyzed. Mass spectrometry of free fatty acids was performed according to[18]. The system was controled by Analyst version 1.4.2 software (MDS Sciex, Concord, ON, Canada) and operated in negative mode in the m/z range from 225–400 amu. Calibration curves were generated using authentic standards to correct for differences in response factors. Data were expressed relative to the protein content of the homogenates as determined by the BCA method Pierce® BCA protein assay kit (Thermo scientific, Rockford, IL, USA) with BSA as standard.

Analysis of prostaglandins using mass spectrometry

DMEM containing 0.5% FBS with or without 10 µM Ca^{2+} ionophore A23187 was added to the HSCs 1 h before harvesting to reduce the background levels of eicosanoids present in serum. Eicosanoids were extracted and analyzed as described elsewhere with slight modifications[19]. Briefly, samples were recovered in a total volume of 1 ml of 15% (v/v) methanol + 0.5% glacial acetic acid in the presence of 10 pmol dimethyl-PGF2α that served as an internal standard. Samples were separated on on C18 solid-phase extraction columns. The eicosanoids were eluted with 2×0.35 ml ethyl acetate and evaporated to dryness under nitrogen. Evaporated samples were reconstituted with 50 µl of 50% ethanol and subject to HPLC–MS analysis. Multiple reaction monitoring (MRM) was used as described in[19].

Statistical analysis

Values for all measurements are expressed as mean ± SD. Each experiment was performed in duplicate and repeated at least three times. Comparisons between two groups were made with paired Student's t test. Differences were considered statistically significant if the P value was less than 0.05.

RESULTS

Specific incorporation of arachidonic acid into triacylglycerol

When hepatic stellate cells (HSCs) become activated in culture, their levels of polyunsaturated triacylglycerol species (PUFA-TAGs) increase 4–5 fold, whereas the amounts of PUFA-containing PL species are not altered under the same conditions[7]. To investigate whether this difference in PUFA accumulation between TAGs and PLs is caused by differential incorporation of exogenously added PUFAs, both quiescent (day 1) and activated (day 7) HSCs were incubated with 25 µM AA-d8 for 24 h. As shown in Fig. 1A, AA-d8 incorporation into TAGs was more than five times higher in activated HSCs compared to quiescent cells, in line with the previously reported increase in TAG-PUFA levels. In contrast, the overall AA-d8 incorporation into PC was already relatively high at
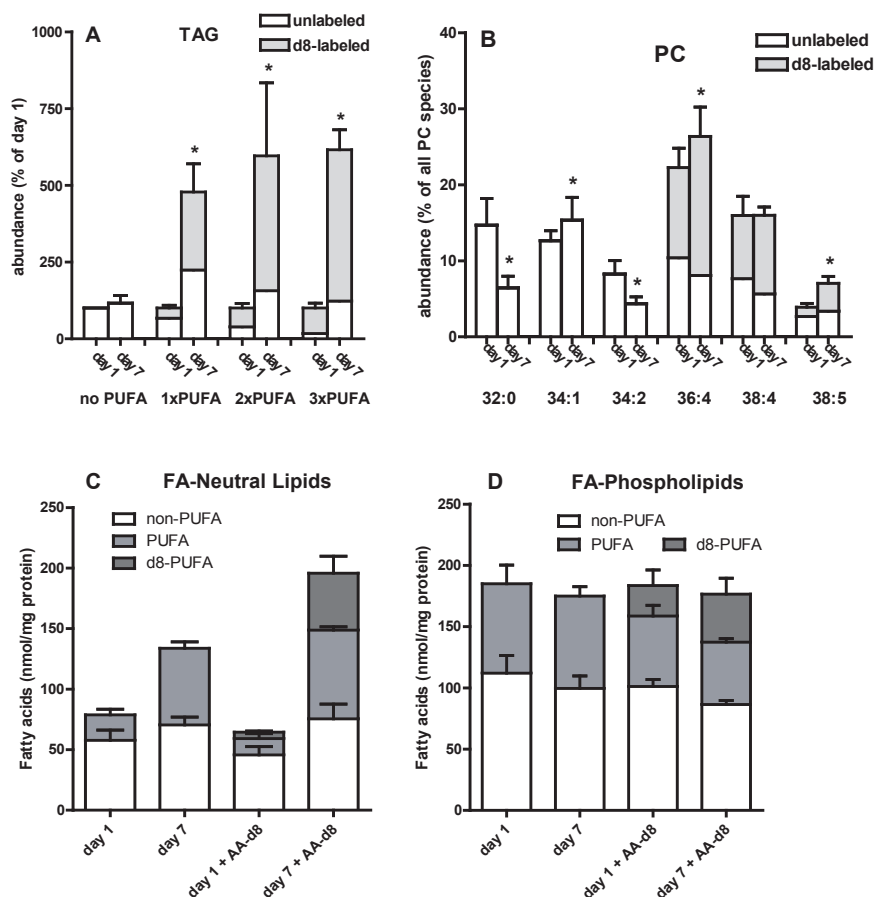
Fig. 1. Incorporation of arachidonic acid in activated HSCs. Freshly isolated HSCs were cultured for 1 or 7 days and additionally incubated for 24 h with 25 µM of AA-*d*8 in medium with 10% FBS at 37 °C. Subsequently, neutral lipids and phospholipids were extracted and analyzed. A. Several representative TAG species with no, 1, 2, or 3 PUFA chains were quantified and unlabeled (white bars) and deuterium labeled variants (gray bars) of the same species were added. Values were normalized to the amount of cholesterol in the sample and expressed relative to the level of the respective TAG species present at day 1. B. The most abundant PC species were quantified, and unlabeled (white bars) and deuterium labeled variants (gray bars) of the same species were added. Values are expressed relative to the total amount of PC in a sample (which did not differ significantly between day 1 and day 7, when normalized to the amount of protein). Data are the means ± SD of 3 experiments performed in duplicate. *P < 0.05. C and D. Freshly isolated HSCs were cultured for 1 or 7 days and additionally incubated for 24 h without or with 25 µM of AA-*d*8 in medium with 10% FBS at 37 °C. Subsequently, lipids were extracted, separated into a neutral (C) and a phospholipid (D) fraction, and hydrolyzed. The released fatty acids were analyzed with HPLC-MS. PUFAs are defined as fatty acids with 20 or more C atoms and 3 or more double bonds. Data are the means ± SD of 2 experiments performed in duplicate.

CHAPTER 2

day 1 and increased only modestly (less than 50%; Fig. 1B) in activated HSCs. This modest increase in deuterium-labeled PUFA PC was partly compensated by a decrease in non-labeled PUFA-PC resulting in overall small changes in PUFA-PC content during the 24 h incubation. These results corroborate that the increase in incorporation of PUFAs in activated HSCs is relatively specific for TAGs.

An exact determination of the contribution of the PUFA-TAG species to the total amount of TAG by the APCI-MS method is hampered by the numerous species (> 1000) and the observation that the various TAG species fragment to a different degree depending on the saturation of their acyl chains as discussed in Section 2.9. Nevertheless, quantitation of a large number of intact and fragmented TAG ions resulted in a conservative estimate that HSCs at day 1 have 15–20% TAGs with one PUFA, 3–5% with two PUFAs, and < 1% with three PUFAs. At day 7 these percentages increased to 30–40%, 20–30% and 6–10%, respectively. To alternatively determine the amount of PUFAs in the neutral lipid fraction, we hydrolyzed the neutral lipids and analyzed the fatty acids released. As shown in Fig. 1C and Supplementary Table S3, the percentage of PUFAs (defined as more than 20 C atoms and 3 double bonds) in HSCs increased from 25% to almost 50% after activation. The addition of 25 µM AA-d8 caused an even larger incorporation of PUFAs, resulting in the majority of the fatty acids in neutral lipids being a PUFA (Fig. 1C, Supplementary Table S3). The total amount of PUFAs in neutral lipids at day 7 (60–70 nmol/mg protein) was almost similar to the total amount of PUFAs in the phospholipid fraction (75–80 nmol/mg protein; Fig. 1D, Supplementary Table S4). Fig. 1D also shows that the amount of PUFAs in the phospholipid fraction did not change upon activation of the HSCs, and that the addition of 25 µM AA-d8 rather caused a replacement of part of the PUFAs by labeled PUFAs, than a net increase in PL-PUFAs, similar as observed for PC (Fig. 1B).

ACSL4 is upregulated in activated HSCs

Uptake and incorporation of long-chain fatty acids is tightly linked to their CoA-esterification[8]. Therefore, to identify key enzymes involved in the enhanced formation of TAG-PUFA species in activated HSCs, we analyzed the expression of various acyl-CoA synthetases (ACSLs). As shown in Fig. 2A, the relative gene expression of all *Acsl* isoforms is downregulated two-fold or approximately two-fold. This implies that *Acsl4* is enriched more than four-fold in relation to the other ACSL family members in activated HSCs when compared to quiescent HSCs. The increase in *Acsl4* mRNA was closely mirrored by the two-fold increase in ACSL4 protein as assessed by western blots (Fig. 2B). We next examined the subcellular localization of ACSL4 in activated and quiescent HSCs. In agreement with its involvement in TAG formation and remodeling, ACSL4 partially localizes around LDs in both quiescent and activated HSCs (Fig. 2C). The ACSL4 staining around the LDs was specific, since it was no longer observed after transfection with *Acsl4*-targeting siRNAs (Fig. 2C).
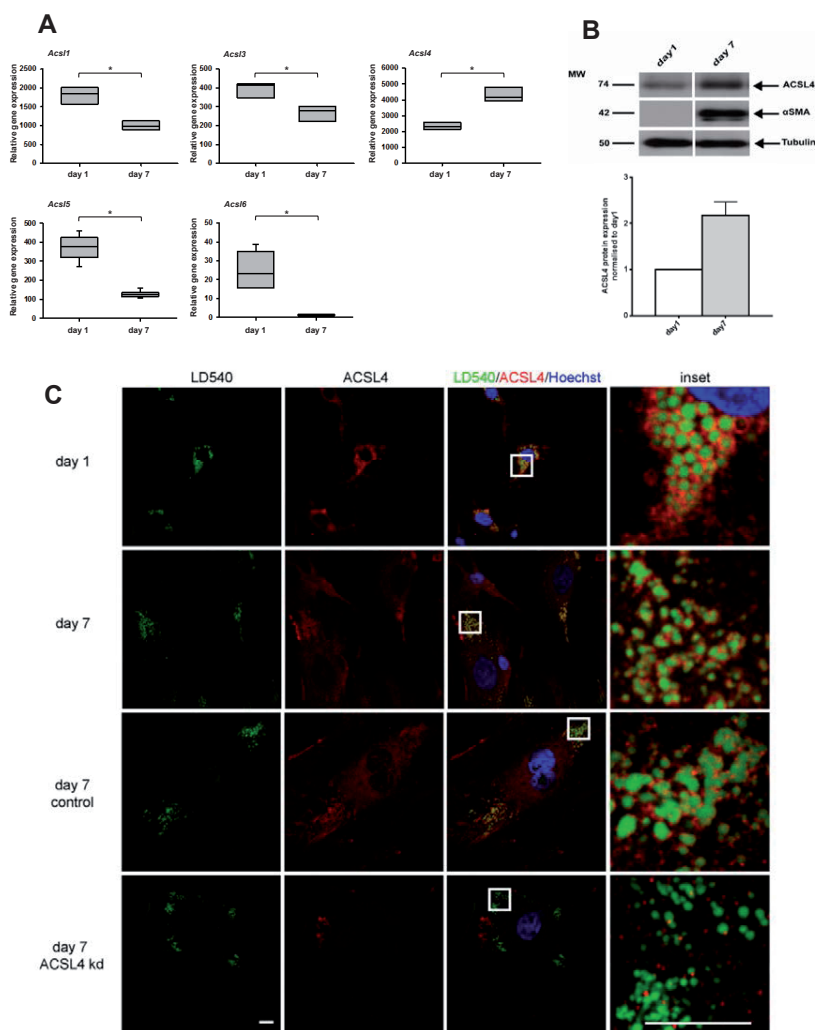
CHAPTER 2

Fig. 2. ACSL4 upregulation in activated HSCs. A. Relative mRNA expression of ACSL isoforms in quiescent (day 1) and activated (day 7) rat HSCs by qPCR. The box plot depicts the median and lower and upper quartile (n = 3). Significant changes are marked by asterisks (P < 0.05). B. Protein expression was measured for ACSL4 in quiescent (day 1) and activated (day 7) rat HSCs by western blotting. αSMA was used as a positive control for HSC activation. Tubulin was used as a loading control. Shown is a representative blot and quantitation by densitometry of the ASCL4 band. Data are the means ± SD of 3 experiments C. Confocal images of ACSL4. Quiescent HSC (day 1) and activated HSC (day 7) lipid droplets were stained with LD540 dye (green), anti ACSL4 antibody (red) and nuclei were stained with Hoechst (blue). Colocalization of LDs with ACSL4 is shown in inset panel. Lower two panels: HSCs were transfected on day 2 with non-targeting siRNA or Acsl4 siRNA and at day 7 stained as above. Images shown are representative for at least 3 independent experiments. Scalebars represent 10 μm.

ACSL4 is involved in enhanced formation of PUFA-TAGs

Because ACSL4 is relatively specific for PUFAs[8] and it localizes to LDs, ACSL4 is a good candidate to mediate the increase in PUFA-TAG species in activated HSCs. To test this hypothesis, HSCs were transfected at day 2 in culture with siRNAs targeted against *Acsl4* and analyzed at day 7. Compared to non-targeting siRNA control, knockdown up to 70% with *Acsl4* siRNA was achieved on mRNA level and to 80–90% on the protein level (Fig. 3A). In order to ascertain whether ACSL4 knockdown impaired incorporation of PUFAs in TAG, the siRNA-treated HSCs were incubated for 24 h with 25 µM AA-d8 and lipids were extracted and analyzed using HPLC-MS. As shown in Fig. 3B,
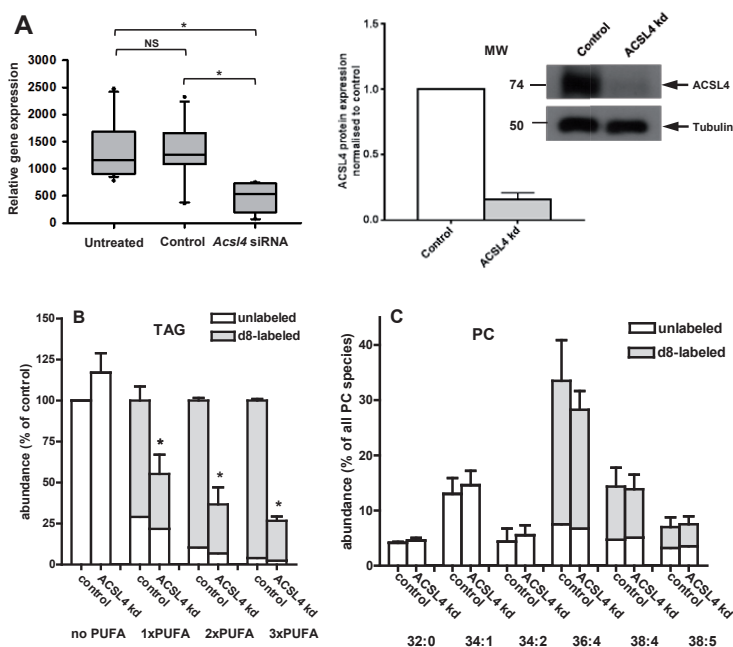

Fig. 3. Acsl4 gene silencing reduces the incorporation of arachidonic acid into TAG. A. relative mRNA expression (left panel) and protein (right panel) of Acsl4 in HSCs 5 days after transfection with non-targeting (control) or Acsl4 siRNA on day 2. Untreated sample represents untransfected HSCs cultured until day 7. NS, not significant. Significant changes are marked by asterisks (P < 0.05). Insert shows representative western blot. B, C. Isolated HSCs were transfected at day 2, and on day 6 incubated with 25 µM AA-d8 for 24 h. Cells were harvested on day 7. Subsequently, neutral lipids and phospholipids were extracted and HPLC-MS was performed as described. B. Several representative TAG species with no, 1, 2, or 3 PUFA chains were quantified and unlabeled (white bars) and deuterium labeled variants (gray bars) of the same species were added. Values were normalized to the amount of cholesterol in the sample and expressed relative to the level of the respective TAG species present in the non-targeting (control) cells. C. The most abundant PC species were quantified, and unlabeled (white bars) and deuterium labeled variants (gray bars) of the same species were added. Values are expressed relative to the total amount of PC in a sample (which did not differ significantly between non-targeting and Acsl4 siRNA transfected cells). Data are the means ± SD of 3 experiments performed in duplicate. *P < 0.05 paired t-test.

ACSL4 knockdown inhibited the incorporation of labeled AA into TAG. Especially the incorporation of two and three exogenous PUFA chains within the same TAG-species (2× and 3 × PUFAs) was strongly inhibited. In contrast, ACSL4 knockdown had little effects on the incorporation of exogenous AA into PC (see Fig. 3C), or into phosphatidylserine and phosphatidylinositol (data not shown).

To further examine the specific involvement of ACSL4 in PUFA metabolism in activated HSCs, cells were treated with rosiglitazone, a pharmacological drug well known for its ability to inhibit ACSL4 activity[20] and[21]. Initially, this inhibition was evaluated by determining the effect of rosiglitazone on the incorporation of exogenous AA-d8 into TAG species in the human stellate cell line LX-2. Rosiglitazone inhibited the incorporation of AA-d8 in the LX-2 cells with an IC_{50} of approximately 30 μM, and near maximal inhibition was reached at a concentration of 100 μM (results not shown).
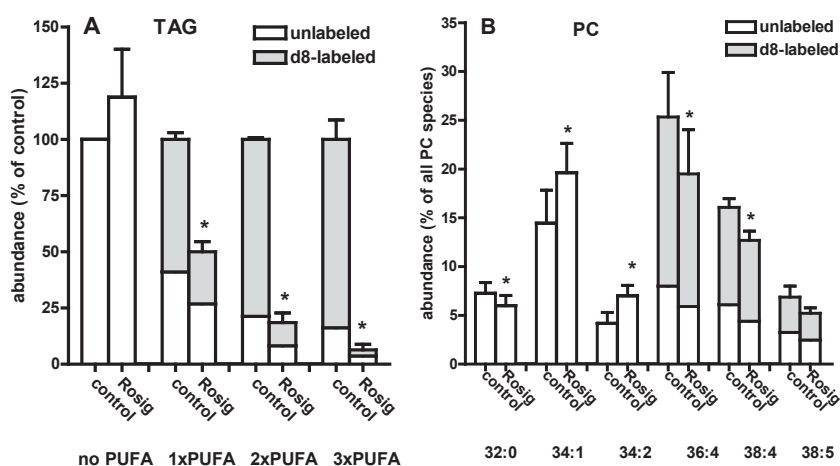

Fig. 4. Rosiglitazone inhibits arachidonic acid incorporation into TAG. Freshly isolated HSCs were cultured for 6 days. Subsequently the cells were incubated for 24 h with 25 μM AA-d8 in the absence (control) or presence of rosiglitazone (Rosig) (100 μM). Cells were harvested on day 7. Subsequently, neutral lipids and phospholipids were extracted and HPLC-MS was performed as described. A. Several representative TAG species with no, 1, 2, or 3 PUFA chains were quantified and unlabeled (white bars) and deuterium labeled variants (gray bars) of the same species were added. Values were normalized to the amount of cholesterol in the sample and expressed relative to the level of the respective TAG species present in the control cells. B. The most abundant PC species were quantified, and unlabeled (white bars) and deuterium labeled variants (gray bars) of the same species were added. Values are expressed relative to the total amount of PC in a sample. Data are the means ± SD of 3 experiments performed in duplicate. *P < 0.05 paired t-test. Rosiglitazone (Rosig) was added from a 25 mM stock in DMSO to final concentration of 100 μM (0.4% DMSO). In control experiments, the equivalent volume of DMSO was added.

Subsequently a concentration of 100 µM rosiglitazone was used to determine its effect on AA-d8 incorporation in activated rat HSCs. As shown in Fig. 4A, in activated rat HSCs incorporation of two and three exogenous PUFA chains within the same TAG-species (2 × and 3 × PUFAs) was inhibited by more than 80% by rosiglitazone. The incorporation of only one PUFA into TAG was inhibited to a somewhat lesser degree, and incorporation of exogenous AA into PC was inhibited only marginally by pharmacological inhibition of ACSL4 (see Fig. 4).

Dose response curve for the incorporation of exogenous AA into TAG and PC

We observed that in activated HSCs, the increased incorporation of PUFAs is relatively specific for TAG (Fig. 1) and that likewise, the inhibition of ACSL4 activity either by siRNA-mediated gene silencing or by rosiglitazone addition, affected the incorporation of AA into TAG to a larger extent than the incorporation of this PUFA into PC (Fig. 3 and Fig. 4). We questioned the reason for this differential incorporation since PUFA-CoA, the product of ACSL4, is the substrate for both PUFA-PC and PUFA-TAG synthesis. We investigated the possibility that the enzymes involved in
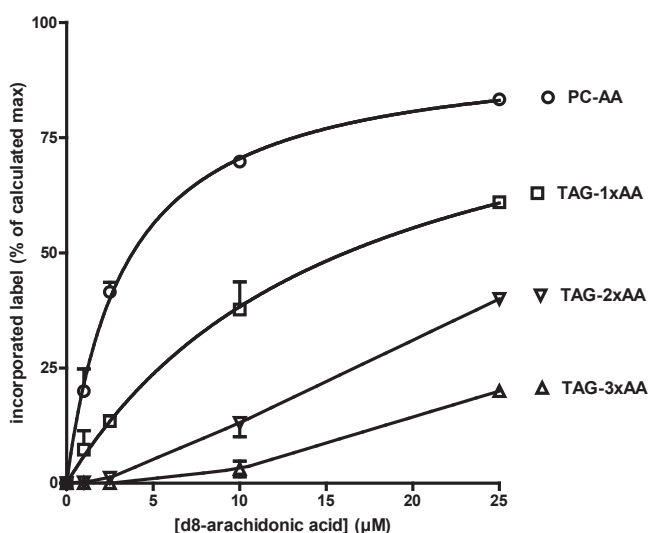

Fig. 5. Kinetics of arachidonic acid incorporated into PC and TAG. Freshly isolated HSCs were cultured for 7 days and additionally incubated with increasing concentrations of AA-d8 for another 3 h at 37 °C. Subsequently, lipids were extracted and HPLC-MS was performed as described. The d8-label in various representative TAG species with 1, 2 and 3 PUFAs (respectively TAG-1xAA, -2xAA, and -3xAA), and in the PC species 36:4, 38:4 and 38:5 (PC-AA) were quantified and summed. Data were fitted to one-site binding model (Michaelis–Menten plot) and the calculated Vmax was set as 100% in case of PC-AA and TAG-1xAA. TAG-2xAA and -3xAA data could not be fitted and were expressed relative to an arbitrary value. Data are the means ± SD of 3 experiments performed in duplicate.

the final step of PUFA-TAG and PUFA-PC synthesis have different affinities for PUFA-CoA. To probe the affinities of these enzymes we performed dose–response curves with exogenous AA-d8 at a relatively short incubation time during which the incorporation was linear with time. As shown in Fig. 5, AA-d8 was incorporated into PC and TAG species containing one molecule of AA-d8 with saturation kinetics fitting to a one binding site Michaelis–Menten model. The exogenous AA concentration at which half-maximal incorporation was observed was 4-fold higher for TAG as compared to PC (approx. 16 μM and 4 μM, respectively). In contrast, the incorporation of multiple AAs into one TAG molecule did not show saturation kinetics (within the concentration range studied), but increased with increasing exogenous AA concentrations. The different dose response curves show that different affinities of the final PC and TAG synthesizing enzymes for PUFAs are a possible explanation for the different responses of TAG and PC species profiles to changes in ACSL4 activity.

Effect of ACSL4 inhibition on HSC lipid composition

To examine whether ACSL4 plays a role in the overall lipid composition of HSCs activated in culture, we analyzed the endogenous TAG and PC species distribution after siRNA-mediated gene silencing of *Acsl4* or after inhibition of ACSL4 for 6 days with rosiglitazone. As shown in Fig. 6, the levels of the TAG-PUFAs were significantly lower in HSCs after the knock down of ACSL4 (see Fig. 6A). The levels of PC-species containing a PUFA were also reduced, but to a much lesser extent (Fig. 6B). The knock down of ACSL4 significantly decreased the ratio of PUFA-PC species to PC species without a PUFA from 1.40 ± 0.35 to 0.85 ± 0.30 (n = 3; P < 0.01 in paired *t*-test). We next questioned whether inhibition of ACSL4 by rosiglitazone would lead to a similar difference in lipid profile in HSCs cultured for 7 days. As shown in Figs. 6C and D, addition of 100 μM rosiglitazone to isolated HSCs at day 1 changed the TAG-PUFA and PC-PUFA levels measured at day 7, causing more than 80% lower levels of PUFA-TAG species when compared to control. Rosiglitazone incubation also lowered the PUFA content of PC by approximately 50% (Fig. 6D). These experiments also show that prolonged inhibition of ACSL4 in the presence of relatively low levels of non-esterified AA (approx. 1–2 μM) present in medium with 10% FBS also affects the levels of PC species containing AA, besides that of PUFA-TAGs. Thus, depending on the experimental conditions (high or low concentrations AA-d8), rosiglitazone had respectively little (Figs. 3B and 4B) or more substantial (Fig. 6D) effect on the incorporation of AA into PC.
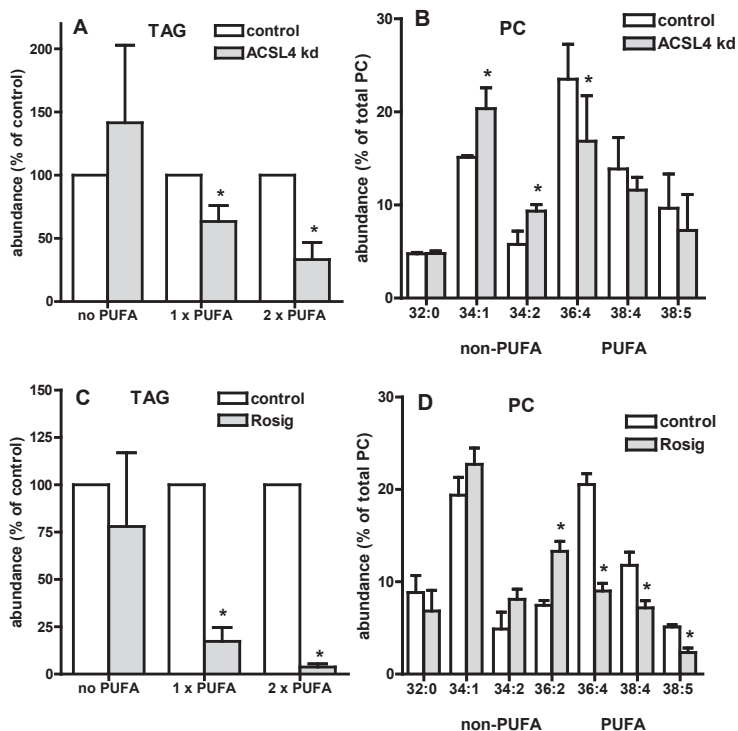
CHAPTER 2

Fig. 6. The effect of ACSL4 inhibition on endogenous lipids in activated HSCs. A,B. Freshly isolated HSCs were transfected with non-targeting (control) targetingor Acsl4 siRNA at day 2 and cultured until day 7, or C,D isolated HSCs were incubated in the absence (control) or presence of rosiglitazone (Rosig) (100 µM) at day 1 and cultured in the continued presence of these substances until day 7. Subsequently, neutral lipids and phospholipids were extracted and HPLC-MS was performed as described. A,C. Several representative TAG species with no, 1, or 2 PUFA chains were quantified and normalized to the amount of cholesterol in the sample. Values and expressed relative to the level of the respective TAG species present in the non-targeting (control) cells (A), or control (C). B, D. The most abundant PC species were quantified and expressed relative to the total amount of PC in a sample. Data are the means ± SD of 3 experiments performed in duplicate. *P < 0.05 paired t-test. Rosiglitazone (Rosig) was added from a 25 mM stock in DMSO to final concentration of 100 µM. In control experiments, the equivalent volume of DMSO was added.

Effect of ACSL4 inhibition on HSC activation

To investigate the role of the increased ACSL4 expression and the increase in PUFA-TAGs on HSC function, we determined the cellular morphology and levels of alpha-smooth muscle actin (αSMA) after knockdown of ACSL4 or pharmacological inhibition. αSMA is considered a marker for HSC activation[22] and was clearly upregulated in the HSCs after 7 days under our culture conditions (Fig. 2B). Treatment of HSCs with siRNA targeted against Acsl4 on day 2 after plating did not cause a significantly different expression of αSMA mRNA (88 ± 18% compared to non-targeting siRNA

(control) transfected; n = 4; non-significant), and no difference in cellular morphology was noted (Figs. 2C and D). However, the transfection with non-targeting siRNA already increased αSMA levels more than two-fold when compared to non-transfected cells, suggesting that the transfection procedure stimulated the activation process, and potentially masked an inhibitory role of ACSL4 knock down. Therefore the effect of rosiglitazone was also assessed on αSMA expression. As shown in Fig. 7, rosiglitazone inhibited αSMA expression in cultured HSC at concentrations that were in a similar range as required for ACSL4 inhibition (IC_{50} = approx. 100 μM). The relatively high concentration of rosiglitazone required to inhibit HSC activation makes it unlikely that PPAR-γ is involved, since rosiglitazone activates this transcription factor at much lower concentrations (≤ 10 μM; [23]). However, rosiglitazone is also known to activate an unknown (PPAR-γ independent) mechanism at concentrations around 100 μM[24]. This latter mechanism can be targeted with 15-dPGJ$_2$[24]. We therefore compared the inhibitory effects of different concentrations of rosiglitazone and 15-dPGJ$_2$ on αSMA expression with their effects on ACSL4 activity. Since 15-dPGJ$_2$ inhibited αSMA expression without affecting ACSL4 activity (Fig. 7), we cannot exclude the possibility that
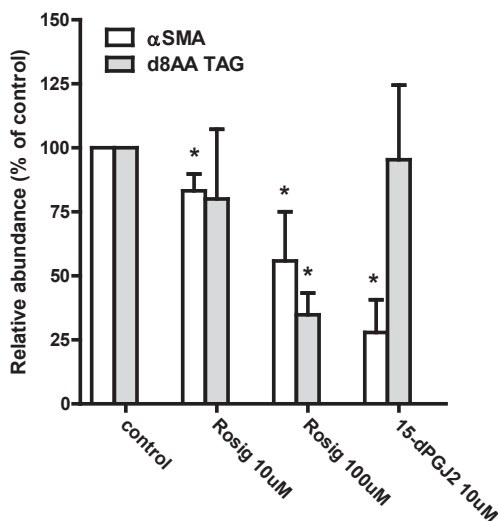

Fig. 7. Effects of rosiglitazone and 15-dPGJ2 on HSC activation and AA incorporation into TAGs. Freshly isolated HSCs were incubated in the absence (control) or presence of rosiglitazone (Rosig) (10 or 100 μM) or 15-deoxy-Δ12,14 prostaglandin J2 (15-dPGJ2; 10 μM) at day 1 and cultured until day 7. Relative gene expression of αSMA (HSC activation marker) was measured by qPCR. In parallel, the incorporation of AA-d8 into TAG was determined by incubation for 24 h with 25 μM AA-d8, similar to Fig. 5. The incorporated d8 label into several representative TAG species with 1, 2 or 3 PUFAs were added. Values are expressed relative to the levels in the control cells and are the means ± SD of 3 experiments. Rosiglitazone or 15-dPGJ2 were added from a 25 mM stock in DMSO to final concentration of 100 μM. In control experiments, the equivalent volume of DMSO was added. *P < 0.05 t-test treatment vs control.
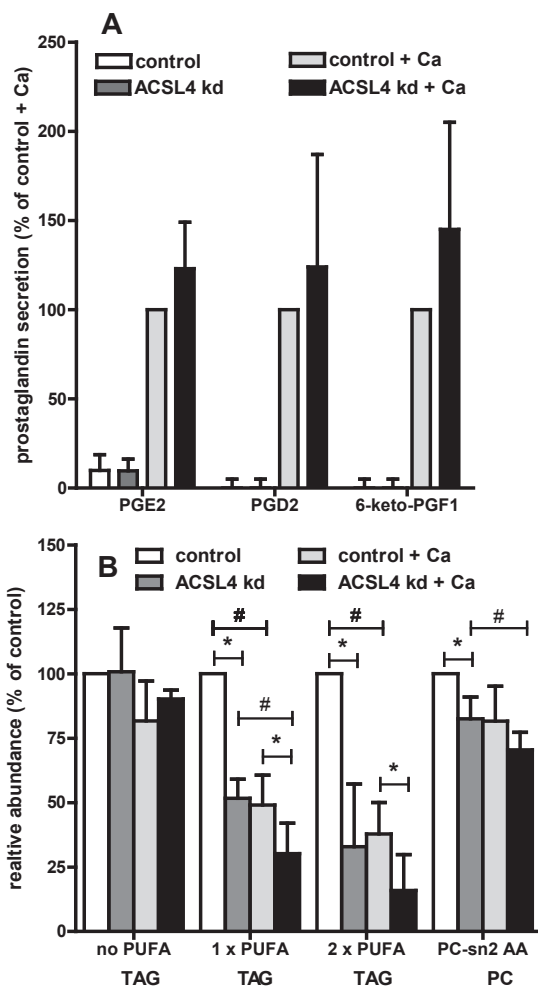
Fig. 8. Effect of Acsl4 gene silencing on prostaglandin secretion by HSCs. Freshly isolated HSCs were transfected with non-targeting (control) or Acsl4 siRNA at day 2 and cultured until day 7. Subsequently the cells were incubated for 1 h with DMEM containing 0.5% FBS either with or without 10 μM of the Ca2 +ionophore A23187. Upper panel: Prostaglandins secreted for 1 h into the low FBS medium were expressed relative to the level secreted by non-targeting (control) cells in the presence of Ca2 + ionophore. Lower panel: neutral lipids and phospholipids were extracted and HPLC-MS was performed as described. PC-sn2 AA is the sum of the PC species 36:4, 38:4, and 38:5. Values are expressed relative to the level of lipid present in non-targeting siRNA (control) transfected cells in the absence of Ca2 + ionophore. Data are the means of 3 experiments performed in duplicate. Data are the means ± SD of 3 experiments. Lower panel, *P < 0.05 paired t-test, ASCL4 kd vs control, #P < 0.05 paired t-test, Ca2 + ionophore vs no Ca2 + ionophore.

rosiglitazone (partly) inhibits HSC activation by another mechanism, independent of its effect on PUFA-TAG formation.

Effect of ACSL4 inhibition on eicosanoid secretion by HSCs

TAG-PUFAs may play a role in the AA/eicosanoid metabolism[10,11], and ACSL4 was suggested to increase eicosanoid synthesis in tumor cells[20]. We therefore studied the effect of ACSL4 knock down on eicosanoid secretion by activated HSCs. A major eicosanoid detected in the medium of HSCs at day 7 was prostaglandin E_2 (PGE_2). However no difference in the basal PGE_2 secretion between non-targeting and *Acsl4* siRNA transfected HSCs was observed (Fig. 8). Stimulation of Ca^{2+} dependent isoforms of phospholipase A_2 by incubation with a Ca^{2+} ionophore A23187 resulted in a more than 10-fold increase in PGE_2 release by the activated HSCs. As shown in Fig. 8, the secretion of PGE_2 and other prostaglandins was not significantly affected by knock down of ACSL4. We observed also detectable levels of thromboxane B_2 and the hydroxyeicosatetraenoic acids (HETEs), 11-HETE and 15-HETE in the medium of the Ca-ionophore stimulated HSCs, which did also not differ after knock down of ACSL4 (results not shown). To determine whether the eicosanoids after the Ca^{2+} stimulus were derived from the PC and/or the PUFA-TAG pool, we performed lipidomic analyses on the HSCs after incubation with and without the Ca^{2+} ionophore. As shown in Fig. 8, stimulation of phospholipase A_2 activity with Ca^{2+} ionophore caused a relatively strong decrease in TAG-PUFA species, that was larger than the decrease in the PC-AA pool in both non-targeting siRNA transfected cells and in HSCs treated with *Acsl4* siRNA. We could estimate from Fig. 8 and Supplementary Tables 3 and 4, that the observed 50–60% loss in PUFA-TAGs would result in the release of 9–12 nmol of AA/mg protein, whereas a loss of 15–20% of AA-containing phospholipids would release 6–9 nmol of AA/mg protein.

This suggests that PUFAs from the TAG pool are used to replenish the PC-PUFA pool after the stimulation of phospholipase A_2. In that case, prostaglandin secretion will only be affected in HSCs containing no or very low levels of TAG-PUFAs. Therefore, HSCs were pre-incubated for 6 days with 100 µM rosiglitazone, resulting in very low levels of TAG-PUFAs (< 20% of control) and 50% of PC-AA (Figs. 6C and D). Under these conditions, Ca^{2+} induced secretion (for 1 h in the absence of rosiglitazone) of PGE_2, PGD_2 and 6-keto-PGF_1-alpha was significantly inhibited by 72 ± 21%, 82 ± 15%, and 69 ± 20%, respectively (n = 3).

DISCUSSION

In this paper, we report that ACSL4 is a key enzyme involved in the increase in PUFA-TAGs in activated rat HSCs. This conclusion is based on the observations that ACSL4, which has a preference for PUFAs[8], i) is the only isoform of the ACSL family which is upregulated in activated HSCs,

whereas the other isoforms are downregulated, ii) ACSL4 localizes around LDs, and, most importantly, iii) siRNA-mediated gene silencing of *Acsl4* or inhibition of ACSL4 activity by rosiglitazone considerably reduces the amounts of PUFA-TAG species.

Because the different ACSL isoforms have different preferences for fatty acids[8,9], the change in ACSL isoform profile during HSC activation will affect the species profile of the newly formed acyl-CoA pool. In activated HSCs this new acyl-CoA pool will be dominated by PUFA-CoA species, as PUFAs are the preferred fatty acids of ACSL4. We previously observed that during HSC activation the PUFAs are almost exclusively accumulating in TAGs and not in PLs[7]. We now propose that this increase in PUFA-TAGs is caused by an increase in ACSL4 during HSC activation. Likewise, knock down of ACSL4 in insulin secreting INS 832/13 cells inhibited the incorporation of labeled AA into TAGs but not into PLs[25]. In contrast, overexpression of ACSL4 in arterial smooth muscle cells caused a relatively larger increase in incorporation of labeled AA into PLs as compared to TAGs[20]. There are three main explanations for the differences in response of the TAG and PL species profile to changes in ACSL activity. One explanation states that there is no general acyl-CoA pool for PC and TAG but that specialized pools exist channeling synthesized acyl-CoAs to either TAGs or PLs[26]. This hypothesis requires that different CoA synthesizing enzymes are coupled to either PL or TAG synthesis/remodeling enzymes, for example by differential intracellular localization. Our finding that ACSL4 localizes to large LDs in HSCs, sites of TAG formation[27], supports a channeling hypothesis. Our data are also in agreement with proteomic screens identifying ACSL4 as a LD associated protein[28-31.] Another, not mutually exclusive, explanation is that the enzymes involved in the final step of TAG formation (i.e. DGAT 1 and/or 2) and in PL remodeling (i.e. LPCAT 3 in case of PC[32]) have different affinities for PUFA-CoAs. Indeed, we observed that exogenous AA was incorporated into PC with a higher affinity than into TAGs. The simplest explanation for the observed difference in affinity for exogenous AA is that the final PC and TAG synthesizing enzymes have different affinities for PUFA-CoA. As a consequence, changes in the intra cellular PUFA-CoA concentration, caused by an up- or downregulation of ACSL4 activity, will differentially affect PC and TAG synthesis. The higher affinity for PUFA-PC synthesis will generate smaller effects on the rate of PUFA-PC synthesis as compared to the formation of PUFA-TAG species, as the former is more readily saturated. Especially the formation of TAG species containing 2 and 3 PUFA moieties are expected to be sensitive to variation in PUFA-CoA levels as their formation rate is linear over a large concentration range. A different affinity of the PC and TAG remodeling enzymes for PUFA-CoA also explains our observation that knock-down of ACSL4 and inhibition of ACSL4 with rosiglitazone only caused an appreciable decrease in PUFA-PC species at the low micro molar levels of AA present in the culture medium (Fig. 6), but not in the presence of the higher concentration of exogenous AA-d8 (25 µM) (Fig. 3 and Fig. 4). Thirdly, the TAG pool, but not the PL pool, is expandable. This implies that the TAG pool can accommodate the extra PUFA-CoAs formed by ACSL4. In contrast, in the

non–expandable PL pool, the higher level of PUFA-CoAs will lead to a somewhat higher rate of replacement, rather than to net higher levels of PUFAs (see Fig. 1B and D).

The role of ACSL4 in the formation of PUFA-TAGs permits an evaluation of the function of the accumulation of PUFA-TAGs during HSC activation by modulating ACSL4 activity. An approximately 80–90% knockdown of ACSL4 obtained by gene silencing caused a strong decrease in PUFA-TAGs, but did not result in a significant change in HSC activation. However this does not exclude a role for ACSL4 or TAG-PUFAs in HSC activation as the remaining PUFA-TAGs may still be sufficient for HSC functioning. A robust inhibition of PUFA-TAG formation was obtained by inhibition of ACSL4 activity using rosiglitazone. Incubation with this ACSL4 inhibitor was indeed associated with a significant inhibition of HSC activation. However rosiglitazone may affect other targets besides ACSL4, which are implicated in the inhibition of a fibrotic response[33,34].

In several types of immune cells esterified AA has been found in isolated LDs[35], and it has been suggested that such LDs serve as an AA reservoir for local activation of essential cellular functions[36]. Furthermore, in several cancer cell lines upregulation of ACSL4 was suggested to control cell proliferation via generation of eicosanoids[37]. HSCs bear some resemblance to dendritic cells involved in the immune system[38]. Therefore, we investigated whether PUFA-TAGs in HSCs play a role in the generation of eicosanoids, allowing signaling with other hepatic cell types like hepatocytes, liver progenitor cells, or macrophages. Gene silencing of *Acsl4* only caused a marginal effect on the secretion of various prostaglandins in activated HSCs. Under the same experimental conditions, we showed that the PUFA-PC levels are not affected, providing an explanation for the observed lack of effect on eicosanoid production by ACSL4 knockdown. In contrast, PUFA-TAG levels are strongly reduced under these conditions, indicating that under conditions of reduced ACSL4 expression, PUFA-TAGs can be used to maintain normal levels PUFA-PC. These experiments point to a possible role of PUFA-TAGs as a reservoir for PL-AA synthesis and thus eicosanoid formation. This was further investigated by generating higher amounts of eicosanoids using Ca^{2+} ionophore A23187. The Ca^{2+} stimulus affected the PUFA-TAG pool much more as compared to the AA-PC pool, suggesting a flux of AA from TAG to PLs or into prostaglandins. A role for TAG-PUFAs as a PUFA buffer was then further corroborated by the experiments where ACSL4 was almost completely inhibited for 6 days with rosiglitazone. Under these conditions, the TAG-PUFA pool was depleted and a strong (70–80%) inhibition of the Ca^{2+} stimulated eicosanoid secretion was observed, despite the presence of 50% PUFA-PC species. Therefore, we suggest that upregulation of ACSL4 during activation serves to protect HSCs against a shortage of PUFAs required for cell growth and eicosanoid production.

CHAPTER 2

ACKNOWLEDGEMENTS

REFERENCES

1. W. S. Blaner, S. M. O'Byrne, N. Wongsiriroj, J. Kluwe, D. M. D'Ambrosio, H. Jiang, R. F. Schwabe, E. M. C. Hillman, R. Piantedosi, and J. Libien. (2009). Hepatic stellate cell lipid droplets: A specialized lipid droplet for retinoid storage. Biochim. Biophys. Acta **1791**, 467-473.

2. S. L. Friedman. (2008). Hepatic stellate cells: protean, multifunctional, and enigmatic cells of the liver. Physiol. Rev. **88**,125-172.

3. N. Uyama, Y. Shimahara, N. Kawada, S. Seki, H. Okuyama, Y. Iimuro, and Y. Yamaoka. (2002). Regulation of cultured rat hepatocyte proliferation by stellate cells. J. Hepatol **36**, 590-599.

4. M. Sato, T. Sato, N. Kojima, K. Imai, N. Higashi, D. R. Wang, and H. (2004). Senoo. 3-D structure of extracellular matrix regulates gene expression in cultured hepatic stellate cells to induce process elongation. Comp. Hepatol. **3** Suppl 1 S4.

5. M. Okuno, H. Moriwaki, S. Imai, Y. Muto, N. Kawada, Y. Suzuki, and S. Kojima. (1997). Retinoids exacerbate rat liver fibrosis by inducing the activation of latent TGF-beta in liver stellate cells. Hepatology **26**, 913-921.

6. S. L. Friedman. (2003). Liver fibrosis -- from bench to bedside. J. Hepatol. **38** Suppl 1 S38-53.

7. N. Testerink, M. Ajat, M. Houweling, J. F. Brouwers, V. V. Pully, H. J. van Manen, C. Otto, J. B. Helms, and A. B. Vaandrager. (2012). Replacement of retinyl esters by polyunsaturated triacylglycerol species in lipid droplets of hepatic stellate cells during activation. PLoS One **7** e34945.

8. L. O. Li, E. L. Klett, and R. A. Coleman. (2010). Acyl-CoA synthesis, lipid metabolism and lipotoxicity. Biochim. Biophys. Acta **1801**, 246-251.

9. D. G. Mashek, L. O. Li, and R. A. Coleman. (2006). Rat long-chain acyl-CoA synthetase mRNA, protein, and activity vary in tissue distribution and in response to diet. J. Lipid Res. **47**, 2004-2010.

10. P. C. Calder, R. F. Grimble. (2002). Polyunsaturated fatty acids, inflammation and immunity. Eur. J. Clin. Nutr. **56** Suppl 3, S14-9.

11. H. Harizi, J. B. Corcuff, and N. Gualde. (2008). Arachidonic-acid-derived eicosanoids: roles in biology and immunopathology. Trends Mol. Med. **14**, 461-469.

12. S. A. Farber, E. S. Olson, J. D. Clark, and M. E. (1999). Halpern. Characterization of Ca2+-dependent phospholipase A2 activity during zebrafish embryogenesis. J. Biol. Chem. **274**, 19338-19346.

13. L. Riccalton-Banks, R. Bhandari, J. Fry, and K. M. Shakesheff. (2003). A simple method for the simultaneous isolation of stellate cells and hepatocytes from rat liver tissue. Mol. Cell. Biochem. **248**, 97-102.

14. F. G. van Steenbeek, L. Van den Bossche, G. C. Grinwis, A. Kummeling, I. H. van Gils, M. J. Koerkamp, D. van Leenen, F. C. Holstege, L. C. Penning, J. Rothuizen, P. A. Leegwater, and B. Spee. (2013). Aberrant gene expression in dogs with portosystemic shunts. PLoS One **8** e57662.

15. E. G. Bligh, W. J. Dyer. (1959). A Rapid Method of Total Lipid Extraction and Purification. Can. J. Biochem. Physiol. 37, 911-917.

16. K. Retra, O. B. Bleijerveld, R. A. van Gesteil, A. G. M. Tielens, J. J. van Hellemond, and J. F. Brouwers. (2008). A simple and universal method for the separation and identification of phospholipid molecular species. Rapid Communications in Mass Spectrometry **22** 1853-1862.

17. M. Kates. (1986). Techniques of lipidology: isolation, analysis and identification of lipids. *In* Laboratory Techniques in Biochemistry and Molecular Biology (2nd ed.)**125**. R. H. Burdon and P. H. Van Knippenberg (Eds.).

18. H. Aardema, F. Lolicato, C. H. van de Lest, J. F. Brouwers, A. B. Vaandrager, H. T. van Tol, B. A. Roelen, P. L. Vos, J. B. Helms, and B. M. Gadella. (2013). Bovine cumulus cells protect maturing oocytes from increased fatty acid levels by massive intracellular lipid storage. Biol. Reprod. **88**,164 1-15.

19. J. C. de Grauw, C. H. van de Lest, and P. R. van Weeren. (2011). A targeted lipidomics approach to the study of eicosanoid release in synovial joints. Arthritis Res. Ther. **13**, R123.

20. D. L. Golej, B. Askari, F. Kramer, S. Barnhart, A. Vivekanandan-Giri, S. Pennathur, and K. E. Bornfeldt. (2011). Long-chain acyl-CoA synthetase 4 modulates prostaglandin E(2) release from human arterial smooth muscle cells. J. Lipid Res. **52**, 782-793.

21. B. Askari, J. E. Kanter, A. M. Sherrid, D. L. Golej, A. T. Bender, J. Liu, W. A. Hsueh, J. A. Beavo, R. A. Coleman, and K. E. Bornfeldt. (2007). Rosiglitazone inhibits acyl-CoA synthetase activity and fatty acid partitioning to diacylglycerol and triacylglycerol via a peroxisome proliferator-activated receptor-gamma-independent mechanism in human arterial smooth muscle cells and macrophages. Diabetes **56**, 1143-1152.

22. F. J. Eng, S. L. Friedman. (2000). Fibrogenesis I. New insights into hepatic stellate cell activation: the simple becomes complex. Am. J. Physiol. Gastrointest. Liver Physiol. **279** G7-G11.

23. L. Al-Alem, R. C. Southard, M. W. Kilgore, and T. E. Curry. (2011). Specific thiazolidinediones inhibit ovarian cancer cell line proliferation and cause cell cycle arrest in a PPARgamma independent manner. PLoS One **6** e16179.

24. H. E. Ferguson, A. Kulkarni, G. M. Lehmann, T. M. Garcia-Bates, T. H. Thatcher, K. R. Huxlin, R. P. Phipps, and P. J. Sime. (2009). Electrophilic peroxisome proliferator-activated receptor-gamma ligands have potent antifibrotic effects in human lung fibroblasts. Am. J. Respir. Cell Mol. Biol. **41**, 722-730.

25. E. L. Klett, S. Chen, M. L. Edin, L. O. Li, O. Ilkayeva, D. C. Zeldin, C. B. Newgard, and R. A. Coleman. (2013). Diminished Acyl-CoA Synthetase Isoform 4 Activity in INS 832/13 Cells Reduces Cellular Epoxyeicosatrienoic Acid Levels and Results in Impaired Glucose-stimulated Insulin Secretion. J. Biol. Chem. **288**, 21618-21629.

26. D. G. Mashek, L. O. Li, and R. A. Coleman. (2007). Long-chain acyl-CoA synthetases and fatty acid channeling. Future Lipidol**. 2**, 465-476.

27. F. Wilfling, H. Wang, J. T. Haas, N. Krahmer, T. J. Gould, A. Uchida, J. X. Cheng, M. Graham, R. Christiano, F. Frohlich, X. Liu, K. K. Buhman, R. A. Coleman, J. Bewersdorf, R. V. Farese Jr, and T. C. Walther. (2013). Triacylglycerol synthesis enzymes mediate lipid droplet growth by relocalizing from the ER to lipid droplets. Dev. Cell. 24, 384-399.

28. P. Liu, Y. Ying, Y. Zhao, D. I. Mundy, M. Zhu, and R. G. Anderson. (2004). Chinese hamster ovary K2 cell lipid droplets appear to be metabolic organelles involved in membrane traffic. J. Biol. Chem. **279**, 3787-3792.

29. D. L. Brasaemle, G. Dolios, L. Shapiro, and R. Wang. (2004). Proteomic analysis of proteins associated with lipid droplets of basal and lipolytically stimulated 3T3-L1 adipocytes. J. Biol. Chem. **279**, 46835-46842.

30. E. Umlauf, E. Csaszar, M. Moertelmaier, G. J. Schuetz, R. G. Parton, and R. Prohaska. (2004). Association of stomatin with lipid bodies. J. Biol. Chem. **279**, 23699-23709.

31. S. Y. Cho, E. S. Shin, P. J. Park, D. W. Shin, H. K. Chang, D. Kim, H. H. Lee, J. H. Lee, S. H. Kim, M. J. Song, I. S. Chang, O. S. Lee, and T. R. Lee. (2007). Identification of mouse Prp19p as a lipid droplet-associated protein and its possible involvement in the biogenesis of lipid droplets. J. Biol. Chem. **282**, 2456-2465.

32. H. Shindou, D. Hishikawa, T. Harayama, M. Eto, and T. Shimizu. (2013). Generation of membrane diversity by lysophospholipid acyltransferases. J. Biochem. **154** 21-28.

33. A. Galli, D. W. Crabb, E. Ceni, R. Salzano, T. Mello, G. Svegliati-Baroni, F. Ridolfi, L. Trozzi, C. Surrenti, and A. Casini. (2002). Antidiabetic thiazolidinediones inhibit collagen synthesis and hepatic stellate cell activation in vivo and in vitro. Gastroenterology **122**,1924-1940.

34. T. Miyahara, L. Schrum, R. Rippe, S. Xiong, H. F. Yee Jr, K. Motomura, F. A. Anania, T. M. Willson, and H. Tsukamoto. (2000). Peroxisome proliferator-activated receptors and hepatic stellate cell activation. J. Biol. Chem. **275** 35715-35722.

35. P. T. Bozza, K. G. Magalhaes, and P. F. Weller. (2009). Leukocyte lipid bodies - Biogenesis and functions in inflammation. Biochim. Biophys. Acta **1791** 540-551.

36. H. J. van Manen, Y. M. Kraan, D. Roos, and C. Otto. (2005). Single-cell Raman and fluorescence microscopy reveal the association of lipid bodies with phagosomes in leukocytes. Proc. Natl. Acad. Sci. U. S. A. **102** 10159-10164.

37. P. M. Maloberti, A. B. Duarte, U. D. Orlando, M. E. Pasqualini, A. R. Solano, C. Lopez-Otin, and E. J. Podesta. (2010). Functional interaction between acyl-CoA synthetase 4, lipooxygenases and cyclooxygenase-2 in the aggressive phenotype of breast cancer cells. PLoS One **5** e15540.

38. H. S. Chou, C. C. Hsieh, H. R. Yang, L. Wang, Y. Arakawa, K. Brown, Q. Wu, F. Lin, M. Peters, J. J. Fung, L. Lu, and S. Qian. (2011). Hepatic stellate cells regulate immune response by way of induction of myeloid suppressor cells in mice. Hepatology **53** 1007-1019.

CHAPTER 2

SUPPLEMENTARY DATA

Table S1. Sequence of the primers used in this study:

Gene	Accession number	Forward primer 5→3	Reverse primer 5→3	Tm
Acsl 1	NM_012820	GTGAACAGAACGAAACCCAAGCC	TGGGTGACCATTGCTCCTTTGG	60℃
Acsl 3	NM_057107	CAAGGGCGTCATTGTACACACC	TGCTGTGAGCTTTCTTGTCCAC	62.4℃
Acsl 4	NM_053623	CCTGCTTTACCTACGGCT	AATCACCCTTGCTTCCCT	59.9℃
Acsl 5	NM_053607	GGCCTTAAATCCTTTGAGCAGGTC	TGGCTTTCAGTGTCGGTGTCAG	65.5℃
Acsl 6	NM_130739	TGTTTGAGCGAATGGTGCAGTC	CGGAGAGCTTTCATGTCGTCTGAG	64.3℃
α-Sma	NM_031004	AGATGGCGTGACTCACAACGTG	AGGAATAGCCACGCTCAGTCAG	65℃
Hprt	NM_012583	GTGTTGGATACAGGCCAGACTTTG	TCCACTTTCGCTGATGACACAAAC	60℃
Hmbs	NM_013168	GCTTCGCTGCATTGCTGAAAGG	ACTCCACCAGTCAGGTACAGTTG	59.7℃
Ywhaz	NM_013011	ACATCTGCAACGACGTACTGTCTC	AGCAGCAACCTCAGCCAAGTAG	58℃

Table S2. Antibodies used in western blot:

Primary antibody	Manufacturer	Catalogue no.	Dilution WB	Diluent	Incubation time	Type sec.AB
ACSL4	Santa Cruz	sc-134507	1:250	TBS+BSA	O/N 4℃	rabbit polyclonal
α-SMA	Thermo Scientific	AM128-5M	1:1000	TBS+BSA	O/N 4℃	mouse monoclonal
Tubulin	Sigma-Aldrich	T6199	1:1000	TBS+BSA	O/N 4℃	mouse monoclonal

WB = Western Blot. sec. = secondary.
AB = antibody. TBS = Tris-buffered saline. BSA = Bovine serum albumin

Table S3. Fatty acid composition of neutral lipids in quiescent and activated HSCs

Fatty acid	day 1 nmol/mg protein	day 7 nmol/mg protein	day 1 + d8-AA nmol/mg protein	day 7 + d8-AA nmol/mg protein
C14:0	1.3 ± 1.5	1.5 ± 0.1	0.7 ± 0.8	2.0 ± 1.3
C16:0	19.5 ± 5.9	14.4 ± 2.9	15.2 ± 4.4	16.2 ± 1.2
C16:1	2.4 ± 0.9	5.5 ± 1.1	1.8 ± 0.6	5.3 ± 0.9
C18:0	5.4 ± 1.2	6.9 ± 1.9	4.0 ± 1.5	7.3 ± 2.3
C18:1	15.9 ± 0.7	29.3 ± 1.4	13.3 ± 1.3	31.2 ± 5.5
C18:2	11.8 ± 1.9	8,7 ± 0,5	9,2 ± 1,6	9,6 ± 2,4
C20:0	0.2 ± 0.2	0.7 ± 0.2	0.5 ± 0.5	0.7 ± 0.3
C20:1	0.6 ± 0.2	2.0 ± 0.2	0.5 ± 0.2	2.0 ± 0.2
C20:2	0.6 ± 0.1	1.4 ± 0.2	0.4 ± 0.2	1.2 ± 0.0

Table S3. Fatty acid composition of neutral lipids in quiescent and activated HSCs (continued)

Fatty acid	day 1 nmol/mg protein	day 7 nmol/mg protein	day 1 + d8-AA nmol/mg protein	day 7 + d8-AA nmol/mg protein
C20:3	1.7 ± 0.3	5.9 ± 0.6	1.0 ± 0.2	7.1 ± 1.5
C20:4 total	11.7 ± 2.9	18.3 ± 0.8	11.9 ± 1.8	61.6 ± 16.0
d8-C20:4			4.6 ± 0.8	37.0 ± 13.5
C20:5	0.2 ± 0.1	1.3 ± 0.1	0.1 ± 0.0	1.7 ± 0.6
C22:4 total	3.2 ± 0.7	13.0 ± 1.0	2.9 ± 0.6	25.9 ± 1.5
d8-C22:4			0.7 ± 0.1	10.0 ± 0.8
C22:5	1.2 ± 0.3	10.5 ± 0.3	0.8 ± 0.1	10.1 ± 1.6
C22:6	3.0 ± 1.2	14.3 ± 4.7	2.0 ± 1.4	13.9 ± 4.7

Freshly isolated HSCs were cultured for 1 or 7 days and additionally incubated for 24 hr without or with 25μM of d8-AA in medium with 10% FBS at 37℃. Subsequently, lipids were extracted, separated into a neutral fraction, and hydrolyzed. The released fatty acids were analyzed with HPLC-MS. Data are means ± SD of 2 experiments performed in duplicate.

Table S4. Fatty acid composition of phospholipids in quiescent and activated HSCs

Fatty acid	day 1 nmol/mg protein	day 7 nmol/mg protein	day 1 + d8-AA nmol/mg protein	day 7 + d8-AA nmol/mg protein
C14:0	1.3 ± 0.8	1.4 ± 0.2	0.9 ± 0.6	1.0 ± 0.1
C16:0	35.0 ± 4.4	24.1 ± 2.2	33.0 ± 1.9	23.1 ± 1.0
C16:1	3.4 ± 0.8	5.5 ± 0.6	3.0 ± 0.2	4.3 ± 0.3
C18:0	33.4 ± 2.8	26.9 ± 2.7	31.1 ± 2.0	26.7 ± 1.1
C18:1	23.8 ± 6.4	31.7 ± 5.4	20.0 ± 1.8	25.6 ± 3.2
C18:2	12.1 ± 2.2	7.8 ± 0.7	10.6 ± 0.9	4.0 ± 0.6
C20:0	0.6 ± 0.2	0.3 ± 0.1	0.4 ± 0.1	0.3 ± 0.1
C20:1	1.4 ± 0.2	1.1 ± 0.1	1.2 ± 0.1	0.9 ± 0.2
C20:2	1.1 ± 0.1	0.8 ± 0.1	0.9 ± 0.1	0.5 ± 0.0
C20:3	4.0 ± 1.1	4.7 ± 1.0	2.8 ± 0.8	2.5 ± 0.4
C20:4 total	48.2 ± 11.2	42.3 ± 5.0	59.4 ± 18.1	62.7 ± 14.9
d8-C20:4			22.1± 11.5	34.4 ± 11.9
C20:5	0.6 ± 0.1	1.1 ± 0.2	0.3 ± 0.0	0.3 ± 0.0
C22:4 total	8.4 ± 2.3	11.1 ± 2.0	10.1 ± 3.0	13.5 ± 2.3
d8-C22:4			2.8 ± 1.3	4.8 ± 1.1
C22:5	3.8 ± 1.2	5.9 ± 1.4	3.1 ± 0.9	4.0 ± 0.7
C22:6	8.0 ± 0.7	10.2 ± 2.1	6.6 ± 1.2	7.1 ± 2.5

Freshly isolated HSCs were cultured for 1 or 7 days and additionally incubated for 24 hr without or with 25μM of d8-AA in medium with 10% FBS at 37℃. Subsequently, lipids were extracted, separated into a phospholipid fraction, and hydrolyzed. The released fatty acids were analyzed with HPLC-MS. Data are means ± SD of 2 experiments performed in duplicate.

CHAPTER 2

ATGL and DGAT1 are involved in the turnover of newly synthesized triacylglycerols in hepatic stellate cells

Maidina Tuohetahuntila[a], Martijn R. Molenaar[a], Bart Spee[b], Jos F. Brouwers[a], Martin Houweling[a], Arie B. Vaandrager[a], and J. Bernd Helms[a,*]

[a] Department of Biochemistry and Cell Biology, Faculty of Veterinary Medicine & Institute of Biomembranes, Utrecht University, Yalelaan 2, 3584 CM, Utrecht, The Netherlands.

[b] Department of Clinical Sciences of Companion Animals, Faculty of Veterinary Medicine, Utrecht University, Yalelaan 104, 3584 CM, Utrecht, The Netherlands.

Chapter

3

ABSTRACT

Hepatic stellate cell (HSC) activation is a critical step in the development of chronic liver disease. During activation, HSCs lose their lipid droplets (LDs) containing triacylglycerol (TAG), cholesteryl esters (CEs) and retinyl esters (REs). Here we aimed to investigate which enzymes are involved in LD turnover in HSC during activation *in vitro*. Targeted deletion of the *Atgl* gene in mice HSCs had little effect on the decrease of the overall TAG, CE and RE levels during activation. However, ATGL-deficient HSCs specifically accumulated TAG species enriched in PUFAs and degraded new TAG species more slowly. TAG synthesis and levels of PUFA-TAGs were lowered by the DGAT1 inhibitor T863. The lipase inhibitor Atglistatin increased the levels of TAG in both wt and ATGL-deficient mouse HSCs. Both Atglistatin and T863 inhibited the induction of activation marker α-SMA in rat HSCs, but not in mouse HSCs. Compared to mouse, rat HSCs have a higher turnover of new TAGs and Atglistatin and the DGAT1 inhibitor T863 were more effective. Our data suggest that ATGL preferentially degrades newly synthesized TAGs, synthesized by DGAT1, and is less involved in the breakdown of pre-existing TAGs and retinyl esters in HSCs. Furthermore a large change in TAG levels has modest effect on rat HSC activation.

Keywords: Vitamin A, lipase, lipolysis and fatty acid metabolism, lipid droplets, lipidomics, heavy isotope labeling, triacylglycerol pools, retinyl esters.

INTRODUCTION

Hepatic stellate cells (HSCs) are the main vitamin A (retinol)-storing cells of the body (1,2). In a healthy liver, HSCs store vitamin A in the form of retinyl esters (REs) in large lipid droplets (LDs), together with triacylglycerols (TAGs) and cholesteryl esters (CEs). HSCs are located in the space of Disse, between the sinusoidal endothelial cells and the hepatocytes. Upon liver injury, quiescent HSCs can transdifferentiate into an activated myofibroblastic phenotype (1). Activated macrophages in concert with the HSCs may initiate this transition by secreting cytokines, such as transforming growth factor beta (TGF-β), which stimulate the synthesis of matrix proteins and the release of retinoids by HSCs (1,3). The loss of retinoids is associated with a gradual disappearance of the LDs inside the HSCs. We previously reported that LD degradation in activated rat hepatic stellate cell occurs in two phases (4). Upon activation of the hepatic stellate cells, the LDs reduce in size, but increase in number during the first 7 days in culture before they disappear in a later phase. Raman and lipidomic studies showed that in the initial phase of HSC activation, the REs are disappearing rapidly, whereas the TAG content is transiently increased (4). Interestingly, this increase in TAGs in rat HSCs is predominantly caused by a large and specific increase in poly-unsaturated fatty acid (PUFA)-containing triacylglycerol species during the first 7 days in culture, mediated by an increase in expression of the PUFA-specific fatty acid CoA synthase (ACSL) 4 and a decrease in expression of the other ACSLs, especially ACSL1 (5). So far, the molecular mechanisms and identity of the enzymes involved in the observed increase in lipid droplet number, and their subsequent breakdown during HSC activation are not well understood. An increase in number can be accomplished by the novo synthesis of new LDs (6) or fission of existing large LDs (7). Breakdown of LDs is best characterized in adipose cells, in which key roles were assigned to adipose triglyceride lipase (ATGL, also known as PNPLA2), its co-activator CGI-58 and hormone sensitive lipase (HSL) (8). The first two proteins are known to have a more general function as deficiencies in either one leads to neutral lipid storage diseases (9). Both ATGL and CGI-58 were present on LDs in the hepatic stellate cell line HSC-T6 (10), and rat HSCs were shown to express ATGL, although it was down regulated upon activation (11). In mouse HSCs, lipid breakdown was shown to be partially mediated by a lipophagic pathway, as inhibition of autophagy increased the amount of LDs (12,13). Because inhibition of autophagy was shown to impair HSC activation in mice and this effect could be partially reversed by addition of exogenous FAs, it was suggested that LD breakdown is required to fulfill the energy demands of HSCs during activation (13). On the other hand, HSC activation was shown to be relatively undisturbed in the absence of REs and LDs in Lecithin:retinol acyl transferase (LRAT) knockout mice (14).

In this study we addressed the question whether a change in lipid metabolism is causally related to the activation process in rat and mouse HSCs. We identified enzymes involved in LD formation

and breakdown in HSCs *in vitro* and studied the effect of inhibition of these enzymes on HSC activation.

MATERIALS AND METHODS

Reagents

D4-palmitate, D8-arachidonate and Atglistatin were purchased from Cayman Chemical (Ann Arbor, MI, USA). Dulbecco's modified Eagle medium (DMEM), fetal bovine serum (FBS), and penicillin/streptomycin were obtained from Gibco (Paisley, UK). Bovine Serum Albumin (BSA) fraction V was obtained from PAA (Pasching, Austria). T863 and Collagenase (Clostridium histolyticum Type I) was obtained from Sigma-Aldrich (St. Louis, MO, USA), and saponin from Riedel-de Haën (Seelze, Germany). The mouse monoclonal antibody against alpha-smooth muscle actin (α-SMA) was from Thermo Scientific (Waltham, MA, USA). Lipid droplet staining dye LD540 was kindly donated by Dr. C. Thiele, Bonn, Germany. Hoechst 33342 was obtained from Molecular Probes (Paisley, UK), paraformaldehyde (PF) (8%) was obtained from Electron Microscopy Sciences (Hatfield, PA, USA). FluorSave was obtained from Calbiochem (Billerica, MA, USA), all HPLC-MS solvents were from Biosolve (Valkenswaard, the Netherlands) with exception of chloroform (Carl Roth, Karlsruhe, Germany) and were of HPLC grade. Silica-G (0.063–0.200 mm) was purchased from Merck (Darmstadt, Germany).

Animals

We used 10-12 week-old male and female *Atgl*^{+/+} (wt) and *Atgl*^{-/-} mice, generated by crosses of *Atgl*^{+/-} C57BL/6J mice (15) and paired on sex and age from the same nest and adult male Wistar rats (300–400 g). Procedures of mouse and rat care and handling were in accordance with governmental and international guidelines on animal experimentation, and were approved by the Animal Experimentation Committee (Dierexperimentencommissie; DEC) of Utrecht University (DEC-numbers: 2010.III.09.110, 2012. III.10.100, and 2013.III.09.065).

HSC isolation and in vitro primary cell culture

Stellate cells were isolated from livers of mice and rats by collagenase digestion followed by differential centrifugation (16) and cultured as described previously (5) in DMEM supplemented with 10% FBS, 100 units/ml penicillin, 100 μg/ml streptomycin and 4 μl/ml Fungizone and cells were maintained in a humidified 5% CO_2 incubator at 37°C. Medium was changed every 3 days.

Gene silencing

Gene-silencing experiments were performed using small interfering RNA (siRNA) for target genes or non-targeting siRNA as a control (ON-TARGETplus SMARTpool of 4 siRNAs, Thermo-Scientific,

Rochester, NY, USA) according to the manufacturer's instructions. Briefly, two days after plating, the cells were treated with 40 nM siRNA using 5 µl/ml RNAiMAX (Invitrogen, Breda, the Netherlands) in antibiotic free complete media (with FBS). After 6 hr of transfection, media was changed to standard culturing conditions up to day 7.

RNA isolation, cDNA synthesis and QPCR

Total RNA was isolated from HSCs grown in a 24-well plate using RNeasy Mini Kit (Qiagen, Venlo, the Netherlands) including the optional on-column DNase digestion (Qiagen RNase-free DNase kit)**.** RNA was dissolved in 30 µl of RNase free water and was quantified spectrophotometerically using a Nanodrop ND-1000 (Isogen Life Science, IJsselstein, the Netherlands). An iScript cDNA Synthesis Kit (Bio-Rad, Veenendaal, the Netherlands) was used to synthesize cDNA. Primer design and qPCR conditions were as described previously (17). Briefly, qPCR reactions were performed in duplicate using the Bio-Rad detection system. Amplifications were carried out in a volume of 25 µl containing 12.5 µl of 2xSYBR green supermix (BioRad), 1ul of forward and reverse primer and 1 µl cDNA. Cycling conditions were as follows: initial denaturation at 95°C for 3 minutes, followed by 45 cycles of denaturation (95°C for 10 seconds), annealing temperature (see Supplementary data, Table S1 and S2) for 30 seconds, and elongation (72°C for 30 seconds). To determine the relative expression of a gene, a 4-fold dilution series from a pool of all samples of all genes tested were used. The amplification efficiency was between 95-105%, amplicon sequencing conformed the specificity and for each sample a melt-curve analysis was performed. IQ5 Real-Time PCR detection system software (BioRad) was used for data analysis. Expression levels were normalized by using the average relative amount of the reference genes. Reference genes used for normalization are based on their stable expression in stellate cells, namely, *tyrosine 3-monooxygenase/tryptophan 5-monooxygenase activation protein zeta (Ywhaz), hypoxanthine phosphoribosyl transferase (Hprt),* and *hydroxylmethylbilane synthase (Hmbs).* Primers of reference and target genes are listed in Supplementary Data, Table S1 and S2.

Immunofluorescence

Freshly isolated HSCs were grown on glass coverslips in 24 well plates at 37°C for 7 days. Staining of cells was performed as follows: cells were fixed in 4% (v/v) PF at room temperature for 30min and stored in 1% (v/v) PF at 4°C for a maximum of 1 week. HSCs were washed twice in PBS, permeabilized (0.1% (w/v) saponin) and blocked with 2% BSA for 1hr at room temperature. After blocking, slides were incubated 1hr with the primary antibody against α-SMA (50-75 ug/mL), washed again, and incubated for 1hr with anti-mouse antibody (15ug/mL) supplemented with Hoechst (4 ug/mL) for nuclear counterstaining and lipid droplet dye LD540 (0.05 ug/ml). Thereafter, coverslips were mounted with FluorSave on microscopic slides. Image acquisition was performed on a Leica TCS SPE-II confocal microscope at the Center of Cellular Imaging, Faculty of Veterinary Medicine, Utrecht University.

CHAPTER 3

To quantify lipid droplet size and numbers per cell, confocal images of LD540 (lipid droplets) and Hoechst33342 (nuclei) were analyzed with CellProfiler v2.1.1. Recognized lipid droplets and nuclei were overlayed on the original image to confirm the identity. The error rate was <5% for lipid droplets and <2% for nuclei.

Determination of TAG turnover

To investigate the dynamics of TAG formation and degradation, we labeled isolated rat HSCs for 1 or 2 days with 25 μM D4-palmitate and 25 μM D8-arachidonate in medium containing 10% fetal calf serum. The labeling medium contained approximately 25 % of unlabeled palmitate and 5% of unlabeled arachidonate from the fetal bovine serum (5-10 μM, and 1-2 μM, respectively; (18)). After the labeling the cells were either harvested or subsequently chased for 1 or 2 days in medium containing 10% fetal calf serum the absence of the stable isotope-labeled FAs to determine the breakdown of the labeled TAGs.

Analysis of neutral lipids by HPLC-MS

Lipids were extracted from a total cell homogenate of HSCs grown in a 12-well plate by the method of Bligh and Dyer (19) after addition of 200 pmol tripentadecanoylglycerol as internal standard. Lipid extracts were dissolved in methanol/chloroform (1/9, v/v), loaded on top of the silica-G column (approximately 10 mg of 0.063–0.200 mm silica) and separated in a neutral and phospholipid fraction (20). Neutral lipids were eluted with two volumes acetone, dried under nitrogen gas and stored at −20°C. Prior to HPLC-MS analysis, the neutral lipid fraction was dissolved in methanol/chloroform (1/1, v/v) and separated on a Kinetex /HALO C8-e column (2.6 micron, 150×3.00 mm; Phenomenex, the Netherlands). A gradient was generated from methanol/H_2O (5/5, v/v) to methanol/isopropanol (8/2, v/v) at a constant flow rate of 0.3 ml/min. Mass spectrometry of neutral lipids (TAGs, CEs, RE, and cholesterol) was performed using Atmospheric Pressure Chemical Ionization (APCI) interface (AB Sciex Instruments, Toronto, ON, Canada) on a Biosystems API-2000 Q-trap. The system was controlled by Analyst version 1.4.2 software (MDS Sciex, Concord, ON, Canada) and operated in positive ion mode using settings described previously (4,5). Typical TAG, CE, and RE ions detected are shown in Supplementary Data, Fig. S1. Cholesterol and CEs give typical ions with a m/z of 369, and REs with a m/z of 269, due to the loss of the FA chain. It is important to note that TAG species have retention times on HPLC that are characteristic for TAGs. Subsequently, ionization of the TAG species by APCI generates some DAG fragments. As these DAG fragments are generated after HPLC, they have HPLC retention times that are the same as the TAG species that they are derived from. In contrast, DAG species present in HSCs have DAG-specific retention times. TAG fragments with two non-, single-, and double-labeled palmitoyl chains (16:0,16:0,x) were quantitated by counting ions with m/z of 551, 555 and 559 respectively. TAG fragments with a non- or single-labeled palmitoyl and an oleoyl chain (16:0,18:1,x) were quantitated by counting ions with m/z of 577 and 581, respectively, and

non-, single-, double- and triple-labeled di-arachidonoyl-palmitoyl-glycerol (20:4, 20:4,16:0) was quantitated by counting ions with m/z of 903, 907+911, 915+919, and 923, respectively. Typical non-labeled, high abundant TAG species quantitated were: non PUFA, 52:3 (m/z 859), and 54:3 (m/z 885); PUFA, 56:5 (m/z 909), 58:6 (m/z 935), 60:9 (m/z 957) and 62:11 (m/z 981). Total TAG was determined by quantitating all ions between m/z 530 and 1050 with a retention time of TAG species and corrected for the presence of second and third isotope peaks. In this mass and retention time range no CEs and REs were detected (See Supplementary Data, Fig. S1). The quantitated lipids were normalized to the amount of cholesterol in the same sample. Cholesterol was found to be a good marker for recovery of cellular material, as the cholesterol/protein ratio was found to be constant during HSC culture.

Statistical analysis

Each experiment was performed in duplicate and repeated at least three times. Comparisons of variables between multiple factors were made by a two-way ANOVA. Comparisons of a variable between two groups were made with unpaired or paired Student's t test depending on whether the data were normalized to a control before analysis. Differences were considered statistically significant if the P value was less than 0.05.

RESULTS

Differential effect of ATGL on TAG breakdown in mouse HSCs

We investigated the dynamics of neutral lipid breakdown in HSCs isolated from wt and $Atgl^{-/-}$ mice. HSCs from $Atgl^{-/-}$ mice have almost 2-fold higher TAG levels compared to wt mice during the cell culture period, but similar levels of CEs and REs (Fig. 1, panels A-C). These results clearly implicate ATGL in TAG metabolism of HSCs. Surprisingly, however, upon culturing and hence activation of HSCs, the TAG levels in ATGL-deficient HSCs dropped with an apparently similar rate as compared to wt (Fig. 1A), indicating that ATGL is not the main lipase in mouse HSCs involved in TAG hydrolysis during activation. Likewise, there was no effect of ATGL knockout on the decrease of CEs and REs levels upon culturing (Fig. 1B and 1C). To look more closely at a possible role of ATGL in lipid breakdown during mouse HSC activation, we quantitated different TAG species individually and expressed the TAG levels as percent of the levels at day 1 (Fig. 1D-F). In particular TAG species with one or more polyunsaturated fatty acid (PUFA) moieties were increased in ATGL deficient HSCs at day 7 and 14, but decreased in wt HSCs. Non-PUFA TAG species decreased at an almost similar rate in $Atgl^{-/-}$ HSCs. An exact determination of the contribution of the PUFA-TAG species to the total amount of TAG by the APCI-MS method is hampered by the numerous species (>1000) and the observation that the various TAG species fragment to a different degree depending on the saturation of their acyl chains (5). Nevertheless, quantitation of a number of representative
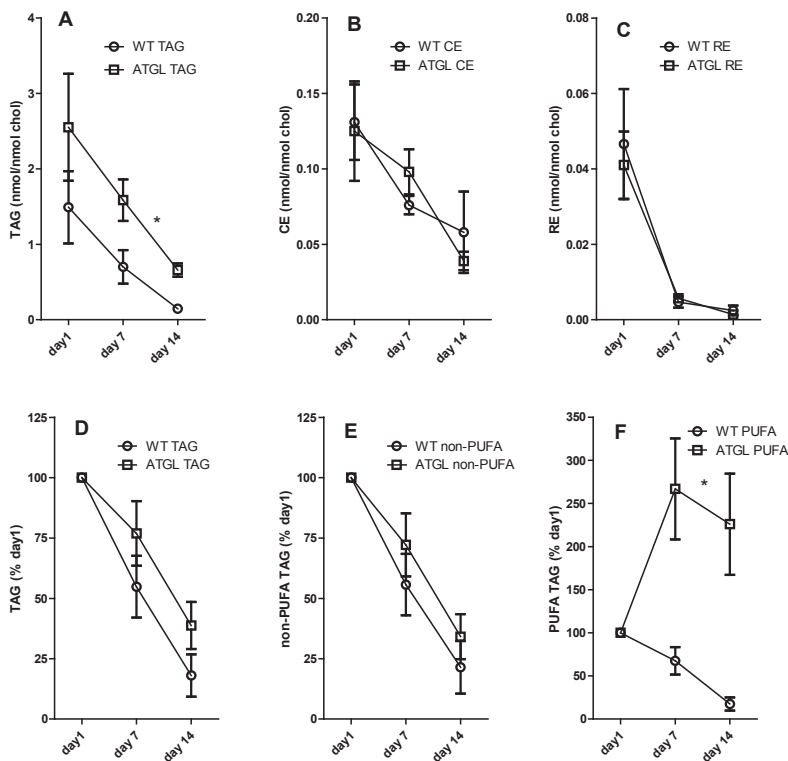
Figure 1. Atgl-deficiency has differential effect on neutral lipids in mouse HSCs. HSCs isolated from wt or Atgl -/- mice were incubated for 1, 7 or 14 days in normal medium. Subsequently, neutral lipids were determined by HPLC-MS. Values of all TAG species (TAG; A), Cholesteryl ester (CE; B) and retinylesters (RE; C) were expressed relative to the amount of cholesterol in the same sample. D, E and F show the relative net loss or gain of all TAG species (D), specific TAG species without a PUFA chain (E), and specific TAG species with one or more PUFA-chains (F) during the incubation as values are expressed relative to level of the respective lipids present at day 1. Data are the means ± SEM of 6 mice. * P< 0.05 ANOVA wt vs Atgl -/-.

intact and fragmented TAG ions allowed us to estimate that wt HSCs at day 1 have 10% TAGs with one or more PUFAs, whereas this was approximately 5% in $Atgl^{-/-}$ HSCs. At day 14, the fraction of PUFA-TAGs in wt HSC was similar as on day 1, but in $ATGL^{-/-}$ cells it was increased to more than 30% (Supplementary Data, Fig. S1D and S2). This allows us to estimate that the PUFA-TAG levels in $Atgl^{-/-}$ HSCs at day 1, 7 and 14 are 0.13, 0.33 and 0.29 nmol/mmol chol, respectively.

We previously reported that the increase in PUFA-TAGs in wt HSCs upon culturing *in vitro* was dependent on a preferential incorporation of exogenous FAs into TAG (4,5). We therefore deter-
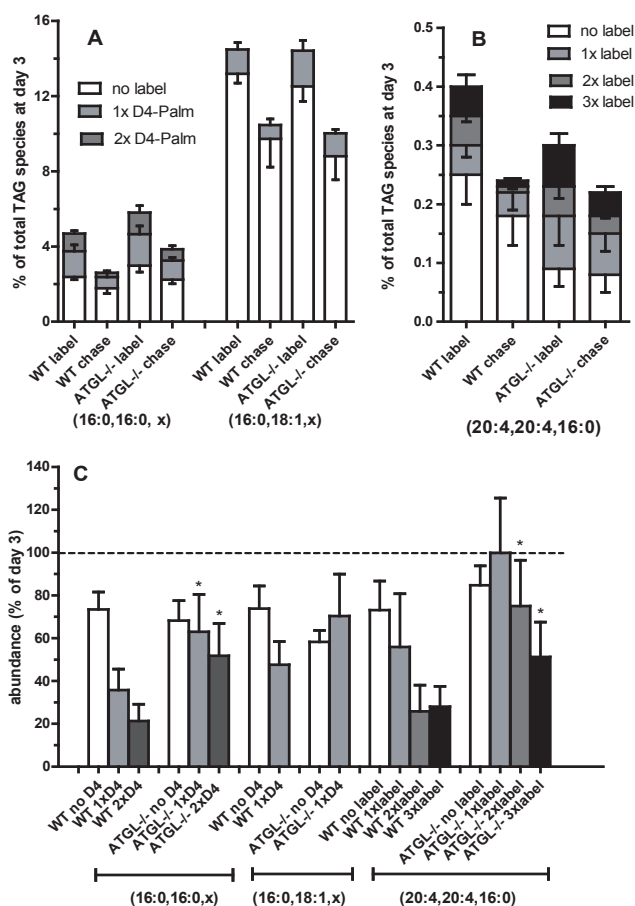
Figure 2. Atgl-deficient mouse HSCs have a lower relative breakdown of newly labeled TAG species. A and B: Primary wt and ATGL-/- mouse HSCs were incubated on day 1 with D4-palmitate and D8-arachidonic acid for 2 days. At day 3, part of the cells were harvested (label), and the remaining HSCs were chased for 48 hrs with normal medium and harvested at day 5 (chase). Subsequently, neutral lipids were extracted and HPLC-MS was performed as described. A: Single or double deuterium-labeled (grey and dark grey bars) and non-labeled (white bars) TAG fragments with 2 palmitoyl chains (16:0,16:0,x) and a palmitoyl and an oleoyl chain (16:0,18:1,x) were quantitated and expressed as percentage of all TAG species. B: Single, double, or triple deuterium-labeled (grey, dark grey, and black bars) and non-labeled (white bars) forms of di-arachidonoyl-palmitoyl glycerol (20:4, 20:4,16:0) were quantitated and expressed as percentage of all TAG species. C: Shows breakdown of the labeled TAG species as the data from the indicated TAG fragments of the cells at day 5, after the chase, were expressed relative to the level of the same TAG species at the beginning of the chase at day 3. Data are the means ± SEM of 5 experiments performed in duplicate. * P< 0.05 t-test versus wt.
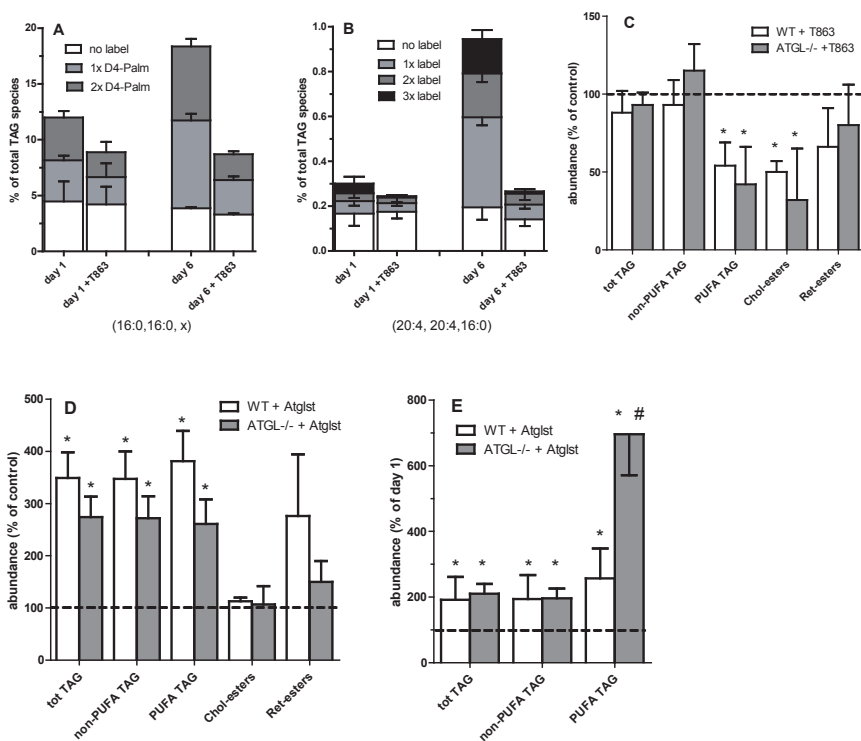
Figure 3. Effect of the DGAT1-inhibitor T863 and Atglistatin on TAG metabolism in wt and ATGL-/- mouse HSCs. A and B: HSCs isolated from wt or Atgl -/- mice were incubated on day 1 or day 6 with D4-palmitate and D8-arachidonic acid for 24 hrs additionally containing vehicle (DMSO) or 20 µM T863. At day 2 or 7 the cells were harvested and neutral lipids were determined with HPLC-MS. A: Single or double deuterium-labeled (grey and dark grey bars) and non-labeled (white bars) TAG fragments with 2 palmitoyl chains (16:0,16:0,x) were quantitated and expressed as percentage of all TAG species. B: Single, double, or triple deuterium-labeled (grey, dark grey, and black bars) and non-labeled (white bars) forms of di-arachidonoyl-palmitoyl glycerol (20:4, 20:4,16:0) were quantitated and expressed as percentage of all TAG species. C, D and E: Isolated wt and ATGL-deficient mouse HSCs were incubated from day 1 to day 7 with vehicle (DMSO; control), 20 µM T863 (C), or 50 µM Atglistatin (Atglst) (D and E). The values of the various neutral lipids were normalized to the amount of cholesterol in the sample, and expressed relative to the level of the respective lipids present in the control cells at day 7 (C and D), or expressed relative to the levels present at the beginning of the incubation (day 1) to show that Atglistatin causes a net increase in TAG (E). Data are the means ± SD of 3 experiments performed in duplicate. C-E: * P< 0.05 ANOVA, treatment versus control, # P< 0.05 ANOVA, wt versus Atgl -/- mice.

mined the incorporation and subsequent chase of deuterium-labeled fatty acids (D4-palmitate and D8-arachidonate) in mouse HSCs. As shown in Fig. 2A, approximately 5% of all the TAG species were labelled with D4-palmitate in either TAG (16:0, 16:0,x) and TAG (16:0, 18:1,x) (sum of labeled species in first and fifth bar). The predominant D4-palmitate labeled species were the TAGs with two palmitoyl groups, from which more than 50% was labeled (Fig.2A, first bar). ATGL is involved in the breakdown of this newly formed TAG pool as the labeled TAG pool was lost at a significantly lower relative rate in $Atgl^{-/-}$ HSCs (half time > 2 days) compared to wt cells (half time < 1 day; Fig. 2C grey and dark grey bars). The breakdown of non-labeled, mainly pre-existing TAGs were not different in the ATGL-deficient cells (Fig. 2C, white bars), assuming an equal re-synthesizis of unlabeled TAG species during the chase in both mice types from FAs from the medium. Similar results were observed for the predominant D8-arachidonate-labeled TAG species (Fig. 2B and 2C), indicating that ATGL is specific for newly formed TAGs, irrespective of the degree of unsaturation of the fatty acid moieties.

We previously reported that the enrichment of PUFAs into newly synthesized TAGs is caused by a down regulation of the general ACSL1 isoform concomitant with an upregulation of the PUFA-specific ACSL4 isoform upon rat HSC activation (5). To see whether a similar shift occurs in mouse HSCs to explain the increase in PUFA-TAGs observed in the ATGL-deficient HSCs, we determined the relative mRNA expression of ACSL1 and ACSL4 in mouse HSCs at day 1, and 7. We found that the ratio of ACSL4 mRNA to ACSL1 mRNA levels increased from 0.8 ± 0.2 at day 1 to 4.6 ± 0.7 at day 7 (n=6). No difference in increase in ACSL4/ACSL1 ratio was observed between wt and ATGL$^{-/-}$ HSCs. This demonstrates a clear enrichment of the PUFA-specific ACSL4 isoform upon activation of mouse HSCs. Furthermore, we observed that D8-arachidonate was incorporated at a higher rate into TAG in activated HSCs at day 6 than in relative quiescent cells at day 1 (Fig. 3B).

DGAT1 is involved in the novo synthesis of TAG during HSC activation

To investigate which of the two Acyl-CoA:Diacylglycerol Acyltransferase (DGAT) enzymes is involved in the formation of the new TAG species in mouse HSCs during activation we determined the DGAT1 and DGAT2 mRNA expression in mouse HSCs at day 1 and day 7. The mRNA levels of DGAT1 were higher compared to those of DGAT2 at day 1 (relative mRNA levels of 118 ± 26 and 35 ± 36, respectively; n=6), and the difference between DGAT1 and DGAT2 mRNA expression increased during activation at day 7 (relative mRNA levels of 136 ± 20 and 14 ± 16, respectively; n=6). To test the role of DGAT1 on the synthesis of new TAGs we determined the incorporation of deuterium-labeled FAs into TAG in the presence of the DGAT1-specific inhibitor T863 (21). As shown in Fig. 3A and 3B, the DGAT1 inhibitor inhibited the incorporation of both D4-palmitate and D8-arachidonate into TAG. The DGAT1-specific inhibitor T863 also caused a clear decrease in the levels of PUFA-TAGs in both wt and in $Atgl^{-/-}$ HSCs during activation, but had almost no effect on the non-PUFA TAG levels (Fig 3C). This indicates that PUFAs are preferential incorporated in the
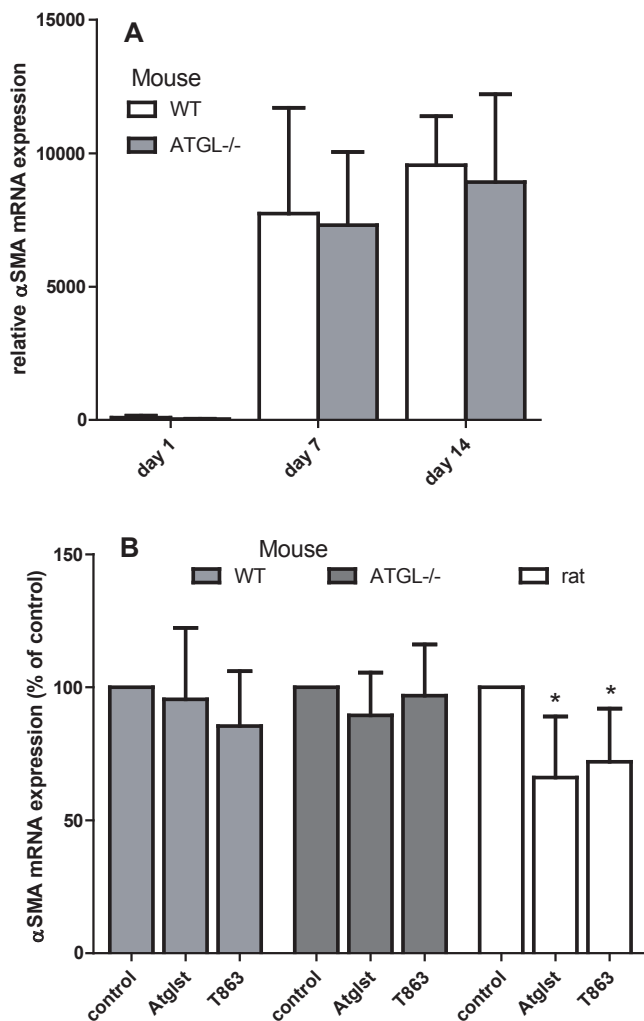
CHAPTER 3

Figure 4. Effect of alterations in TAG metabolism on activation of rat and mouse HSCs. Relative gene expression of α-SMA (HSC activation marker) was measured by qPCR. A: HSCs isolated from wt or Atgl -/- mice were incubated for 1, 7 or 14 days in normal medium (n=6). B: HSCs isolated from wt or Atgl -/- mice or from rats were incubated from day 1 to day 7 with vehicle (DMSO; control), 50 μM Atglistatin (Atglst), or 20 μM T863. Relative mRNA levels of α-SMA were expressed relative to the levels in the control-treated cells (n=3). Data are the means ± SD. * P< 0.05 t-test versus control.
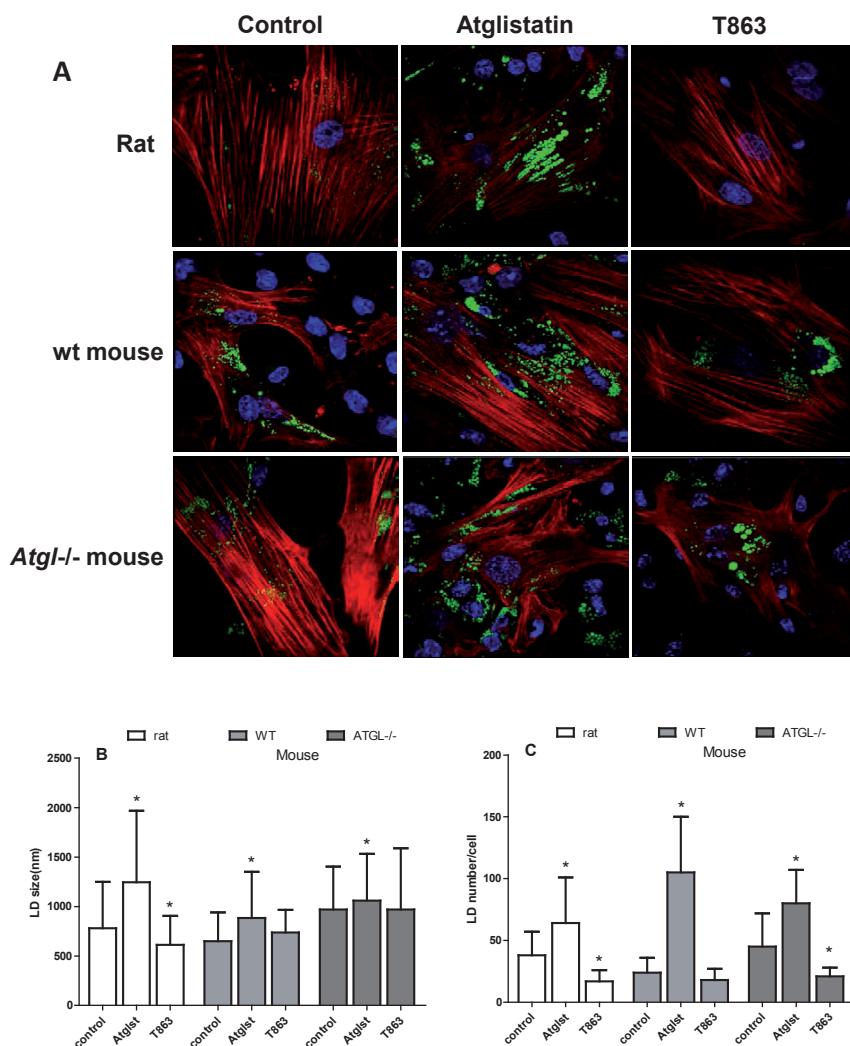
Figure 5. Effect of Atglistatin and the DGAT1-inhibitor T863 on LDs and on the activation marker α-SMA in rat and mouse HSCs. A: Confocal images of HSCs isolated from rats, and wt or Atgl -/- mice, which were incubated from day 1 to day 7 with vehicle (DMSO; control), 50 μM Atglistatin (Atglst), or 20 μM T863. Lipid droplets were stained with LD540 dye (green), anti α-SMA antibody (red) and nuclei were stained with Hoechst (blue). Shown are representative pictures from 3 experiments. B and C: Images were analyzed with CellProfiler v2.1.1. B: LD size was expressed in diameter (nm). C: LD numbers were expressed as a ratio of scored lipid droplets and scored nuclei per image. Image analysis of rat hepatic stellate cells was based on 40 cells and 2500 lipid droplets per condition and for mouse HSCs both wild-type and Atgl -/- animals on 85 cells and 3000 lipid droplets per condition. Data are the means ± SD. * P< 0.05 t-test versus control.

newly formed TAG pool in mouse, similar to observed in rat HSCs. As shown in Fig 3C, the levels of CEs were lower in T863-treated mouse HSCs, suggesting that this drug may also affect cholesterol acylation.

Atglistatin inhibits the predominant lipase in mouse HSCs

The *Atgl* $^{-/-}$ mice also provided a model to study the specificity of the ATGL-specific inhibitor Atglistatin in HSCs (22). Surprisingly, Atglistatin-treatment for 6 days resulted in an almost similar increase in TAG levels in *Atgl* $^{-/-}$ as compared to wt HSCs (Fig. 3D). This amounted to a 2-fold net increase in the total TAG levels in both wt and *Atgl* $^{-/-}$ HSCs, when compared to the original TAG levels at day 1 (Fig. 3E). This clearly demonstrates that Atglistatin not only inhibits ATGL but also targets another, as yet unknown, TAG lipase, which plays a major role in the degradation of the TAG pool in mouse HSCs.

Effect of TAG metabolism on HSC activation

To investigate whether a change in LD size and number is causally related to the activation process, we determined the expression levels of α-smooth muscle actin (α-SMA) after the various treatments to alter TAG content of the HSCs and determined the cellular morphology of the cells. α-SMA is considered a marker for HSC activation and was clearly upregulated in mouse HSCs (Fig. 4A). However, neither deletion of ATGL nor addition of the lipase inhibitor Atglistatin or the DGAT1-inhibitor T863 affected the expression of the activation marker α-SMA in mouse HSCs (figs 4A and 4B). In contrast, we observed a 30 % inhibition of α-SMA expression by both Atglistatin and T863 in rat HSCs (Fig. 4B).

Imaging studies show that Atglistatin increased both the number and size of LDs in rat and mouse HSCs, whereas the DGAT1-inhibitor T863 decreased these parameters in rat HSCs (Fig. 5). In HSCs from wt mice, T863 had no effect on LD size or number, but T863 decreased the number of LDs in *Atgl*$^{-/-}$ HSCs (Fig. 5).

Rat HSCs have a higher TAG turnover as compared to mouse HSCs

As we observed effects of Atglistatin and the DGAT-inhibitor T863 on activation and LD number and size in rat HSCs, we investigated neutral lipid metabolism in isolated HSCs from this rodent in more detail. The dynamics of TAG formation and degradation in rat HSC was assessed by labeling freshly isolated rat HSCs for 2 days with deuterated FAs followed by a 1 day chase. As shown in Fig. 6A (sum of labeled species in first and third bar), 20 % of all the TAG species were labelled with D4-palmitate after 2 days. From the TAG species containing two palmitoyl groups even 80% was labeled (first bar). This suggests that a large part of the total TAG pool is renewed if we assume that palmitoyl-containing TAG species behave similar to the other TAG species. Most of the label was replaced after the 24 h chase, especially in the doubly labeled TAGs, which lost more than 90%
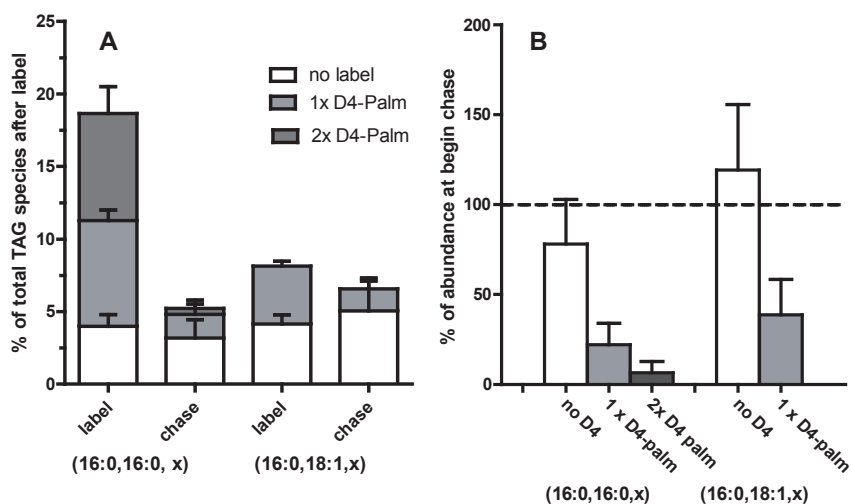
Figure 6. High turnover of TAG in rat HSCs. A and B: Primary rat HSCs were incubated on day 1 with D4-palmitate for 2 days. At day 3, part of the cells were harvested (label), and the remaining HSCs were chased for 24 hrs with normal medium and harvested at day 4 (chase). Subsequently, neutral lipids were extracted and HPLC-MS was performed as described. A: Single or double deuterium-labeled (grey and dark grey bars) and non-labeled (white bars) TAG fragments with 2 palmitoyl chains (16:0,16:0,x) and a palmitoyl and an oleoyl chain (16:0,18:1,x) were quantitated and expressed as percentage of all TAG species. B: Shows breakdown of the labeled TAG species as the data from the indicated TAG fragments of the cells at day 4, after the chase, were expressed relative to the level of the same TAG species at the beginning of the chase at day 3. Data are the means ± SD of 3 experiments performed in duplicate.

of their label (see Fig. 6A, chase and 6B). Similar results were observed for the D8-arachidonate-labeled TAG species upon addition of D8-arachidonate to HSCs for two days (results not shown; cf. (4)). This indicates that rat HSCs contain a large and highly dynamic TAG pool with turn-over rates of less than 8 hrs. In comparison to mouse HSCs, rat cells incorporated more labeled FAs, but also lost their newly made TAGs at a higher relative rate (cf. Figs 2A and 2B to 6A and 6B).

ATGL and DGAT1 are involved in TAG turnover in rat HSCs

Next we tested the effects of the DGAT1-specific inhibitor T863 and Atglistatin on TAG formation and breakdown in rat HSCs. As shown in Fig. 7A, T863 inhibited the incorporation of D4-labeled palmitate in TAG by 80% and caused a similar decrease in the unlabeled TAGs, presumably due to inhibition of the incorporation of unlabeled palmitate from the fetal calf serum. Atglistatin prevented the breakdown of labeled TAG almost completely and also increased the level of non-labeled TAG almost 4-fold during the 2 day chase. This latter observation is caused most likely by inhibition of degradation of the newly formed unlabeled TAGs (Fig. 7A, and 7B). When rat HSCs were incubated for 6 days with Atglistatin the TAG levels were even 10-fold higher compared to
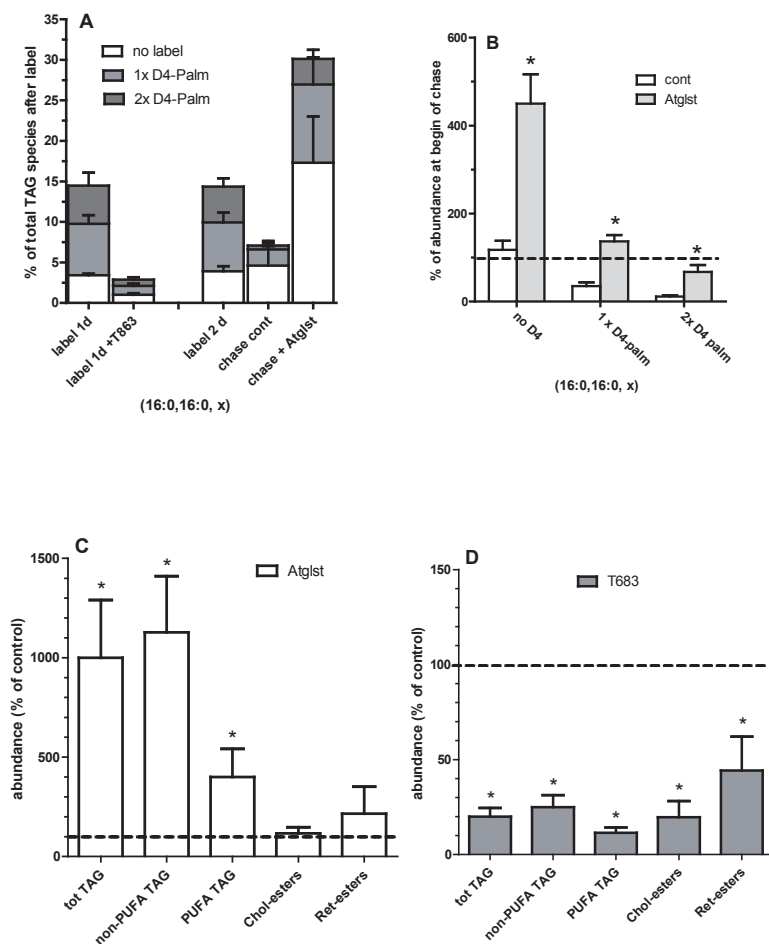
CHAPTER 3

Figure 7. Effect of Atglistatin and the DGAT1-inhibitor T863 on TAG metabolism in rat HSCs. A and B: Isolated rat HSCs were either labeled on day 6 with D4-palmitate for 1 day in the presence or absence of 20 μM T863 (label 1d), or labeled for 2 days from day 1 to day 3 (label 2d), and subsequently chased for another 2 days in the presence of vehicle (DMSO; chase cont) or 50 μM Atglistatin (chase + Atglst). Neutral lipids were determined by HPLC-MS. A: Single or double deuterium-labeled (grey and dark grey bars) and non-labeled (white bars) TAG fragments with 2 palmitoyl chains (16:0,16:0,x) were quantitated and expressed as percentage of all TAG species. B: Shows breakdown of the D4-palmitate-labeled TAG species as the data from the cells after the chase, were expressed relative to the level of the same TAG species at the beginning of the chase. C and D: Isolated rat HSCs were incubated from day 1 to day 7 with vehicle (DMSO; control), 50 μM Atglistatin (Atglst; C), or 20 μM T863 (D). Subsequently, neutral lipids were determined by HPLC-MS. The values were normalized to the amount of cholesterol in the sample, and expressed relative to the level of the respective lipids present in the control cells at day 7. Data are the means ± SD of 3 experiments performed in duplicate. * P< 0.05 t-test versus control.
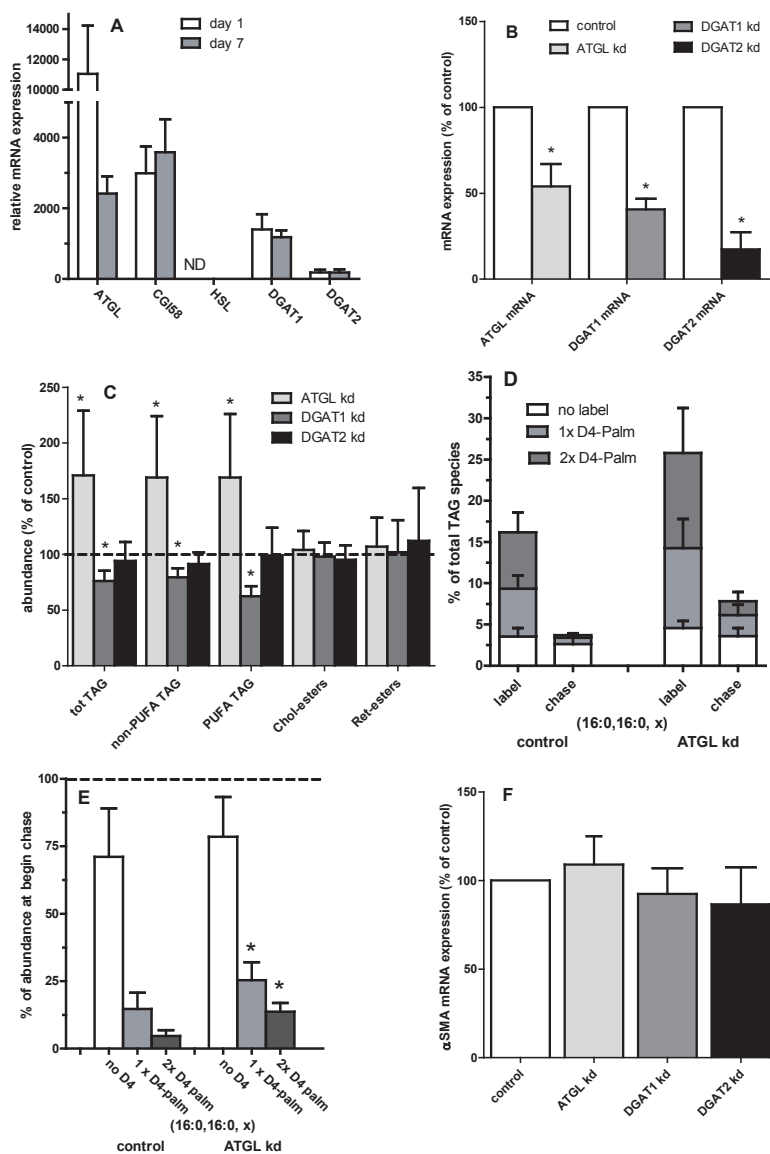
CHAPTER 3

Figure 8. Atgl and Dgat1 affects TAG metabolism in rat HSCs. A: Relative mRNA expression of genes involved in TAG breakdown and synthesis in quiescent (day 1; white bars) and activated (day 7; grey bars) rat HSCs by qPCR. B, C and F: Isolated rat HSCs were transfected at day 2 with non-targeting (control; white bars) or siRNAs targeting Atgl (light grey bar), Dgat1 (grey bar), or Dgat2 (black bar). B. HSCs were harvested 3 days after transfection at day 5 after isolation, and relative mRNA expression of indicated genes were determined with qPCR and expressed relative to their levels in the control-transfected cells. C: Transfected HSCs were harvested on day 7 and neutral lipids were determined by HPLC-MS. The values were normalized to the amount of cholesterol in the sample, and expressed relative to the level of the respective lipids present in the control-transfected cells. D and E: Isolated

HSCs were transfected at day 2 with non-targeting (control) or siRNAs targeting ATGL. One day after transfection, cells were incubated with D4-palmitate for 2 days from day 3 to day 5. After the labeling period, part of the cells were harvested (label), and the remaining HSCs were chased for 2 days with normal medium from day 5 to day 7 (chase). Subsequently, neutral lipids were determined by HPLC-MS. D: Single or double deuterium-labeled (grey and dark grey bars) and non-labeled (white bars) TAG fragments with 2 palmitoyl chains (16:0,16:0,x) were quantitated and expressed as percentage of all TAG species. E: Shows breakdown of the D4-palmitate-labeled TAG species as the data from the cells after the chase, were expressed relative to the level of the same TAG species at the beginning of the chase. F: Transfected HSCs were harvested on day 7 and relative mRNA levels of α-SMA were measured by qPCR and were expressed relative to the levels in the control-transfected cells. All Data are the means ± SD of 3 experiments performed in duplicate. * P< 0.05 t-test versus control.

control incubated cells (Fig. 7C). This experiment demonstrates the large capacity of rat HSCs to synthesize TAG, since net TAG formation is now unmasked by the virtual absence of the normally large concurrent degradation pathway. The DGAT1-specific inhibitor T863 caused 80% lower TAG levels after a 6 day incubation (Fig. 7D), suggesting that DGAT1 is the principal enzyme in the high TAG formation in activated rat HSCs. The levels of cholesterol esters and retinyl esters, were also lowered by T863, indicating that either these neutral lipids require the presence of the major LD core lipid TAG, or that T863 also affects the enzymes involved in CE and RE synthesis.

T863 and Atglistatin might be not completely specific for DGAT1 and ATGL, respectively, as was clearly found in case of Atglistatin in mouse HSCs. Therefore, we wanted additional evidence for a role of ATGL and DGAT1 in the rapid turn-over in rat HSCs. To this end we measured the expression of various TAG-metabolizing genes in quiescent (day 1) and activated (day 7) rat HSCs. Of the tested genes, *Atgl*, in combination with its regulator CGI-58, and *Dgat*1 are likely to play a role in the rapid rat HSC lipid turnover, as HSL mRNA was not detectable and *Dgat*2 expression was relatively low (Fig. 8A). We found no indication that the expression level of these genes was up-regulated during activation. In contrast, ATGL expression was down-regulated during the 7 day culture of the HSCs. We next explored the function of the candidate genes *Atgl*, *Dgat*1 and *Dgat*2 by siRNA-mediated silencing. The efficiency of silencing was between 80% and 50% as shown in Fig. 8B. In line with the mRNA expression data, knock-down of *Atgl* and *Dgat*1, but not *Dgat*2, affected the levels of TAG in rat HSCs (Fig. 8C). *Atgl* knock-down clearly inhibited the relative loss of labeled palmitate during the chase and caused a higher level of labeled palmitate containing TAGs at the beginning of the chase, probably by an inhibition of breakdown during the labeling period (see Fig. 8D and 8E). A more quantitative estimation of the roles of ATGL and DGAT1 on TAG levels in rat HSCs was hampered by the relatively low knock-down efficiency in these primary cells (50 % and 60 %, respectively, on mRNA levels; Fig. 8B). The relatively small effects on TAG levels by the knock-down of ATGL and DGAT1 did not cause an effect on HSC activation, since we could find no effect on α-SMA expression by siRNA-mediated knock down of *Atgl*, *Dgat*1 and *Dgat*2 in rat HSCs (Fig. 8F).

DISCUSSION

Our study with ATGL-deficient HSCs showed that ATGL has a limited, but specific role in lipid degradation in this cell type. We could not confirm a significant role of this lipase in the degradation of retinyl esters in culture-activated mouse HSCs as suggested by Taschler et al. (23). Knockout of *Atgl* did not prevent a decrease in most TAG species without PUFA chains, but caused a preferential accumulation of PUFA-TAG species. This differential behavior was not expected, as no clear preference of ATGL for specific acyl chains has been described (24). We here propose that, rather than an acyl-chain preference, the observed difference in TAG species distribution reflects a preference of ATGL for newly synthesized TAGs, as i) the degradation of newly formed TAGs was specifically decreased in the ATGL-deficient mouse HSCs, ii) PUFAs are preferentially incorporated in newly synthesized TAG in HSCs upon activation by an enrichment of ACSL4 (5), that we now observe also in mouse HSCs, and iii) the DGAT1-specific inhibitor T863, which inhibited the formation of new TAGs in mouse HSCs, also specifically affected the levels of PUFA-TAGs in activated mouse HSCs.

The suggestion that ATGL specifically targets newly synthesized TAGs, would imply that in activated HSCs two pools of TAG exist. A original pool of TAG present in the relatively large pre-existing LDs, and a novel pool, made preferential by DGAT1 in combination with ACSL4, and thus enriched in PUFAs. This latter pool may well be located in newly formed, and therefore relatively small LDs. In activated rat HSCs we previously observed that LDs reduce in size, but increase in number and are localized in cellular extensions (4). We speculated that this was caused by fission of the LDs and extensive migration to the periphery (4). Our new data favors an alternative explanation, i.e. that the apparent redistribution of LDs is due to a degradation of the lipid content (both TAGs and RE) of original LDs concurrent with an rapid resynthesis of TAGs in novel lipid droplets by DGAT1 in the cell periphery. Interestingly, DGAT1 has been associated with the formation of small new LDs, whereas DGAT2 was involved in the enlargement of existing LDs in model cells (25).

In wild type mice, the accumulation of these new PUFA-TAGs is less apparent as this pool is probably degraded by ATGL at an equal rate as it is formed. In rat HSCs, however, the formation of new TAGs, preferential containing PUFAs, was shown to be much higher and is apparently not balanced by ATGL. We have strong evidence that DGAT1 is a key enzyme in this rapid TAG synthesis, as TAG levels were affected by siRNA-mediated knock down of DGAT1, but not DGAT2 in rat HSCs, and the DGAT1-specific inhibitor T863 affected the synthesis of new TAGs and resulted in a large drop in TAG species during activation. In rat HSCs, the relatively high rate of TAG synthesis must be compensated by an almost equal rate of degradation to obtain the small net gain of TAG observed (4). The breakdown of the novel TAGs was indeed found to be very high in rat cells, as more than 80-90% of the newly formed TAGs is degraded within 1 day. Furthermore, we found that inhibition of TAG breakdown by Atglistatin caused a massive increase in total levels of TAG,

which was estimated to be more than a doubling of the original amount of TAG in one day (as 2 days of Atglistatin resulted in a 4-fold higher level of TAG, and 6 days of inhibition led to a 10-fold higher level; Fig. 7). The higher turnover of new TAGs in rat HSCs would suggest a larger role of ATGL in TAG homeostasis in rats compared to mice. This was corroborated by the clear effect of a limited siRNA-mediated knockdown of ATGL on total TAG levels (Fig. 8).

The observation that ATGL-deficient mouse HSCs still lose their TAG content, indicates that another as yet unknown lipase is the main TAG-degrading enzyme in mouse cells. This other lipase, like ATGL, is sensitive to Atglistatin as TAG levels were 3-4 fold increased by this inhibitor in both wt and $Atgl^{-/-}$ HSCs (Fig. 3). This would eliminate monoglyceride lipase, hormone sensitive lipase, lipoprotein lipase and pancreatic lipase, as well as patatin-like phospholipase domain containing (PNPLA) 6 and PNPLA 7, which were shown to be unaffected by this drug (22). PNPLA3, also called adiponutrin (ADPN), is also an unlikely candidate since this enzyme is rather involved in TAG remodeling, than in net lipolysis (26). In human HSCs, PNPLA3 was shown to play a role in retinyl ester degradation (27), rather than TAG breakdown. But, interestingly, a variant of this gene was associated with steatohepatitis by an as yet unknown mechanism (28). Another candidate would be lysosomal acidic lipase (LAL/Lipa), the putative TAG degrading lipase in the lipophagy/autophagy pathway. Inhibition of autophagy was shown to result in TAG accumulation in mouse HSCs (12,13). We have no direct information whether Atglistatin inhibits LAL/Lipa. However, we did not observe an increase in CEs after treatment with Atglistatin, as would be expected in case of LAL/Lipa inhibition (29).

In general, this study also points out that HSCs from different species are not using metabolic pathways in a quantitatively similar way, not even in related animals as rat and mice. This may be relevant to explain the differences observed between mice and rats in the effect of strategies to alter lipid metabolism on HSC activation. The detection of two potent inhibitors of TAG synthesis and degradation in rat HSCs, T863 and Atglistatin, respectively, allowed us to address the question whether a change in TAG metabolism is causally related to the activation process in rat and mouse HSCs. Intriguingly, both inhibitors significantly attenuated activation in rat HSCs to a similar, albeit relatively low degree (30%, Fig. 4). Although we cannot exclude the possibility that these drugs affect HSCs activation by other, non-lipid related pathways, their effects on HSC activation correlated with their effect on TAG levels, as Atglistatin and T863 had less effect on TAG levels in mouse HSCs and did not affect the expression of the activation marker α-SMA in these cells. As inhibition of TAG formation had the same effect as inhibiting its breakdown, rat HSCs seem to require an available TAG pool for optimal functioning. This pool may act as a buffer for FAs required for energy (13), or synthesis of membranes or bioactive lipids, like prostanoids (5). Our study with the DGAT-specific inhibitor T863 is in line with previous studies showing that knockdown of *Dgat*1 in rat liver inhibited activation of HSCs *in vitro* (30), whereas knockout of *Dgat*1 in mice had no effect

on subsequent HSC activation in culture (31). Interestingly in the latter study also indicated that a limited effect *in vitro*, might be meaningful *in vivo*, as the DGAT1-deficient mice were less sensitive to induction of liver fibrosis (31).

ACKNOWLEDGEMENTS

CHAPTER 3

REFERENCES

1.   Blaner, W. S., S. M. O'Byrne, N. Wongsiriroj, J. Kluwe, D. M. D'Ambrosio, H. Jiang, R. F. Schwabe, E. M. Hillman, R. Piantedosi, and J. Libien. (2009). Hepatic stellate cell lipid droplets: a specialized lipid droplet for retinoid storage. *Biochim. Biophys. Acta* **1791:** 467-473.

2.   Friedman, S. L. (2008). Hepatic stellate cells: protean, multifunctional, and enigmatic cells of the liver. *Physiol. Rev.* **88:** 125-172.

3.   Pellicoro, A., P. Ramachandran, J. P. Iredale, and J. A. Fallowfield. (2014). Liver fibrosis and repair: immune regulation of wound healing in a solid organ. *Nat. Rev. Immunol.* **14:** 181-194.

4.   Testerink, N., M. Ajat, M. Houweling, J. F. Brouwers, V. V. Pully, H. J. van Manen, C. Otto, J. B. Helms, and A. B. Vaandrager. (2012). Replacement of retinyl esters by polyunsaturated triacylglycerol species in lipid droplets of hepatic stellate cells during activation. *PLoS One* **7:** e34945.

5.   Tuohetahuntila, M., B. Spee, H. S. Kruitwagen, R. Wubbolts, J. F. Brouwers, C. H. van de Lest, M. R. Molenaar, M. Houweling, J. B. Helms, and A. B. Vaandrager. (2015). Role of long-chain acyl-CoA synthetase 4 in formation of polyunsaturated lipid species in hepatic stellate cells. *Biochim. Biophys. Acta* **1851:** 220-230.

6.   Wilfling, F., J. T. Haas, T. C. Walther, and R. V. Farese Jr. (2014). Lipid droplet biogenesis. *Curr. Opin. Cell Biol.* **29:** 39-45.

7.   Long, A. P., A. K. Manneschmidt, B. VerBrugge, M. R. Dortch, S. C. Minkin, K. E. Prater, J. P. Biggerstaff, J. R. Dunlap, and P. Dalhaimer. (2012). Lipid droplet de novo formation and fission are linked to the cell cycle in fission yeast. *Traffic* **13:** 705-714.

8.   Zechner, R., P. C. Kienesberger, G. Haemmerle, R. Zimmermann, and A. Lass. (2009). Adipose triglyceride lipase and the lipolytic catabolism of cellular fat stores. *J. Lipid Res.* **50:** 3-21.

9.   Schweiger, M., A. Lass, R. Zimmermann, T. O. Eichmann, and R. Zechner. (2009). Neutral lipid storage disease: genetic disorders caused by mutations in adipose triglyceride lipase/PNPLA2 or CGI-58/ABHD5. *Am. J. Physiol. Endocrinol. Metab.* **297:** E289-96.

10. Eichmann, T. O., L. Grumet, U. Taschler, J. Hartler, C. Heier, A. Woblistin, L. Pajed, M. Kollroser, G. Rechberger, G. G. Thallinger, R. Zechner, G. Haemmerle, R. Zimmermann, and A. Lass. (2015). ATGL and CGI-58 are lipid droplet proteins of the hepatic stellate cell line HSC-T6. *J. Lipid Res.* **56:** 1972-1984.

11. Mello, T., A. Nakatsuka, S. Fears, W. Davis, H. Tsukamoto, W. F. Bosron, and S. P. Sanghani. (2008). Expression of carboxylesterase and lipase genes in rat liver cell-types. *Biochem. Biophys. Res. Commun.* **374:** 460-464.

12. Thoen, L. F., E. L. Guimaraes, L. Dolle, I. Mannaerts, M. Najimi, E. Sokal, and L. A. van Grunsven. (2011). A role for autophagy during hepatic stellate cell activation. *J. Hepatol.* **55:** 1353-1360.

13. Hernandez-Gea, V., Z. Ghiassi-Nejad, R. Rozenfeld, R. Gordon, M. I. Fiel, Z. Yue, M. J. Czaja, and S. L. Friedman. (2012). Autophagy releases lipid that promotes fibrogenesis by activated hepatic stellate cells in mice and in human tissues. *Gastroenterology* **142:** 938-946.

14. Kluwe, J., N. Wongsiriroj, J. S. Troeger, G. Y. Gwak, D. H. Dapito, J. P. Pradere, H. Jiang, M. Siddiqi, R. Piantedosi, S. M. O'Byrne, W. S. Blaner, and R. F. Schwabe. (2011). Absence of hepatic stellate cell retinoid lipid droplets does not enhance hepatic fibrosis but decreases hepatic carcinogenesis. *Gut* **60:** 1260-1268.

15. Haemmerle, G., A. Lass, R. Zimmermann, G. Gorkiewicz, C. Meyer, J. Rozman, G. Heldmaier, R. Maier, C. Theussl, S. Eder, D. Kratky, E. F. Wagner, M. Klingenspor, G. Hoefler, and R. Zechner. (2006). Defective lipolysis and altered energy metabolism in mice lacking adipose triglyceride lipase. *Science* **312:** 734-737.

16. Riccalton-Banks, L., R. Bhandari, J. Fry, and K. M. Shakesheff. (2003). A simple method for the simultane-ous isolation of stellate cells and hepatocytes from rat liver tissue. *Mol. Cell. Biochem.* **248:** 97-102.

17. van Steenbeek, F. G., L. Van den Bossche, G. C. Grinwis, A. Kummeling, I. H. van Gils, M. J. Koerkamp, D. van Leenen, F. C. Holstege, L. C. Penning, J. Rothuizen, P. A. Leegwater, and B. Spee. (2013). Aberrant gene expression in dogs with portosystemic shunts. *PLoS One* **8:** e57662.

18. Aardema, H., F. Lolicato, C. H. van de Lest, J. F. Brouwers, A. B. Vaandrager, H. T. van Tol, B. A. Roelen, P. L. Vos, J. B. Helms, and B. M. Gadella. (2013). Bovine cumulus cells protect maturing oocytes from increased fatty acid levels by massive intracellular lipid storage. *Biol. Reprod.* **88:** 164.

19. Bligh, E. G., W. J. Dyer. (1959). A rapid method of total lipid extraction and purification. *Can. J. Biochem. Physiol.* **37:** 911-917.

20. Retra, K., O. B. Bleijerveld, R. A. van Gestel, A. G. Tielens, J. J. van Hellemond, and J. F. Brouwers. (2008). A simple and universal method for the separation and identification of phospholipid molecular species. *Rapid Commun. Mass Spectrom.* **22:** 1853-1862.

21. Cao, J., Y. Zhou, H. Peng, X. Huang, S. Stahler, V. Suri, A. Qadri, T. Gareski, J. Jones, S. Hahm, M. Perreault, J. McKew, M. Shi, X. Xu, J. F. Tobin, and R. E. Gimeno. 2011. Targeting Acyl-CoA:diacylglycerol acyltrans-ferase 1 (DGAT1) with small molecule inhibitors for the treatment of metabolic diseases. *J. Biol. Chem.* **286:** 41838-41851.

22. Mayer, N., M. Schweiger, M. Romauch, G. F. Grabner, T. O. Eichmann, E. Fuchs, J. Ivkovic, C. Heier, I. Mrak, A. Lass, G. Hofler, C. Fledelius, R. Zechner, R. Zimmermann, and R. Breinbauer. (2013). Development of small-molecule inhibitors targeting adipose triglyceride lipase. *Nat. Chem. Biol.* **9:** 785-787.

23. Taschler, U., R. Schreiber, C. Chitraju, G. F. Grabner, M. Romauch, H. Wolinski, G. Haemmerle, R. Brein-bauer, R. Zechner, A. Lass, and R. Zimmermann. (2015). Adipose triglyceride lipase is involved in the mobilization of triglyceride and retinoid stores of hepatic stellate cells. *Biochim. Biophys. Acta* **1851:** 937-945.

24. Eichmann, T. O., M. Kumari, J. T. Haas, R. V. Farese Jr, R. Zimmermann, A. Lass, and R. Zechner. (2012). Studies on the substrate and stereo/regioselectivity of adipose triglyceride lipase, hormone-sensitive lipase, and diacylglycerol-O-acyltransferases. *J. Biol. Chem.* **287:** 41446-41457.

25. Wilfling, F., H. Wang, J. T. Haas, N. Krahmer, T. J. Gould, A. Uchida, J. X. Cheng, M. Graham, R. Christiano, F. Frohlich, X. Liu, K. K. Buhman, R. A. Coleman, J. Bewersdorf, R. V. Farese Jr, and T. C. Walther. (2013). Triacylglycerol synthesis enzymes mediate lipid droplet growth by relocalizing from the ER to lipid droplets. *Dev. Cell.* **24:** 384-399.

26. Ruhanen, H., J. Perttila, M. Holtta-Vuori, Y. Zhou, H. Yki-Jarvinen, E. Ikonen, R. Kakela, and V. M. Olk-konen. (2014). PNPLA3 mediates hepatocyte triacylglycerol remodeling. *J. Lipid Res.* **55:** 739-746.

27. Pirazzi, C., L. Valenti, B. M. Motta, P. Pingitore, K. Hedfalk, R. M. Mancina, M. A. Burza, C. Indiveri, Y. Ferro, T. Montalcini, C. Maglio, P. Dongiovanni, S. Fargion, R. Rametta, A. Pujia, L. Andersson, S. Ghosal, M. Levin, O. Wiklund, M. Iacovino, J. Boren, and S. Romeo. (2014). PNPLA3 has retinyl-palmitate lipase activity in human hepatic stellate cells. *Hum. Mol. Genet.* **23:** 4077-4085.

CHAPTER 3

28.   Krawczyk, M., P. Portincasa, and F. Lammert. (2013). PNPLA3-associated steatohepatitis: toward a gene-based classification of fatty liver disease. *Semin. Liver Dis.* **33:** 369-379.

29.   Du, H., M. Duanmu, D. Witte, and G. A. Grabowski. (1998). Targeted disruption of the mouse lysosomal acid lipase gene: long-term survival with massive cholesteryl ester and triglyceride storage. *Hum. Mol. Genet.* **7:** 1347-1354.

30.   Yamaguchi, K., L. Yang, S. McCall, J. Huang, X. X. Yu, S. K. Pandey, S. Bhanot, B. P. Monia, Y. X. Li, and A. M. Diehl. (2008). Diacylglycerol acyltranferase 1 anti-sense oligonucleotides reduce hepatic fibrosis in mice with nonalcoholic steatohepatitis. *Hepatology* **47:** 625-635.

31.   Yuen, J. J., S. A. Lee, H. Jiang, P. J. Brun, and W. S. Blaner. (2015). DGAT1-deficiency affects the cellular distribution of hepatic retinoid and attenuates the progression of CCl4-induced liver fibrosis. *Hepatobiliary. Surg. Nutr.* **4:** 184-196.

SUPPLEMENTARY DATA

Table S1. Rat primer sequence for the target and reference genes used in qPCR

Gene	Accession Number	Forward primer 5 → 3	Reverse primer 5 → 3	Tm
Pnpla2	NM_001108509	CACCCTTTCCAACATGCT	GTCTGCTCCTTCATCCAC	63ºC
CGI-58	NM_212524	GCATTGACTCCCTTTAACCC	TGTACTCTGTCACCGTGTC	65ºC
HSL	NM_012859	TCAAAGTCAAACCCTCCA	TGTCATTGTGCGTAAATCC	*61.5*ºC
Dgat1	NM_053437	TTTCTGCTACGGCGGGTTCTTG	GATAGTAGGGACCATCCACTGCTG	65ºC
Dgat2	NM_001012345	TACAGTGGGTCCTATCCT	CAGCCAGGTGAAGTAGAG	65ºC
α-SMA	NM_031004	AGATGGCGTGACTCACAACGTG	AGGAATAGCCACGCTCAGTCAG	65ºC
Hprt	NM-012583	GTGTTGGATACAGGCCAGACTTTG	TCCACTTTCGCTGATGACACAAAC	60ºC
Hmbs	NM_013168	GCTTCGCTGCATTGCTGAAAGG	ACTCCACCAGTCAGGTACAGTTG	59.7ºC
Ywhaz	NM_013011	ACATCTGCAACGACGTACTGTCTC	AGCAGCAACCTCAGCCAAGTAG	58ºC

Table S2. Mouse primer sequence for the target and reference genes used in qPCR

Gene	Accession Number	Forward primer 5 → 3	Reverse primer 5 → 3	Tm
Acsl1	NM_001302163	TCTTTCTTGCCTCTCGCC	GTCGTCCATAAGCAGCCT	66.5ºC
Acsl4	NM_001033600	GCCAGTGTGAACGTATCC	GTGAAGAGTATCCAATCCTACAG	61.5ºC
Dgat1	NM_010046.2	CAGCAATTATCGTGGTATCCT	TCCTTCAGAAACAGAGACAC	*59.5*ºC
Dgat2	NM_026384.3	TTCCGAGACTACTTTCCCA	GTTACAGAAGGCACCCAG	61.5ºC
α-SMA	NM_007392	TCTTCCAGCCATCTTTCATTGGG	CCTGACAGGACGTTGTTAGCATAG	61ºC
Hprt	NM_013556	TCAGTCAACGGGGGACATAAA	GGGGCTGTACTGCTTAACCAG	64ºC
Hmbs	NM_001110251	ACTCTGCTTCGCTGCATTG	AGTTGCCCATCTTTCATCACTG	58ºC
Ywhaz	NM_001253805	AACAGCTTTCGATGAAGCCAT	TGGGTATCCGATGTCCACAAT	64ºC

CHAPTER 3

SUPPLEMENTARY FIGURE S1

Lipidomic analysis of neutral lipids from HSCs

Contour plots in the m/z range of 250 to 1050 of a HPLC-APCI-MS analysis.

A: TAG standard (100 pmol of sunflower oil, enriched in TAGs with unsaturated FAs like 18:1 and 18:2), showing both intact TAG fragments in the m/z 800–1000 region and fragments in the m/z region of 530-650 resulting from the loss of one FA chain, and in the m/z region of 350-300 resulting from the loss of two FA chains.

B. CE standard (100 pmol of cholesterol oleate), showing a characteristic cholesterol fragment of m/z 369 resulting from the complete loss of the FA chain.

C. RE standard (100 pmol of retinyl palmitate), showing a characteristic retinol fragment of m/z 269 due to the complete loss of the FA chain.

D Neutral lipids extracted from wt and ATGL-/- mouse HSC at day 1 and 14 in culture.

IS = tripentadecanoylglycerol as internal standard which is detected as a fragment with a m/z of 523 resulting from the complete loss of one FA chain.

Box denotes the range used for total TAG analysis

A sunflower oil

TAGs

intact

fragments
1 FA loss

B cholesteryloleate

TAGs

CEs

C Retinylpalmitate

TAGs

RP

D WT day 1

TAGs

intact

fragments
1 FA loss

IS

CEs

WT day 14

TAGs

intact

fragments
1 FA loss

IS

CEs

ATGL
day 1

TAGs

intact

fragments
1 FA loss

IS

CEs

ATGL
day 14

TAGs

intact

fragments
1 FA loss

IS

CEs

m/z

Time (min)
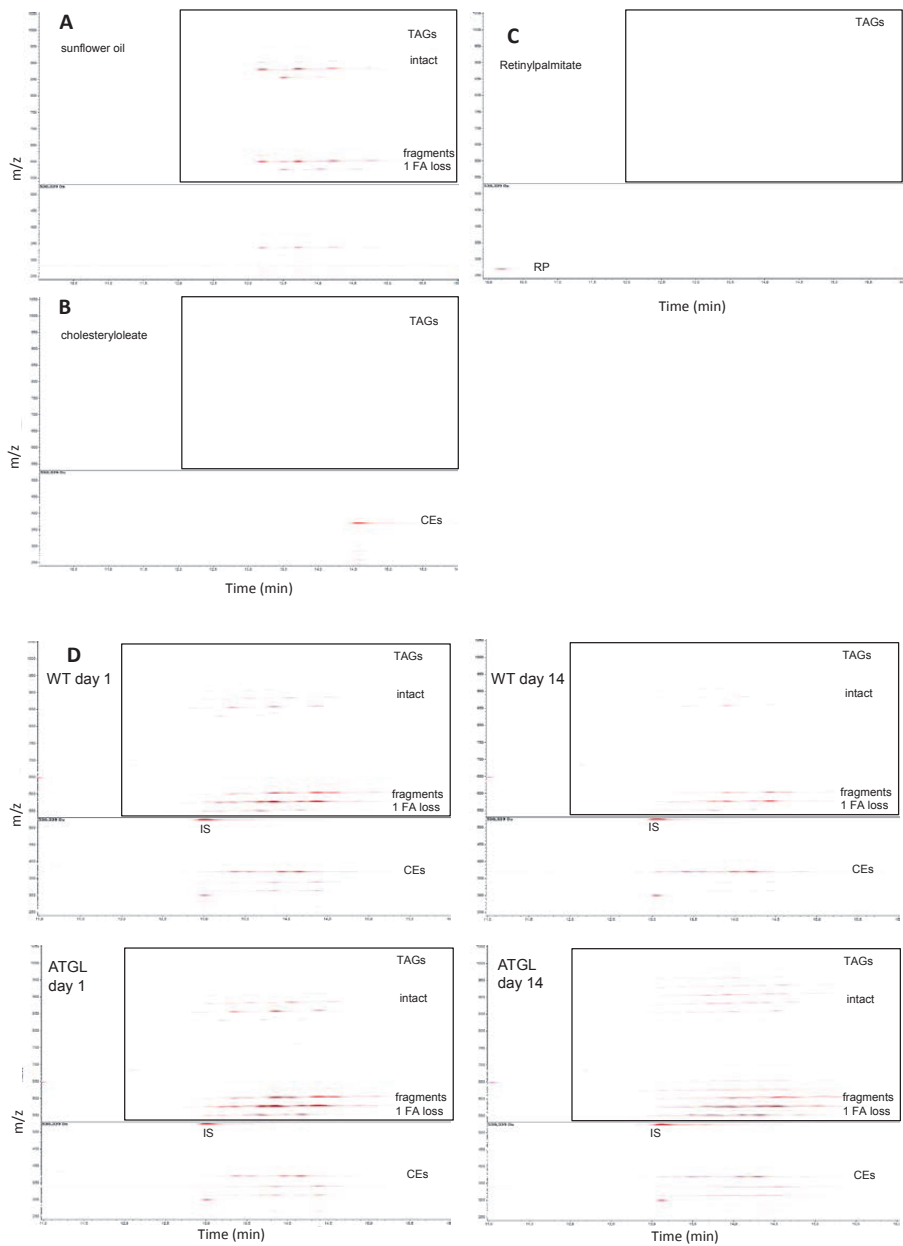
SUPPLEMENTARY FIGURE S2

HSCs of ATGL-/- mice accumulate PUFA-TAGs during activation.

Contour plots of HPLC-APCI-MS analysis of mouse HSC at day 1, 7 and 14, showing an increase in long chain fatty acid-containing TAG species at day 7 and 14 in ATGL-/- HSCs. From every ion in the m/z 800–1000 region its relative abundance (amount of blackness) and retention time in the HPLC separation is shown. TAG species with the same total number of carbon atoms in the three acyl chains (denoted on the left hand side), but different number of double bonds (:n) form diagonal "stripes" at specifc m/z regions. In general TAGs with 56 C atoms or more contain at least one PUFA, whereas TAGs with 54 C atoms may contain one or no PUFAs. Shown is at typical experiment.
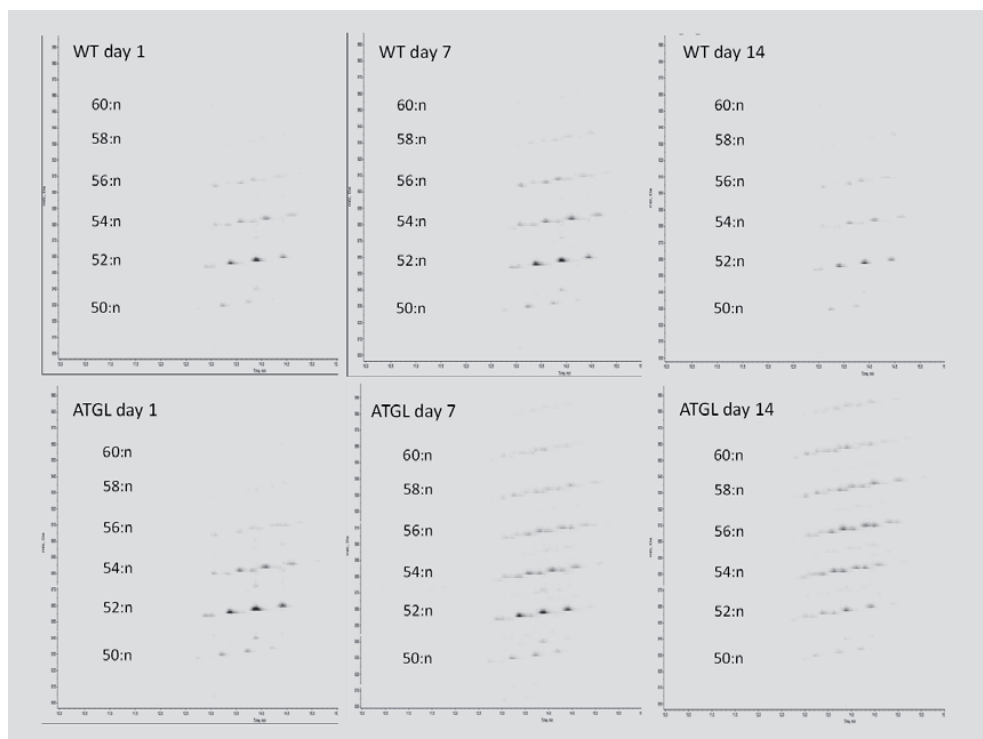
Lysosomal acid lipase inhibitor affects retinyl ester breakdown and hepatic stellate cell activation

Maidina Tuohetahuntila[a], Martijn R. Molenaar[a], Bart Spee[b], Jos F. Brouwers[a], Richard Wubbolts[a] , Martin Houweling[a],Cong Yan[c] , Hong Du[c], Arie B. Vaandrager[a], and J. Bernd Helms[a]

[a] Department of Biochemistry and Cell Biology, Faculty of Veterinary Medicine & Institute of Biomembranes, Utrecht University, Yalelaan 2, 3584 CM, Utrecht, The Netherlands.

[b] Department of Clinical Sciences of Companion Animals, Faculty of Veterinary Medicine, Utrecht University, Yalelaan 104, 3584 CM, Utrecht, The Netherlands.

[c] Indiana University School of Medicine, 975 W Walnut St., Indianapolis, IN 46202, USA

ABSTRACT

Activation of hepatic stellate cells (HSCs) is a critical step in the development of liver fibrosis. During activation, HSCs lose their lipid droplets (LDs) containing triacylglycerol (TAG), cholesteryl esters (CEs) and retinyl esters (REs) and the autophagy pathway is stimulated. Here we aimed to investigate whether lysosomal acid lipase (LAL/Lipa) is involved in LD degradation in HSCs during activation *in vitro* by studying the effect of lalistat, a specific LAL-inhibitor. The LAL-inhibitor increased the levels of TAG, CE and RE in both rat and mouse HSCs, but was less potent in inhibiting the degradation of newly synthesized TAG species compared to a more general lipase inhibitor orlistat. Lalistat inhibited the degradation of TAG and RE when novo synthesis of these lipids was limited, and induced the presence of RE-containing LDs in an acid compartment. However, targeted deletion of the Lipa gene in mice had little effect on the liver levels of RE, whereas the levels of CE and TAG were strongly increased. Lalistat partially inhibited the induction of activation marker α-SMA in rat and mouse HSCs. Our data suggest that LAL/Lipa is involved in the degradation of pre-existing LDs, delivered to the lysosomal compartment by an autophagy pathway, and that inhibition of this lipophagic path has a modest effect on HSC activation.

Keywords: Vitamin A, lipase, lipolysis and fatty acid metabolism, lipid droplets, lipidomics, heavy isotope labeling, triacylglycerol pools, retinyl esters.

INTRODUCTION

The majority of vitamin A (retinol) is stored as retinyl esters (REs) in specific liver cells, the so called hepatic stellate cells (HSCs) [1,2]. HSCs are located in the spaces of Disse, between sinusoidal endothelial cells and hepatocytes. In a healthy liver, HSCs contain large lipid droplets filled with REs, triacylglycerols (TAGs) and cholesteryl esters (CEs). After liver injury, quiescent HSCs can transdifferentiate into an activated myofibroblastic phenotype [1]. Activated macrophages in concert with HSCs may initiate this transition by secreting cytokines such as transforming growth factor beta (TGF-β), which stimulate the synthesis of matrix proteins and the release of retinoids by HSCs [1,3]. The loss of retinoids is associated with a gradually disappearance of LDs inside the HSCs. We previously reported that LD degradation in activated rat HSCs occurs in two phases [4]. Upon activation of HSCs, the LDs reduce in size, but increase in number during the first 7 days in culture. The LDs migrate to cellular extensions in this first phase, before they disappear in a later phase. Raman and lipidomic studies showed that in the initial phase of HSC activation, the REs are disappearing rapidly, whereas the TAG content is even transiently increased [4]. Interestingly, this increase in TAGs in rat HSCs is predominantly caused by a large and specific increase in poly-unsaturated fatty acid (PUFA)-containing triacylglycerol species during the first 7 days in culture, mediated by the increase in the ratio of the PUFA-specific fatty acid CoA synthase (ACSL)4 to the non-specific ACSLs, especially ACSL1 [5]. So far, the molecular mechanisms and identity of the enzymes involved in the observed increase in lipid droplet number, and their subsequent breakdown during HSC activation are unknown. An increase in number can be accomplished by the novo synthesis of new LDs [6] or fission of existing large LDs [7]. We have previously suggested that the former possibility is more likely as HSCs were shown to have a dynamic lipid metabolism, in which new TAGs are synthesized and hydrolyzed at relatively high rates [8]. Breakdown of LDs is best characterized in adipose cells, in which key roles were assigned to adipose triglyceride lipase (ATGL, also known as PNPLA2), its co-activator CGI-58 and hormone sensitive lipase (HSL) [9]. The first two proteins are known to have a more general function as deficiencies in either one leads to neutral lipid storage diseases [10]. Rat HSCs were shown to express ATGL but not HSL [8,11]. In mouse and rat HSCs, ATGL was found to be involved specifically in breakdown of newly synthesized TAGs rather than in degrading pre-existing TAGs. This suggests the existence of another lipolysis pathway [8]. In mouse HSCs, lipid breakdown was shown to be partially mediated by a lipophagic pathway, as inhibition of autophagy increased the amount of LDs [12,13]. Because inhibition of autophagy was shown to impair HSC activation in mice and this effect could be partially reversed by addition of exogenous FAs, it was suggested that LD breakdown is required to fulfill the energy demands of HSCs during activation [13]. The lipase active in lipophagy is thought to be lysosomal acid lipase (LAL) coded by the Lipa gene [14], which is also responsible for the degradation of lipoprotein derived CEs and TAGs taken up by endocytosis [15]. Targeted deletion of Lipa in mice leads to severe CE and TAG accumulation in hepatocytes [16] and LAL deficiency in humans results in either Wolman disease

or its milder variant, Cholesteryl Ester Storage Disease (CESD), depending on the mutation in the Lipa gene [17].

In this study, we addressed the question, whether inhibition of LAL affects lipid metabolism in HSCs and the activation process in rat and mouse HSCs. We therefore studied the effect of the LAL-specific inhibitor lalistat [18-20] and the more general lipase inhibitor orlistat [18] on HSC lipid metabolism and activation.

MATERIALS AND METHODS

Reagents

Lalistat (lalistat-2; 3,4-disubstituted thiadiazole carbamate, compound 12 from ref. [19]) was a gift from Paul Helquist (University of Notre Dame, IN, USA). D4-palmitate and 3-Methyladenine were purchased from Cayman Chemical (Ann Arbor, MI, USA). D7-Cholesterylpalmitate was from Avanti polar lipids. Dulbecco's modified Eagle medium (DMEM), fetal bovine serum (FBS), and penicillin/streptomycin were obtained from Gibco (Paisley, UK). Bovine Serum Albumin (BSA) fraction V was obtained from PAA (Pasching, Austria). T863, Chloroquine diphosphate salt, Bafilomycin A, L-α-Phosphatidylcholine, retinol palmitate (RP), collagenase (Clostridium histolyticum Type I) and basic chemicals were obtained from Sigma-Aldrich (St. Louis, MO, USA). The mouse monoclonal antibody against alpha-smooth muscle actin (α-SMA) was from Thermo Scientific (Waltham, MA, USA). Lipid droplet staining dye LD540 was kindly donated by Dr. C. Thiele, Bonn, Germany. Hoechst 33342 was obtained from Molecular Probes (Paisley, UK), paraformaldehyde (PF) (8%) was obtained from Electron Microscopy Sciences (Hatfield, PA, USA). FluorSave was obtained from Calbiochem (Billerica, MA, USA), all HPLC-MS solvents were from Biosolve (Valkenswaard, the Netherlands) with exception of chloroform (Carl Roth, Karlsruhe, Germany) and were of HPLC grade. Silica-G (0.063–0.200 mm) was purchased from Merck (Darmstadt, Germany). Delipidated FBS was made from FBS by extraction with diisopropylether and n-Butanol (FBS/diisopropylether/n-Butanol, 10/8/4 v/v/v), followed by extensive dialysis against phosphate buffered saline (PBS) at 4 °C.

Animals

We used adult male Wistar rats (300–400 g) and 10-12 week-old male and female C57BL/6J mice for HSC isolation. Lipa^{-/-} mice were generated as described [16].

Procedures of rat and mouse care and handling were in accordance with governmental and international guidelines on animal experimentation, and were approved by the Animal Experi-

mentation Committee (Dierexperimentencommissie; DEC) of Utrecht University (DEC-numbers: 2010.III.09.110, 2012. III.10.100, and 2013.III.09.065).

HSC isolation and in vitro primary cell culture

Stellate cells were isolated from livers of rats and mice by collagenase digestion followed by differential centrifugation [21]. After isolation, HSCs were plated in 24, 12 or 6 well plates at a density of $2x10^4$, $5x10^4$ or $1x10^5$ cells/well, respectively. Cells were maintained in DMEM supplemented with 10% FBS, 100 units/ml penicillin, 100 μg/ml streptomycin and 4 μl/ml Fungizone and cells were maintained in a humidified 5% CO_2 incubator at 37°C and were protected from light by covering with aluminium foil. Medium was changed every 3 days.

RNA isolation, cDNA synthesis and QPCR

Total RNA was isolated using RNeasy Mini Kit (Qiagen, Venlo, the Netherlands) including the optional on-column DNase digestion (Qiagen RNase-free DNase kit)**.** RNA was dissolved in 30 μl of RNase free water and was quantified spectrophotometerically using a Nanodrop ND-1000 (Isogen Life Science, IJsselstein, the Netherlands). An iScript cDNA Synthesis Kit (Bio-Rad, Veenendaal, the Netherlands) was used to synthesize cDNA. Primer design and qPCR conditions were as described previously [22]. Briefly, qPCR reactions were performed in duplicate using Bio-Rad detection system. Amplifications were carried out in a volume of 25 μl containing 12.5 μl of 2xSYBR green supermix (BioRad), 1ul of forward and reverse primer and 1 μl cDNA. Cycling conditions were as follows: initial denaturation at 95°C for 3-minute, followed by 45 cycles of denaturation (95°C for 10 seconds), annealing temperature (see Table 1 and 2) for 30 seconds, and elongation (72°C for 30 seconds). A melting curve analysis was performed for every reaction. To determine relative expression of a gene, a 4-fold dilution series from a pool of all samples were used. IQ5 Real-Time PCR detection system software (BioRad) was used for data analysis. Expression levels were normalized by using the average relative amount of the housekeeping genes. Reference genes used for normalization are, based on their stable expression in stellate cells, namely, *tyrosine 3-monooxygenase/tryptophan 5-monooxygenase activation protein, zeta (Ywhaz), hypoxanthine phosphoribosyl transferase (Hprt),* and *hydroxylmethylbilane synthase (Hmbs)*. Primers of reference genes are as described [8], and primers of target genes are listed in Supplementary Data, Table S1.

Immunofluorescence

Freshly isolated HSCs were grown on glass coverslips in 24 well plates at 37°C for 7 days. Staining of cells was performed as follows: cells were fixed in 4% (v/v) PF at room temperature for 30min and stored in 1% (v/v) PF at 4°C for a maximum of 1 week. HSCs were washed twice in PBS, permeabilized (0.1% (w/v) saponin (PBS-S; Riedel-de Haën, Seelze, Germany)) and blocked with 2% BSA for 1hr at room temperature. After blocking, slides were incubated 1hr with the primary antibody against αSMA (50-75 ug/mL), washed again, and incubated for 1hr with anti-mouse

antibody (15ug/mL) supplemented with Hoechst (4 ug/mL) for nuclear counterstaining and lipid droplet dye LD540 (0.05 ug/ml). Thereafter, coverslips were mounted with FluorSave on microscopic slides and Image acquisition was performed at the Center of Cellular Imaging, Faculty of Veterinary Medicine, Utrecht University, on a Leica TCS SPE-II confocal microscope. Images were adjusted in ImageJ (freeware available at www.download-imagej.com).

Live cell imaging

For live cell imaging, cells (200 µL cell suspensions, approximately 2×10^5 cells/mL) were plated on a 8 well glass-bottom slide of Ibidi (Ibidi, Germany). Cells were cultured under similar conditions as described above in the presence or absence of lalistat for 3 days. At the 4th day after isolation, media were changed with fresh media for 2 hrs before imaging. Just before imaging, 100ul Lysotracker Red DND99 (Life Technologies, final concentration of 75nM) was added and Bodipy 493/503 (Molecular Probes, final concentration of 200nM) for 30 minutes in the incubator. Images of the samples were recorded using a NIKON A1R confocal microscope equipped with a humidified imaging chamber set to 5% CO2 and 37 ºC (TOKAI hit, Japan) at the Center for Cell Imaging (CCI), Faculty of Veterinary Medicine, Utrecht University.

Retinyl esterase (REH) and cholesteryl esterase (CEH) activity assay

REH was assayed essential as described [23]. In short an aliquot of mouse liver homogenate or rat hepatocyte (400 ug of protein) were incubated in sodium citrate buffer (60 mM; pH 4.1) or with HEPES buffer (60mM; pH 7) to a final reaction volume of 100 µl at 37°C in a shaking water bath for 45 min in presence of 1.9 mM retinyl palmitate (RP) and/or 1.5 mM D7-cholesteryl palmitate (D7-CE) incorporated into liposomes. Liposomes were made by dissolving 20 mg of L-α-phosphatidylcholine and 0.5 mg of (RP) and/or 0.5 mg of D7-CE in chloroform, and after solvent evaporation, the lipids were suspended in 1 ml of 50mM NaCl, and 10mM Tris, pH 7.4, by sonication and was centrifuged at 13000 RPM for 10 min to sediment large vesicles. The reaction was stopped by the addition of 100 µl ethanol, and lipids were determined by HPLC-MS using multiple reaction monitoring (MRM).

Analysis of neutral lipids by HPLC-MS

Lipids were extracted from a total cell homogenate of HSCs grown in a 12-well plate by the method of Bligh and Dyer [24] after addition of 200pmol tripentadecanoylglycerol as internal standard. Extracted lipids were separated in a neutral and phospholipid fraction and analyzed on HPLC-MS as described [8]. In short, the neutral lipid fraction was reconstituted in methanol/chloroform (1/1, v/v) and separated on a Kinetex /HALO C8-e column by a gradient of methanol/H$_2$O (5/5, v/v) to methanol/isopropanol (8/2, v/v). Mass spectrometry of neutral lipids (TAGs, CEs, RE, and cholesterol) was performed using Atmospheric Pressure Chemical Ionization (APCI) interface (AB Sciex Instruments, Toronto, ON, Canada) on a Biosystems API-2000 Q-trap. The system was controlled

by Analyst version 1.4.2 software (MDS Sciex, Concord, ON, Canada) and operated in positive ion mode. TAG fragments with two non-, single-, and double-labeled palmitoyl chains (16:0,16:0,x) were quantitated by counting ions with m/z of 551, 555 and 559 respectively and TAG fragments with a non- or single-labeled palmitoyl and an oleoyl chain (16:0,18:1,x) had m/z of 577 and 581 respectively. Typical TAG species quantitated were: non PUFA, 52:3 (m/z 859), and 54:3 (m/z 885); PUFA, 56:5 (m/z 909), 58:6 (m/z 935), 60:9 (m/z 957) and 62:11 (m/z 981). For the quantification of the various (deuterated) RE and CE species, we used multiple reaction monitoring (MRM) in positive ion mode by monitoring molecule specific transitions as described in Supplementary Data, Table S2. The quantitated lipids were normalized to the amount of cholesterol or protein in the same sample. Cholesterol was found to be a good marker for both recovery and cellular material, as the cholesterol/protein ratio was found to be constant during HSC culture.

RESULTS

Neutral lipid breakdown in HSCs by lysosomal acidic lipase

Lysosomal acidic lipase could play an important role in the breakdown of neutral lipids via activation of the autophagy pathway during the activation phase of HSCs. Primary rat HSCs in culture have an active autophagy pathway as judged by the relative high ratio of the lipidated to unlipidated form of the autophagy protein LC3B, (see Fig. 1B). Similar results have been described
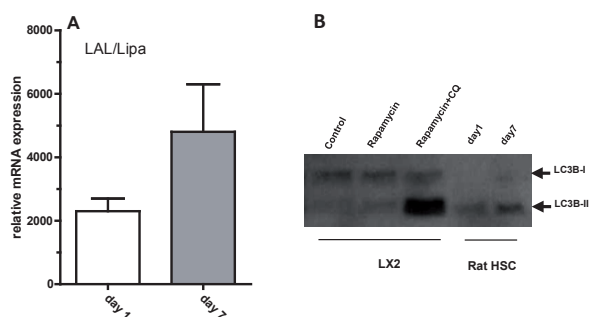
CHAPTER 4

Figure 1. Expression of Lipa and activation of autophagy in rat HSCs. A: Relative mRNA expression of lysosomal acidic lipase LAL/Lipa in quiescent (day 1; white bar) and activated (day 7; grey bar) rat HSCs was determined by qPCR. Data are the means ± SD of 3 experiments performed in duplicate. * P< 0.05 paired t-test versus day 1. B: Immunoblot probed with LC3B antibody of total proteins (10 μg) of quiescent (day 1) and activated (day 7) rat HSCs and the human stellate cell line LX2 incubated for 4 hrs with vehicle (control), the autophagy inducer rapamycin (200 nM), or rapamycin in the presence of 20 μM chloroquine to prevent breakdown of LC3B in the lysosome. LCB-I is the non-activated form, and LC3B-II is the activated form containing the lipid phosphatidyl ethanolamine. Shown is a representative blot from 3 experiments.
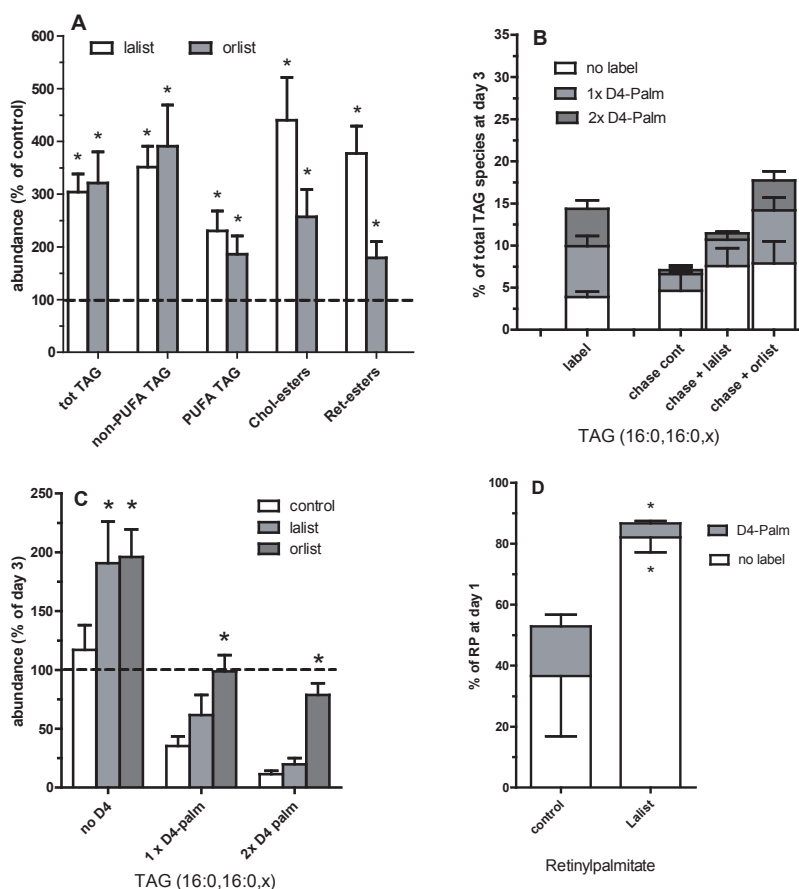
Figure 2. Effect of the lipase inhibitors lalistat and orlistat on neutral lipid levels and degradation in rat HSCs. A: Isolated rat HSCs were incubated from day 1 to day 7 in medium with 10% FBS containing vehicle (DMSO; control), 100 μM lalistat (lalist; white bars), or 40 μM orlistat (orlist; grey bars). Subsequently, neutral lipids were determined by HPLC-MS. The values were normalized to the amount of cholesterol in the sample, and expressed relative to the level of the respective lipids present in the control cells at day 7. B and C: Effect of lipase inhibitors on the breakdown of newly synthesized TAGs. Primary rat HSCs were incubated on day 1 with 25 μM D4-palmitate for 48 hrs. At day 3, part of the cells were harvested (label), and the remaining HSCs were chased for 48 hrs with normal medium with vehicle (DMSO; cont), 100 μM lalistat (lalist), or 40 μM orlistat (orlist) and harvested at day 5 (chase). B: Single or double deuterium-labeled (grey and dark grey bars) and non-labeled (white bars) TAG fragments with 2 palmitoyl chains (16:0,16:0,x) were quantitated and expressed as percentage of all TAG species. C: Shows breakdown of the labeled TAG species. The levels of the indicated TAG fragments at day 5, after the chase, were expressed relative to the level of the same TAG species at the beginning of the chase at day 3. D: Primary rat HSCs were either harvested at day 1, or incubated for 3 days with 25 μM D4-palmitate (from day 1 to day 4). Non-labeled and D4-labeled retinylpalmitate (RP) levels were quantitated by multiple reaction monitoring (MRM) and were expressed relative to the RP levels at day 1. Data are the means ± SEM of 6 experiments performed in duplicate (A) or the means ± SD of 5 (B and C) or 3 (D) experiments performed in duplicate. * P< 0.05 t-test versus control.

for mouse HSCs [12, 13]. Determination of Lipa mRNA expression in quiescent (day 1) and activated (day 7) rat HSCs shows that Lipa mRNA is upregulated during activation *in vitro* (Fig.1A).

The contribution of LAL/lipa to neutral lipid breakdown was studied by incubating rat HSCs with the LAL-specific inhibitor lalistat (100 µM) during the early activating phase (day 1 - day 7). As shown in Fig. 2A, lalistat caused a 3-4 fold increase in the levels of all neutral lipids including TAGs, CEs and REs. The effect of lalistat was compared to orlistat, a more general lipase inhibitor that was used at a concentration known to affect LAL to a lesser extent (40uM). Orlistat had a similar effect on TAG levels, but a smaller effect on CE and RE levels when compared to lalistat (Fig. 2A). We recently described the existence of two pools of TAGs in HSCs, a pre-existing pool and a highly dynamic pool that can be readily labeled by adding deuterated fatty acids to the medium [8]. To investigate the effect of the lipase inhibitors on TAG degradation in different TAG pools, we labeled freshly isolated rat HSCs for 2 days with 25 µM D4-palmitate in medium containing 10% fetal bovine serum, followed by a 2 day chase without stable isotope-labeled palmitate, but in the presence of lalistat or orlistat. As shown in Fig. 2B and 2C, a large percentage of TAGs can be labeled with D4-palmitate. In the absence of inhibitors the doubly labeled TAG species are almost completely degraded during the 2 day chase (Fig. 2A). Lalistat could not prevent the breakdown of these labeled TAGs, although both lalistat and orlistat increased the amount of unlabeled TAGs during the chase to a similar level (Fig. 2B and C). This suggests that lalistat preferentially inhibits the degradation of a pool of unlabeled, pre-existing TAGs, whereas orlistat mostly affects the breakdown of a pool of newly synthesized (i.e. labeled) TAGs.

Besides the expected massive incorporation of D4-labeled palmitate in to TAGs (cf. [8]), we also observed that approx. 30% of the retinylpalmitate (RP) was D4-labeled after a 3 day incubation with 25 µM D4-palmitate (Fig. 2D). This indicates that a significant part of the RE pool is resynthesized under our culture conditions, presumably from retinol derived from the breakdown of endogenous REs as the medium contained almost no retinol nor REs (data not shown). In line with this we found that lalistat, which was shown to inhibited the breakdown of the existing REs (Fig.1) and thus expected to prevent the release of free retinol, clearly prevented the incorporation of D4-palmitate into REs (Fig. 2D).

To verify that lalistat predominantly targets the existing pool of lipids, we limited the contribution of new, exogenous, lipids to the HSC neutral lipid pool during the inhibitor treatment by culturing the cells in medium with delipidated serum. The levels of TAG species containing PUFAs and the levels of CEs were much lower in the absence of lipids in the medium (Fig. 3A), in line with the notion that PUFA-TAGs are synthesized from exogenous PUFAs [5] and that CEs are derived from lipoproteins from te medium. The levels of non-PUFA TAGs and REs were less affected by growing the HSCs in delipidated medium. Nevertheless the levels of these non-PUFA TAGs and REs

were increased by lalistat to similar levels when compared to cells grown in normal medium (cf. Figs 2A and 3A). As expected, orlistat was less effective in raising the levels of TAG in HSCs when lipids were omitted from the medium (Figs 3A and 2A). During the incubation with delipidated medium, TAGs might be still (re)synthesized from endogenous FAs, derived from TAG and phospholipid breakdown. We therefore also studied the effect of lalistat in delipidated medium in the presence of T863, a DGAT1 inhibitor, which was shown to inhibit TAG synthesis in rat HSCs for more than 80 % [8]. When resynthesis is inhibited, the amount of non-PUFA TAGs is almost halved during the 3 day incubation, similar to the approx. 60 % decrease in RE levels (Fig. 3B). As shown in Fig. 3B, lalistat now completely prevented the degradation of these lipids, clearly indicating that this Lipa-inhibitor prevented the breakdown of existing lipids.
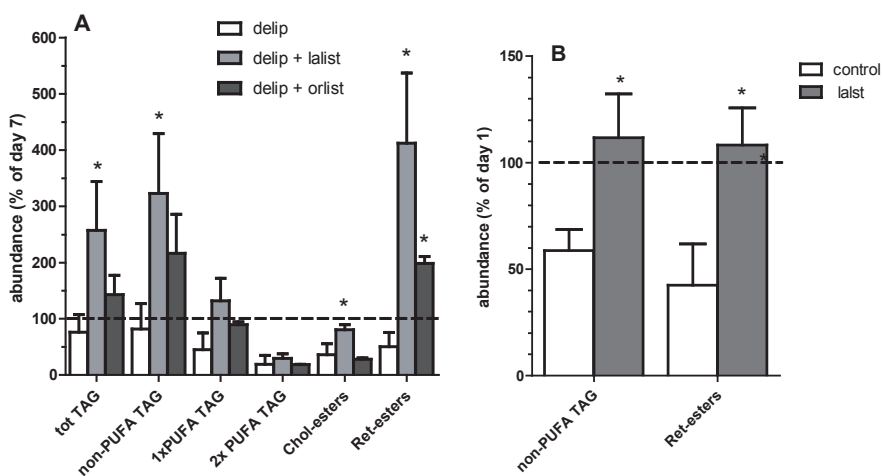

Figure 3. Effect of lalistat and orlistat on neutral lipid levels in rat HSCs in the absence of lipids in the medium. A: Isolated rat HSCs were incubated from day 1 to day 7 in medium with 10% FBS or with 10% delipidated FBS containing vehicle (DMSO; delip; white bars), 100 µM lalistat (delip lalist; grey bars), or 40 µM orlistat (delip orlist; dark grey bars). Subsequently, neutral lipids were determined by HPLC-MS. The values were normalized to the amount of cholesterol in the sample, and expressed relative to the level of the respective lipids present in the cells at day 7 incubated with normal FBS. B: Isolated rat HSCs were incubated from day 1 to day 4 in medium with delipidated FBS and 10 µM of the DGAT1 inhibitor T863, additionally containing vehicle (DMSO; control; white bars), or 100 µM lalistat (lalist; grey bars). The values were normalized to the amount of cholesterol in the sample, and expressed relative to the level of the respective lipids present in the cells at day 1. All Data are the means ± SD of 3 (A) or 4 (B) experiments performed in duplicate. * P< 0.05 paired t-test versus control.
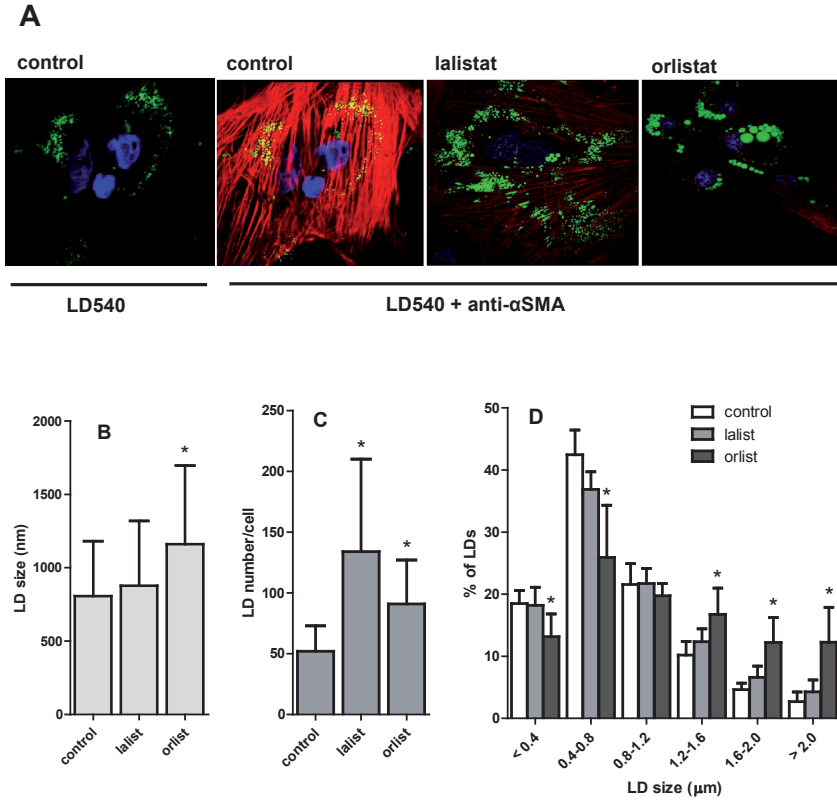
Figure 4. Effect of lalistat and orlistat on LD morphology and on the activation marker α-SMA in rat HSCs. A: Confocal images of HSCs isolated from rats incubated from day 1 to day 7 with vehicle (day7), 100 μM lalistat, or 40 μM orlistat. Lipid droplets were stained with LD540 dye (green), anti α-SMA antibody (red) and nuclei were stained with Hoechst (blue). In the first panel the red channel was omitted for better visibility of the LDs. Shown are representative pictures from 4 experiments. B, C, and D: Images were analyzed with CellProfiler v2.1.1. B: LD size was expressed in diameter (nm). C: LD numbers were expressed as a ratio of scored lipid droplets and scored nuclei per image. D: LDs distribution is expressed as percentage of LDs with the specified size (in μm). Image analysis was based on at least 50 cells and 3000 lipid droplets per condition. Data are the means ± SD. * $P < 0.05$ t-test versus control.

Examination of lipid droplet morphology in HSCs by fluorescence microscopy showed that lalistat induces an increase in the number, but not in the size of the LDs, whereas orlistat increased both these parameters resulting in a specific increase in big LDs (> 2 μm) (Fig.4). These data are in agreement with the fact that these drugs affect different lipid breakdown pathways.

To verify that lalistat inhibit lipid breakdown in the lysosomal compartment, we imaged LDs in HSCs after staining the acidic compartments with Lysotracker red (Fig 5). In control cells we observed that approx. 20 % of the lysotracker positive structures were close to RE-containing
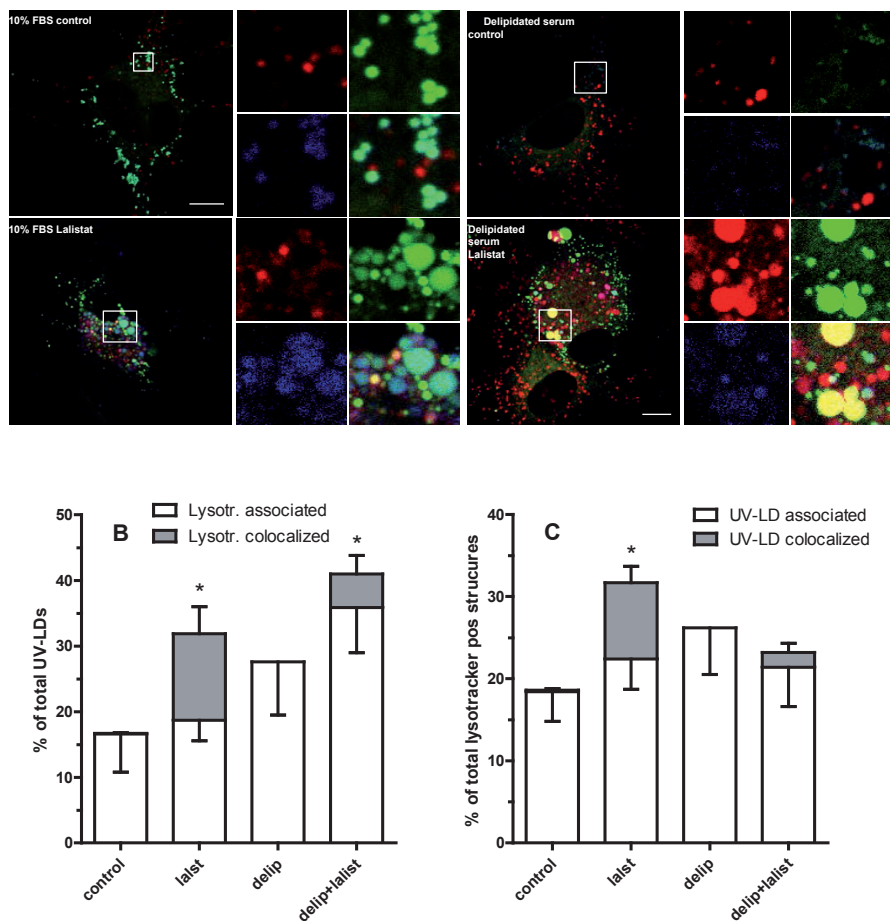
Figure 5. Lalistat increases colocalization of LD and the lysosomal compartment in rat HSCs. A: Confocal images of HSCs isolated from rats incubated from day 1 to day 4 in medium with 10% FBS or with 10% delipidated serum in the presence of vehicle (control), or 100 µM lalistat. Live HSCs were stained with Lysotracker Red DND99 (red) and Bodipy (LD dye, green) for 30 min before imaging. Blue is the UV autoflorescence signal from REs. In the boxes higher magnification of the separate channels and the merge are shown. White bar is 10 µm. B: UV-positive LDs were counted and classified manually. Classifications were: i) not in contact with Lysotracker red structures, ii) in contact or surrounded by Lysotracker red structures (Lysotr. Associated; white bars) or completely colocalized with Lysotracker red structures (Lysotr. colocalized; grey bars). C: Lysotracker red structures were counted and classified as i) not in contact with UV-positive LDs, ii) in contact or around UV-positive LDs (UV-LD associated; white bars) or colocalized with UV-positive LDs (UV-LD colocalized; grey bars). Image analysis was based on 40 cells from 4 independent experiments. Data are the means ± SEM. * P< 0.05 t-test versus control.

LDs, but colocalization was not observed. Only in the HSCs incubated with lalistat, we detected a consistent colocalization of these structures, suggesting that the lipids were inside the lysosomes (see Fig. 5). After incubation with lalistat, we also noticed HSCs that clearly contained two populations of LDs, one that contained retinoids (UV autofluorescent) and one that did not (Fig. 5A and Supplementary data Fig. S1). Typically, the latter population was localized at the periphery of the cell, whereas the former was present around the nucleus together with the Lysotracker red positive structures.

Since endogenous lipids are thought to traffic to the lysosomal compartment by the autophagy pathway, we tried to compare the effect of lalistat in rat HSCs with that of the autophagy inhibitors 3-Methyladenine (5 mM) and Bafilomycin A1 (7.5 nM) and the inhibitor of lysosomal degradation chloroquine (5 uM). However all the inhibitors caused massive death of the rat HSCs within 12 hrs. These doses were effective in other cells including the LX-2 human stellate cell line and did not affect the viability of the LX-2 cells (Fig 1B; results not shown). When we studied the autophagy inhibitors in rat HSCs at lower concentrations that were tolerated, we could not find an effect of these inhibitors on autophagy or lysosomal acidification as analyzed with the LC3B I to II ratio and imaging with Lysotracker red (results not shown), suggesting that autophagy is essential for activated rat HSCs under our culture conditions.

Retinyl ester breakdown in HSCs by lysosomal acidic lipase

The observed inhibitory effect of lalistat on RE degradation is surprising as RE hydrolytic (REH) activity has not yet been attributed to the Lipa gene product. An acidic REH has been described that was different from LAL/Lipa as judged from its insensitivity to bivalent metal ions like Ca^{2+} and Mg^{2+} [23, 25]. We also found that the main REH in an homogenate of rat HSCs and rat hepatocytes has an optimum at pH 4 (Figs 6A and 6B). However we could not observe a difference in inhibition by bivalent cations between the REH in comparison to the CE hydrolase activity, assayed simultaneously (Fig. 6B). We also found that both activities were inhibited by lalistat (Fig. 6B), with a similar IC_{50} around 1-3 μM. Furthermore, the acidic REH activity was absent in liver homogenates from Lipa^{-/-} mice and could be induced in CHO homogenates by transfecting the CHO cells with recombinant rat Lipa (Figs 6C and 6D). These latter experiments clearly show that Lipa has REH activity *in vitro*.
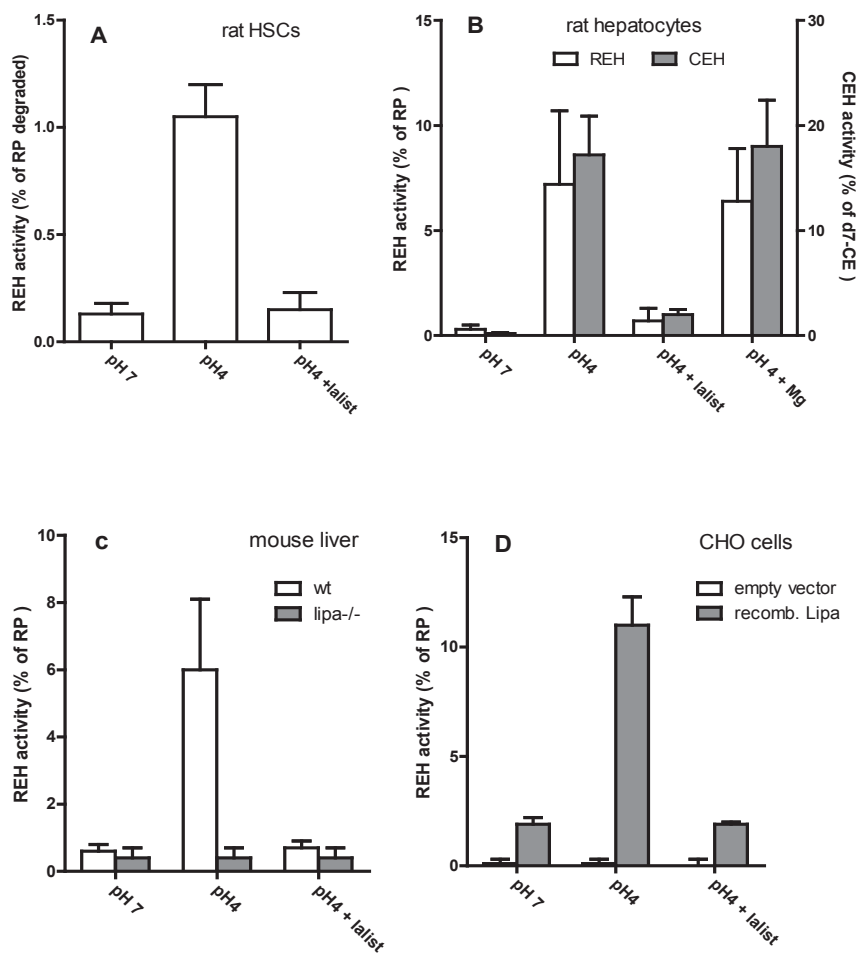
Figure 6. LAL/Lipa has retinyl esterase activity in vitro. Retinyl esterase activity (REH) was assayed with RP presented in liposomes as substrate in a buffer with pH 7, pH 4 and pH 4 containing 10 µM lalistat, or pH4 containing 10 mm MgCl2 in homogenates of A: primary rat HSCs cultured for 4 days (16 µg of protein), B: freshly isolated rat hepatocytes (400 µg of protein), C: whole mouse livers (400 µg of protein). or D: cultured CHO cells 1 day after transfection with an empty expression vector or with an expression vector containing rat Lipa cDNA (40 µg of protein). In B cholesterol esterase activity (CEH) was assayed with D7-cholesterol oleate as substrate presented in liposomes together with RP. Free retinol, RP, D7-cholesterol, and D7-CE levels were quantitated by HPLC-MS in the multiple reaction monitoring (MRM) mode. Retinol and D7-cholesterol were expressed relative to the levels of their respective esters present at the start of the incubation. Data are the means ± SD of 3 experiments performed in duplicate.
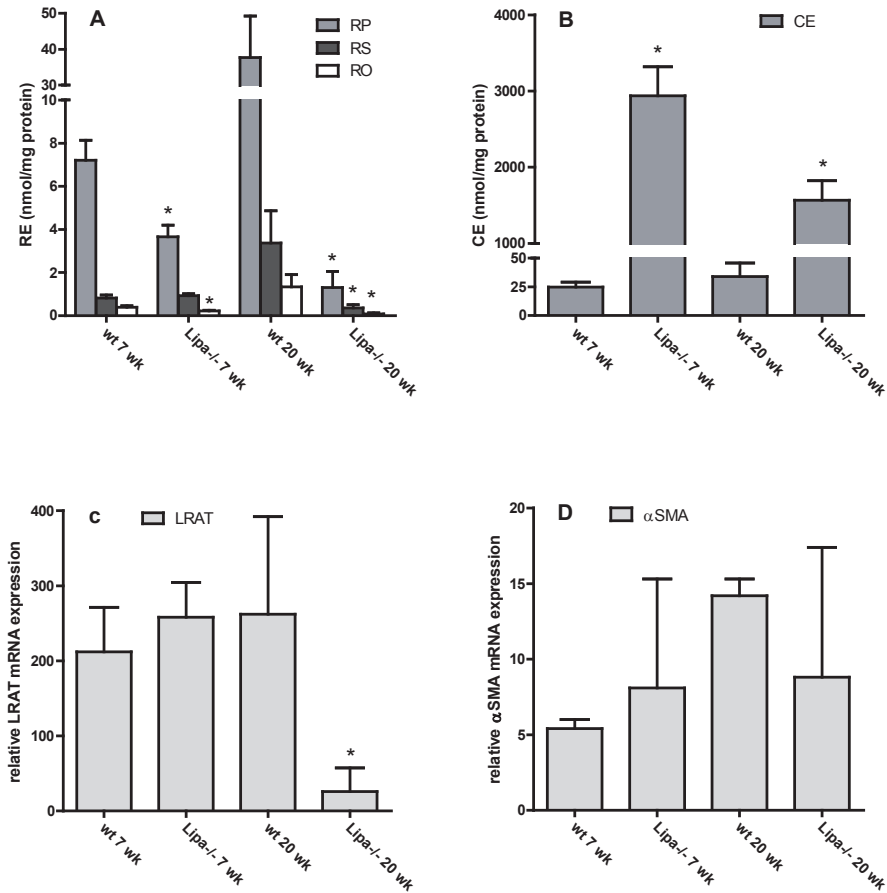
Figure 7. Retinyl esters do not accumulate in livers of LAL-deficient mice. Livers were obtained from either wt and Lipa-/- mice at an age of 7 weeks (wk) or between 4 and 5 months (20 wk). A: Retinyl palmitate (RP; grey bars panel A), retinyl stearate (RS; dark grey bars) and retinyl oleate (RO; white bars) and CEs (panel B) were quantitated by HPLC-MS in the multiple reaction monitoring (MRM) mode, and the relative mRNA expression of LRAT (a marker for quiescent HSCs; panel C) and α-SMA (HSC activation marker; Panel D) was measured by qPCR. Data are the means ± SD of 5 mice (20 wk) or 4 mice (7 wk), assayed in duplicate. * P< 0.05 t-test versus wt.

CHAPTER 4

To investigate the effect of Lipa on RE metabolism in HSCs, we attempted to isolate HSCs from Lipa$^{-/-}$ mice. However, isolation of Lipa$^{-/-}$ HSCs was not possible, most likely due to the massive accumulation of lipids in the Lipa-/- livers [16]. Therefore, we analyzed the RE content in livers of Lipa deficient and corresponding wt mice. We found that despite the 100-fold higher levels of CEs, the levels of the REs were similar (retinyl stearate) or lower (retinyl palmitate and retinyl oleate) in the livers of 7 week old Lipa$^{-/-}$ mice (Fig 7A,7B). In older mice (4 to 5 months; average 20 weeks), the difference between the wt and the Lipa deficient mice became even larger, as the wt mice continued to accumulate REs and the Lipa$^{-/-}$ mice lost most of their REs (Fig 7A).

The low levels of REs in the livers of the 4-5 months old Lipa$^{-/-}$ mice were accompanied by a decrease in the expression LRAT mRNA, considered a marker for quiescent HSCs [26], but not by an upregulation of the HSC activation marker α-smooth muscle actin (α-SMA; Figs 7C and 7D). This suggests that the livers of the Lipa$^{-/-}$ mice gradually lose their quiescent HSCs.
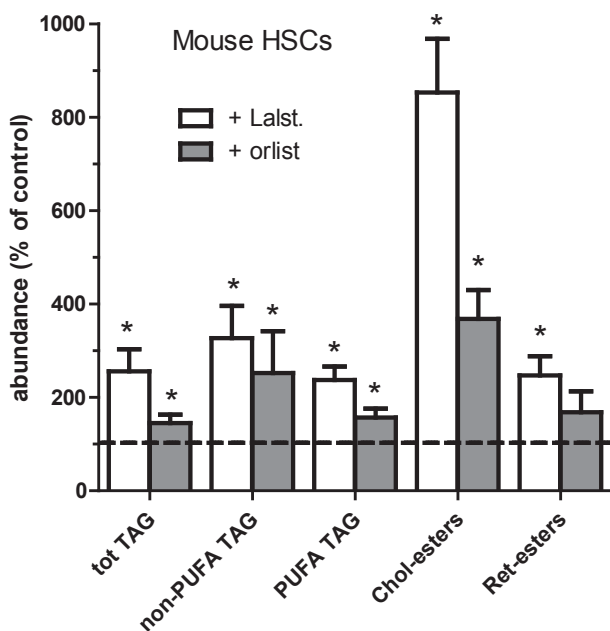
Figure 8. Effect of the lipase inhibitors lalistat and orlistat on neutral lipid levels in mouse HSCs. Isolated mouse HSCs were incubated from day 1 to day 7 in medium with 10% FBS containing vehicle (DMSO; control), 100 µM lalistat (lalist; white bars), or 40 µM orlistat (orlist; grey bars). Subsequently, neutral lipids were determined by HPLC-MS. The values were normalized to the amount of cholesterol in the sample, and expressed relative to the level of the respective lipids present in the control cells at day 7. Data are the means ± SEM of 6 experiments performed in duplicate. * P< 0.05 t-test versus control.

To exclude that the apparent discrepancy between the lack of effect of Lipa knock out in mice *in vivo* on RE storage and the observed effect of the Lipa-inhibitor lalistat on RE levels in rat HSCs *in vitro* is caused by species differences between rat and mouse, we compared the effect of lalistat on neutral lipid levels in primary mouse HSCs in cultured for 6 days with its effect on rat HSCs (Fig. 2A). As shown in Fig. 8, we found that lalistat also caused an increase in TAGs, CEs and REs in mouse HSCs. In comparison to rat HSCs, the lalistat-induced increase in RE level in mouse was somewhat lower (2.5-fold versus almost 4-fold). As also shown in Fig. 8, orlistat was less effective in mouse HSCs compared to lalistat in increasing the levels of TAGs, CEs and REs.

Lalistat and HSC activation

We determined the effect of lalistat and orlistat on HSC activation. We observed a clear inhibition of the expression of the activation marker α-SMA by both lalistat and orlistat in rat HSCs, both on protein and mRNA level (Figs 4A and 9). In mouse HSCs lalistat, but not orlistat, inhibited HSC activation (Fig. 9). The lack of inhibition of orlistat in the activation of mouse HSCs is surprising as it has been reported that TAG degradation is required for the generation of FAs for energy during HSC activation in mouse stellate cell line JS1 [13]. We therefore tested whether FAs derived from TAGs are required for the energy demand of rat HSCs under our culture conditions, by treating
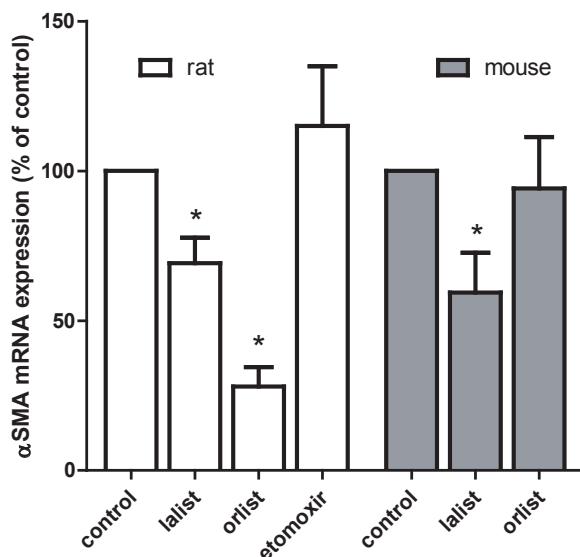
Figure 9. Effect of alterations in neutral lipid metabolism on activation of rat and mouse HSCs. Relative gene expression of α-SMA (HSC activation marker) was measured by qPCR. HSCs isolated from rats or mice were incubated from day 1 to day 7 with vehicle (DMSO; control), 100 µM lalistat (lalist), 40 µM orlistat (orlist) or 50 µM etomoxir (etomox). Relative mRNA levels of α-SMA were expressed relative to the levels in the control-treated cells (n=5). Data are the means ± SD. * P< 0.05 t-test versus control.

the cells with etomoxir, an inhibitor of FA oxidation. However we did not observe an effect of this inhibitor on rat HSC activation (Fig. 9), although we could see a two-fold increase in TAG levels in the presence of this FA oxidation-inhibitor (results not shown). Thus, we consider it more likely that the hydrolysis of a specific lalistat-sensitive pool of TAGs is involved in HSC activation.

DISCUSSION

We here show that lalistat, a specific inhibitor of the Lipa gene product LAL, affects the levels of three classes of neutral lipids, i.e CEs, TAGs and REs, in rat and mouse HSCs. The lalistat-induced increase in CEs is in line with the established function of LAL in degrading CEs from lipoproteins in the lysosome [16, 17]. As expected the increase was much lower in medium depleted of lipoproteins. The residual increase in the absence of exogenous lipoproteins may be caused by inhibiting the degradation of CEs delivered to the lysosome by the autophagy pathway, similarly as has been described in macrophages [14, 27]. Orlistat was less potent in comparison to lalistat in inhibiting the breakdown of CEs, indicating that it inhibited LAL to a lesser degree in HSCs at the concentration used.

LD pools

The comparison between the effects of the inhibitors lalistat and orlistat on TAG levels clearly indicated the existence of different pools of TAGs. Orlistat was more potent at inhibiting the degradation of newly synthesized TAGs, as judged from its large inhibitory effect on the breakdown of labeled TAGs. In contrast, lalistat was more potent in inhibiting the "old"/pre-existing lipid pool as it did not inhibit the degradation of newly labeled TAGs, but prevented the breakdown of existing TAGs, when new TAG synthesis was blocked. We have additional evidence for metabolically different TAG pools in HSCs from studies with ATGL^{-/-} mice and the DGAT1 inhibitor T863 [8]. We there reported that the TAG lipase ATGL specifically targets newly synthesized TAGs, made preferential by DGAT1 in combination with ACSL4, and thus enriched in PUFAs. These newly formed TAGs are likely to form new LDs. Now, in the presence of lalistat, we also observe two pools of LDs by live cell-imaging of rat HSCs. One containing retinoids, located predominately around the nucleus and a pool present in the periphery of the HSCs that did not contain REs. The combined breakdown of LDs in one place and resynthesis in another, would explain our previous observations in activated rat HSCs i.e. that LDs reduce in size, but increase in number and are localized in cellular extensions [4]. We originally speculated that the new small LDs were caused by fission of the ''old'/large LDs and subsequent extensive migration to the periphery, as we observed by Raman spectroscopy that in activated rat HSCs all LDs had a similar lipid spectrum containing a low amount of REs [4]. To explain that both the new and the old LDs contain small amounts of REs at day 7, we have to

assume that REs are incorporated in the new LDs. From D4-palmitate labeling studies we have now evidence that indeed REs, like TAGs, are partly resynthesized during activation.

The lipase inhibitors orlistat and lalistat also caused a different effect on the morphology of the LDs. Lalistat increased the number but not the size of the LDs, whereas orlistat and Atglstatin [8] also increased the size of the LDs. This suggests that inhibition of lipase activity on the new LDs allow them to grow beyond a certain limit maintained under normal conditions by the consorted action of the TAG synthesizing enzyme (presumably DGAT1) and the TAG degrading activity (presumably ATGL). If we assume that Lipa/LAL is the predominant target of Lalistat, and that the cytosolic TAG is routed to the lysosomes by autophagy [12, 13], this would implicate that the autophagy pathway engulfs lipid fragments of the size of the new LDs around 0.8 µm (Figure 4B). This would be compatible with the reported sizes of autophagosomes ranging between 0.50 and 1.5 µm [28, 29], and with the observation in rat HSCs analyzed by EM, that the sub population of LDs that was surrounded by lysosomes, was smaller than the cytosolic LDs [30].

Lipa and retinyl ester hydrolysis

Besides inhibiting the degradation of CEs and TAGs, lalistat proved to be potent inhibitor of RE degradation. As we observed REs in the acidic compartment after treatment with lalistat, a lysosomal lipase is involved in the breakdown of REs in activated HSCs. The most likely REH is Lipa/LAL and we found that it has clear REH activity *in vitro*. The REs are most likely delivered to the lysosomes by the autophagy pathway known to be active in activated HSCs [12, 13] (Figure 1). Unfortunately we could not quantitatively asses the contribution of the autophagy pathway in the degradation of REs since inhibitors of this pathway affected the viability of the rat and mouse HSCs under our conditions.

The presence of a non Lipa/non-autophagy degradation pathway for REs likely exist in mouse HSCs. RE levels in mouse HSC drop by approx. 90 % from day 1 to day 7 [8], implying that only 10 % is left at day 7. The 2.5-fold increase seen in the presence of lalistat indicates that still 75% of the RE pool has disappeared from the mouse HSCs in the presence of the LAL-inhibitor. For comparison, rat HSCs at day 7 still have 30-20 % of the RE content of day 1 in the absence of lalistat [4], and retain most of their REs in the presence of this inhibitor (Fig 3B). A number of neutral carboxyl esterases was found to have REH activity, including ES4, ES10 and ES22 [31]. The patatin-like phospholipase domain-containing 3 (PNPLA3) protein was also shown to have retinyl-palmitate lipase activity in human hepatic stellate cells [32]. However the relative contribution of any of these enzymes in RE degradation in HSCs upon activation is unknown.

CHAPTER 4

Lipa and HSC function

Despite the absence of LAL, a clear decrease of REs was found in livers from 20 week old mice as compared to livers of younger mice (7 weeks old). this could indicate the presence of a different REH activity but it turned out to be related to the presence of HSCs per se. Retinoid storage in the liver is thought to be comprised of two stages. First REs packaged in chylomicron remnants are taken up by hepatocytes and degraded in a non-lysosomal compartment [33]. Subsequently, retinol is transferred from the hepatocytes to HSCs, where it is esterified by LRAT and stored in LDs [31]. The absence of a role of Lipa/lysosomal compartment in the uptake RE in the liver was also suggested by our observation that the RE levels in the livers of the young (7 week old mice) Lipa^{-/-} mice were not accumulated as was observed for the cholesterol levels, but were even somewhat lower. As LRAT expression was not affected in the young Lipa^{-/-} mice, the REs are presumably stored predominantly in HSCs similarly as in wt mice. The observed loss of REs in the older mice (week 20) is however most likely occurring in HSCs of the liver. This is corroborated by the concomitant loss of LRAT, a marker for quiescent HSCs [26]. The HSCs were not yet fully activated in the 20 week old *Lipa*^{-/-} mice, as we found no upregulation of the HSC activation marker α-SMA. In earlier studies on the Lipa^{-/-} mice it was described that in young mice (1.5 months) lipid (CE/TAG) was predominantly accumulated in hepatocytes, but that in older mice (5-8 months) macrophages, became the major lipid storing cells [34]. This suggests that the influx of macrophages might be the cause of the disappearance of quiescent HSCs in the 20 week old Lipa^{-/-} mice. The absence of quiescent HSCs is probably followed by a fibrotic stage as in older (24 weeks) Lipa-deficient mice clear liver fibrosis was detected [35]. Likewise humans with mutations in Lipa are known to develop liver fibrosis [17].

The effect of lalistat and orlistat on lipid levels in rat and mouse HSCs generally correlated with their effect on HSC activation. Lalistat increased all classes of neutral lipids in both rat and mouse HSCs and attenuated activation in rat and mouse HSCs to a similar, albeit relatively low degree (30-40%, Fig. 9). Orlistat was more potent in rat HSCs as compared to mouse cells, both in increasing neutral lipid levels and preventing activation. The inhibitory effect of lalistat and orlistat on rat HSC activation was comparable to the effect of another lipase inhibitor, Atglistatin [8]. In comparison with lalistat, Atglistatin is more potent in inhibiting TAG breakdown, but less potent in preventing RE and CE degradation. Although we cannot exclude the possibility that these drugs affect HSCs activation by other, non-lipid related pathways, their effects on HSC activation correlated with their effect on of neutral lipid breakdown. Therefore, it seems that HSCs require an available TAG/RE pool for optimal functioning. This pool may act as a buffer for FAs required for energy [13], or synthesis of membranes or bioactive lipids, like prostanoids. In rat HSCs we could not find evidence for a requirement for FA as source of energy, as the beta–oxidation inhibitor etomoxir did not affect activation. Another possibility would be that the neutral lipids by their physical presence in the cytosol, interfere with adaptations needed for activation, like ER and

Golgi expansion. This would also explain that mouse HSCs containing almost no LDs by a lack of LRAT show a normal activation response to liver injury [26].

ACKNOWLEDGEMENTS

CHAPTER 4

REFERENCES

1. Blaner, W. S. *et al*. (2009). Hepatic stellate cell lipid droplets: a specialized lipid droplet for retinoid storage. *Biochim. Biophys. Acta* **1791**, 467-473.

2. Friedman, S. L. (2008). Hepatic stellate cells: protean, multifunctional, and enigmatic cells of the liver. *Physiol. Rev.* **88**, 125-172.

3. Pellicoro, A., Ramachandran, P., Iredale, J. P. & Fallowfield, J. A. (2014). Liver fibrosis and repair: immune regulation of wound healing in a solid organ. *Nat. Rev. Immunol.* **14**, 181-194.

4. Testerink, N. *et al*. (2012). Replacement of retinyl esters by polyunsaturated triacylglycerol species in lipid droplets of hepatic stellate cells during activation. *PLoS One* **7**, e34945.

5. Tuohetahuntila, M. *et al*. (2015). Role of long-chain acyl-CoA synthetase 4 in formation of polyunsaturated lipid species in hepatic stellate cells. *Biochim. Biophys. Acta* **1851**, 220-230.

6. Wilfling, F., Haas, J. T., Walther, T. C. & Farese, R. V.,Jr. (2014). Lipid droplet biogenesis. *Curr. Opin. Cell Biol.* **29**, 39-45.

7. Long, A. P. *et al*. (2012). Lipid droplet de novo formation and fission are linked to the cell cycle in fission yeast. *Traffic* **13**, 705-714.

8. Tuohetahuntila, M. *et al*. (2016). ATGL and DGAT1 are involved in the turnover of newly synthesized triacylglycerols in hepatic stellate cells. *J. Lipid Res.*

9. Zechner, R., Kienesberger, P. C., Haemmerle, G., Zimmermann, R. & Lass, A. (2009). Adipose triglyceride lipase and the lipolytic catabolism of cellular fat stores. *J. Lipid Res.* **50**, 3-21.

10. Schweiger, M., Lass, A., Zimmermann, R., Eichmann, T. O. & Zechner, R. (2009). Neutral lipid storage disease: genetic disorders caused by mutations in adipose triglyceride lipase/PNPLA2 or CGI-58/ABHD5. *Am. J. Physiol. Endocrinol. Metab.* **297**, E289-96.

11. Mello, T. *et al*. (2008). Expression of carboxylesterase and lipase genes in rat liver cell-types. *Biochem. Biophys. Res. Commun.* **374**, 460-464.

12. Thoen, L. F. *et al*. (2011). A role for autophagy during hepatic stellate cell activation. *J. Hepatol.* **55**, 1353-1360.

13. Hernandez-Gea, V. *et al*. (2012). Autophagy releases lipid that promotes fibrogenesis by activated hepatic stellate cells in mice and in human tissues. *Gastroenterology* **142**, 938-946.

14. Ouimet, M. *et al*. (2011). Autophagy regulates cholesterol efflux from macrophage foam cells via lysosomal acid lipase. *Cell. Metab.* **13**, 655-667.

15. Brown, M. S. & Goldstein, J. L. (1986). A receptor-mediated pathway for cholesterol homeostasis. *Science* **232**, 34-47.

16. Du, H., Duanmu, M., Witte, D. & Grabowski, G. A. (1998). Targeted disruption of the mouse lysosomal acid lipase gene: long-term survival with massive cholesteryl ester and triglyceride storage. *Hum. Mol. Genet.* **7**, 1347-1354.

17. Anderson, R. A., Bryson, G. M. & Parks, J. S. Lysosomal acid lipase mutations that determine phenotype in Wolman and cholesterol ester storage disease. *Mol. Genet. Metab.* **68**, 333-345 (1999).

18. Rosenbaum, A. I. *et al*. (2009). Chemical screen to reduce sterol accumulation in Niemann-Pick C disease cells identifies novel lysosomal acid lipase inhibitors. *Biochim. Biophys. Acta* **1791**, 1155-1165.

19.   Rosenbaum, A. I. *et al*. (2010). Thiadiazole carbamates: potent inhibitors of lysosomal acid lipase and potential Niemann-Pick type C disease therapeutics. *J. Med. Chem.* **53**, 5281-5289.

20.   Hamilton, J., Jones, I., Srivastava, R. & Galloway, P. (2012). A new method for the measurement of lysosomal acid lipase in dried blood spots using the inhibitor Lalistat 2. *Clin. Chim. Acta* **413**, 1207-1210.

21.   Riccalton-Banks, L., Bhandari, R., Fry, J. & Shakesheff, K. M. (2003). A simple method for the simultaneous isolation of stellate cells and hepatocytes from rat liver tissue. *Mol. Cell. Biochem.* **248**, 97-102.

22.   van Steenbeek, F. G. *et al*. (2013). Aberrant gene expression in dogs with portosystemic shunts. *PLoS One* **8**, e57662.

23.   Mercier, M., Forget, A., Grolier, P. & Azais-Braesco, V. (1994). Hydrolysis of retinyl esters in rat liver. Description of a lysosomal activity. *Biochim. Biophys. Acta* **1212**, 176-182.

24.   Bligh, E. G. & Dyer, W. J. (1959). A rapid method of total lipid extraction and purification. *Can. J. Biochem. Physiol.* **37**, 911-917.

25.   Azais-Braesco, V. *et al*. (1995). Vitamin A contained in the lipid droplets of rat liver stellate cells is substrate for acid retinyl ester hydrolase. *Biochim. Biophys. Acta* **1259**, 271-276.

26.   Kluwe, J. *et al*. (2011). Absence of hepatic stellate cell retinoid lipid droplets does not enhance hepatic fibrosis but decreases hepatic carcinogenesis. *Gut* **60**, 1260-1268.

27.   Robinet, P., Ritchey, B. & Smith, J. D. (2013). Physiological difference in autophagic flux in macrophages from 2 mouse strains regulates cholesterol ester metabolism. *Arterioscler. Thromb. Vasc. Biol.* **33**, 903-910.

28.   Bains, M., Florez-McClure, M. L. & Heidenreich, K. A. (2009). Insulin-like growth factor-I prevents the accumulation of autophagic vesicles and cell death in Purkinje neurons by increasing the rate of autophagosome-to-lysosome fusion and degradation. *J. Biol. Chem.* **284**, 20398-20407.

29.   Mizushima, N., Ohsumi, Y. & Yoshimori, T. (2002). Autophagosome formation in mammalian cells. *Cell Struct. Funct.* **27**, 421-429.

30.   Yamamoto, K. & Ogawa, K. (1983). Fine structure and cytochemistry of lysosomes in the Ito cells of the rat liver. *Cell Tissue Res.* **233**, 45-57.

31.   Schreiber, R. *et al*. (2012). Retinyl ester hydrolases and their roles in vitamin A homeostasis. *Biochim. Biophys. Acta* **1821**, 113-123.

32.   Pirazzi, C. *et al*. (2014). PNPLA3 has retinyl-palmitate lipase activity in human hepatic stellate cells. *Hum. Mol. Genet.* **23**, 4077-4085.

33.   Blomhoff, R., Eskild, W., Kindberg, G. M., Prydz, K. & Berg, T. (1985). Intracellular transport of endocytosed chylomicron [3H]retinyl ester in rat liver parenchymal cells. Evidence for translocation of a [3H] retinoid from endosomes to endoplasmic reticulum. *J. Biol. Chem.* **260**, 13566-13570.

34.   Du, H. *et al*. (2001). Lysosomal acid lipase-deficient mice: depletion of white and brown fat, severe hepatosplenomegaly, and shortened life span. *J. Lipid Res.* **42**, 489-500.

35.   Sun, Y. *et al*. (2014). Reversal of advanced disease in lysosomal acid lipase deficient mice: a model for lysosomal acid lipase deficiency disease. *Mol. Genet. Metab.* **112**, 229-241.

CHAPTER 4

SUPPLEMENTARY DATA

Table1. Rat primer sequence for the target genes used in qPCR

Gene	Accession Number	Forward primer 5 → 3	Reverse primer 5 → 3	Tm
α-SMA	NM_031004	AGATGGCGTGACTCACAACGTG	AGGAATAGCCACGCTCAGTCAG	65ºC
Lipa	NM_012732	TCACAGATGCCTGAACTGGCAAAG	TGCTTCTGCCCAAACAAGTCCTC	63ºC

Mouse primer sequence for the target genes used in qPCR

Gene	Accession Number	Forward primer 5 → 3	Reverse primer 5 → 3	Tm
α-SMA	NM_007392	TCTTCCAGCCATCTTTCATTGGG	CCTGACAGGACGTTGTTAGCATAG	61ºC
Lrat	NM_023624	CAGATATGGCTCTCGGATCAG	GACAATAGATGCTAATCCCAAGAC	65ºC

Table 2. MRM-transitions of HPLC-MS/MS

Analyte	Q1	Q3	dwell time	declustering potential	collision energy
	(m/z)	(m/z)	(msec)	(V)	(V)
cholesterol, cholesteryl esters	369.3	287.3	20	80	27
D7-cholesterol, D7-cholesteryl esters	376.3	293.3	20	80	27
retinol, retinyl esters	269.2	93.1	100	50	33
retinyl palmitate (C16:0)	525.5	269.2	150	75	26
retinyl palmitate-D4 (C16:0-D4)	529.5	269.2	150	75	26
retinyl oleate (C18:1)	551.5	269.2	150	75	26
retinyl stearate (C18:0),	553.5	269.2	150	75	26
retinyl arachidonate (C20:4)	573.6	269.2	150	75	26
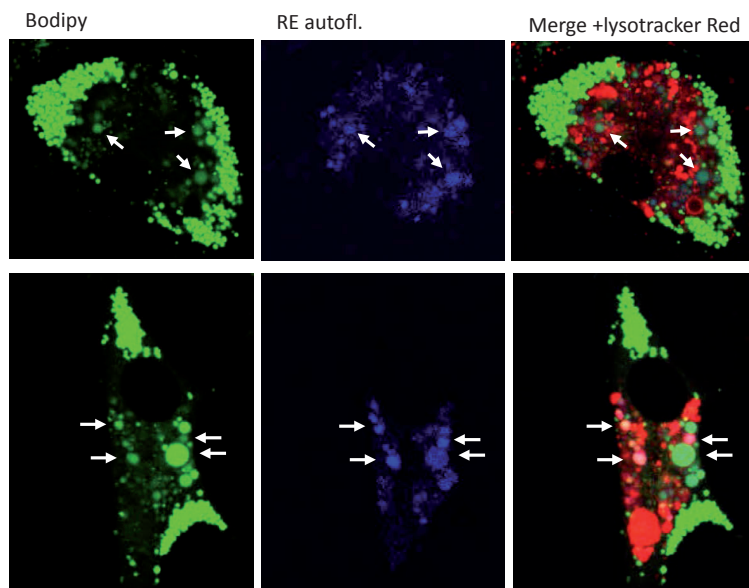
Figure S1. Lalistat induces two population of LDs in rat HSCs. Confocal images of HSCs isolated from rats incubated from day 1 to day 4 in medium with 10% FBS serum in the presence of 100 μM lalistat. Live HSCs were stained with Lysotracker Red DND99 (red) and Bodipy (LD dye, green) for 30 min before imaging. Blue is the UV autoflorescence signal from REs. White arrows point out some RE-containing LDs.

Chapter

Role of eicosanoid secretion in mouse and rat hepatic stellate cell activation

5

Maidina Tuohetahuntila[1], Pawel W. Stachowiak[1],
Chris H. van de Lest[1], Christian Wolfrum[2], Martin Houweling[1],
Arie B. Vaandrager[1], and J. Bernd Helms[1]

[1] Department of Biochemistry and Cell Biology, Faculty of Veterinary Medicine
& Institute of Biomembranes, Utrecht University, Utrecht, The Netherlands.

[2] Swiss Federal Institute of Technology, ETH Zürich, Institute of Food Nutrition
and Health, Schwerzenbach, Switzerland

ABSTRACT

Liver fibrosis is mediated by a complex interplay of both pro- and anti-fibrotic factors, including eicosanoids like prostaglandins (PGs) and leukotrienes (LTs). Hepatic stellate cells (HSCs) play a central role in liver fibrosis as they can transdifferentiate into a myofibroblastic state. During this so-called activation, HSCs were shown to accumulate arachidonic acid, a known precursor for eicosanoid production. To assess whether HSCs can be a source of eicosanoids during liver fibrosis, we analyzed the eicosanoid secretion pattern of primary mouse and rat HSCs by HPLC-MS. We observed that quiescent mouse and rat HSCs can secrete substantial amounts of prostanoids, predominantly PGE_2 and PGD_2, but almost no LTs. Upon activation, the profile, but not the total amount of the prostanoids has changed, and this change was different in mouse and rat cells. Notably, in activated mouse HSCs, PGI_2/prostacyclin secretion was upregulated, but in activated rat HSCs, thromboxane A_2 synthesis was increased. Overall there was a good correlation between the changes in secretion of a specific prostanoid and the mRNA expression level of its respective synthase. Inhibitors of PG synthesis, indomethacin and celecoxib, did not affect expression of the activation marker α-SMA in HSCs at concentrations that inhibited PG secretion. However, exogenous PGE_2 stimulated rat HSCs activation. In conclusion this study shows that HSCs can be an important source of PGs and that PGs can affect HSC activation during liver injury and repair.

Keywords: Hepatic stellate cells, prostaglandins, eicosanoids, lipidomics, gene expression

INTRODUCTION

Hepatic stellate cells (HSCs), perisinusoidal mesenchymal cells residing in the subsinusoidal space of Disse, are the primary effector cells that play a pivotal role in the fibrogenic cascade [1]. They represent 5-8% of the total number of resident cells in normal liver [2]. In a healthy liver, HSCs are found in the quiescent state functioning to store vitamin A in the form of retinyl esters together with triacylglycerol (TAG) and cholesteryl esters in their lipid droplets (LDs). Upon liver injury, the number of activated HSCs dramatically increases at sites of inflammation, thus promoting excessive deposition of extracellular matrix components, predominantly type I collagen [3]. A number of compounds derived from the injured hepatocytes or activated Kupffer cells may initiate this transition, such as transforming growth factor beta (TGF-β). Production of TGF-β and other hormones by activated HSCs can further stimulate the transdifferentiation in an autocrine manner, leading to the formation of scar tissue in the liver [1-3].

During the transdifferentiation into myofibroblasts, HSCs gradually lose their LDs. We previously reported that LD degradation in activated HSCs is a highly dynamic and regulated process [4, 5]. During the first 7 days of HSC culture, the LDs reduce in size. In addition, small LDs appear at cellular extensions in this first phase, before all LDs disappear in a later phase. During the initial phase of HSC activation, the retinyl esters disappear and concomitantly, a large and specific increase in poly-unsaturated fatty acid (PUFA)-containing TAG species was observed. The increase in PUFA-TAGs was caused by a large increase in the uptake of PUFAs including arachidonic acid (AA) [4]. Elevation of TAG-PUFA species may be physiologically relevant as storage pools for PUFAs, waiting to be incorporated in phospholipids (PLs) [6]. Phospholipids containing PUFAs render the membrane more flexible, which reduces the energy required for deformation [7]. Elevation of PUFA-TAGs may also be relevant as a source of AA for eicosanoid synthesis. Eicosanoids are signaling lipids that play a role in a broad range of processes, such as modulation of inflammation and blood pressure [8]. In white blood cells there are significant correlations between lipid droplet formation and enhanced eicosanoid generation [9], suggesting that the presence of LDs in cells, as observed in HSCs, enhances the capacity to secrete eicosanoids.

Eicosanoid synthesis typically starts with the release of AA from the sn-2 position of PLs by specific Ca^{2+}-dependent phospholipases in response to hormones/cytokines [10]. Subsequently AA is converted to various eicosanoids like prostaglandins (PGs), thromboxanes (TXs), or leukotrienes (LTs), depending on the relative activity of their respective synthases [8, 11]. The first step in the synthesis of prostaglandins and thromboxanes is catalyzed by prostaglandin-endoperoxide synthase (PTGS) 1 and/or 2, which convert AA into prostaglandin H_2. These enzymes are also known as COX-1 and COX-2, respectively. COX-1 (PTGS1) is constitutively expressed in most cells, whereas COX-2 (PTGS2) is induced during stimulation. COX-2 is a key executor of inflammation and its

inhibition represents a major target in the treatment of inflammatory disorders [12]. It was reported that human HSCs express COX-2 only after activation, suggesting that the COX-2 pathway has a role in hepatic fibrogenesis [13]. Prostaglandin H_2 is subsequently converted into the various prostaglandins and thromboxanes by different synthases named after their main product. Some of the produced eicosanoids are rather labile and are non-enzymatically converted to more stable metabolites. For example, 6-keto-$PGF_{1\alpha}$ and thromboxane B_2 (TXB_2) are derived by hydrolysis of prostacyclin (prostaglandin I_2) and TXA_2, respectively [8].

The synthesis of leukotrienes (LTs) starts with the conversion of AA by various lipoxygenases (LOXs) into hydroxyeicosatetraenoic acids (HETEs). The potent bioactive leukotrienes, LTB_4 and the cysteinyl leukotrien LTC_4, for instance, are derived from 5-hydroxyeicosatetraenoic acid (5-HETE), the product of the conversion of AA by 5-LOX [14].

Studies with inhibitors of eicosanoid producing enzymes, like PTGS1 and 2 and 5-LOX, or with mice with genetic alterations in these enzymes, point to important, although as yet conflicting, roles of eicosanoids in liver fibrosis [15-21]. Some studies point to a protective effect of eicosanoids against liver fibrosis [15, 16, 19, 21], whereas others report a contributing function of these inflammatory agents to liver fibrosis [17, 20]. Yet some report no effects of eicosanoids produced by PTGS2/COX-2 on liver fibrosis [18].

Due to the multitude of cell types in the liver besides HSCs like hepatocytes, Kupffer cells, liver progenitor cells and endothelial cells, and the various different types of eicosanoids, it is not clear what the role of HSCs is in eicosanoid signaling in the liver. Therefore, we characterized the eicosanoid secretion potential of quiescent and activated mouse and rat HSCs by analyzing a number of eicosanoid metabolites and expression of eicosanoid related genes. To investigate whether eicosanoid secretion does affect HSC activation in an auto/ paracrinic way, we also studied the effects of pharmacological inhibitors of eicosanoid secretion on the expression of the HSC activation marker α-smooth muscle actin (α-SMA).

MATERIALS AND METHODS

Reagents

Dulbecco's modified Eagle medium (DMEM), fetal bovine serum (FBS), and penicillin/streptomycin were obtained from Gibco (Paisley, UK). Collagenase (Clostridium histolyticum Type I), Ca^{2+} ionophore A23187 were obtained from Sigma-Aldrich (St. Louis, MO, USA). The cAMP-analogs, N6-Mono-tert.Butylcarbamoyladenosine-3',5'-cyclic monophosphate (6-MBC-cAMP) and 5,6-Dichlorobenzimidazole riboside-3',5'-cyclic monophosphorothioate, Sp-isomer (Sp-5,6-

DCI-cBIMPS) were from BIOLOG Life Science Institute (Bremen, Germany). Eicosanoid standards, including PGE_2, were from Cayman Chemical (Ann Arbor, MI, USA), and HPLC-MS solvents were from Biosolve (Valkenswaard, the Netherlands).

Isolation and culture of rat and mouse hepatic stellate cells and hepatocytes

Primary HSCs and hepatocytes were isolated from 10-12 week-old C57BL/6J mice or adult male Wistar rats (300–400 g) by collagenase digestion followed by differential centrifugation as described [5]. After isolation, cells were plated in 12 well plates at a density of 5×10^4 cells/well, and maintained in DMEM supplemented with 10% FBS, 100 units/ml penicillin, 100 µg/ml streptomycin and 4 µl/ml Fungizone in a humidified 5% CO_2 incubator at 37 °C. Procedures of mouse and rat care and handling were in accordance with governmental and international guidelines on animal experimentation, and were approved by the Animal Experimentation Committee (Dierexperimentencommissie; DEC) of Utrecht University (DEC-numbers: 2010.III.09.110, 2012. III.10.100, and 2013.III.09.065).

Microarray analysis

Gene expression profiling was performed in mouse hepatic stellate cells grown for 1 day or 7 days in 24 well plates in DMEM containing 10 % FBS. RNA was isolated with the RNeasy® Mini Kit (Qiagen, Venlo, the Netherlands). cRNA synthesis and hybridization to Mouse Genome 430 2.0 arrays (Affymetrix, Freiburg) were performed at the Functional Genomics Center Zürich (Switzerland) according to standard protocols. CustomCDF by Brainarray with Entrez based gene definitions (Entrez basic version 13) was used to annotate the arrays [22].

RNA isolation, cDNA synthesis and QPCR

Total RNA was isolated from rat and mouse HSCs grown in a 24-well plate using RNeasy Mini Kit (Qiagen, Venlo, the Netherlands) including the optional on-column DNase digestion (Qiagen RNase-free DNase kit). RNA was dissolved in 30 µl of RNase free water and was quantified spectrophotometerically using a Nanodrop ND-1000 (Isogen Life Science, IJsselstein, the Netherlands). An iScript cDNA Synthesis Kit (Bio-Rad, Veenendaal, the Netherlands) was used to synthesize cDNA, and a SYBR Green based quantitative RT-PCR (Q-PCR) was performed on a Bio-Rad My-IQ detection system as described previously [5] for up to 45 cycles. Details of the primers and PCR conditions are listed in Tables S1 and S2 in the Supplemental data. Sequencing reactions confirmed amplification of the specific primer products in the Q-PCR reaction. Normalization was based on their stable expression in stellate cells by using at least three independent reference genes namely, *tyrosine 3-monooxygenase/tryptophan 5-monooxygenase activation protein, zeta (Ywhaz), hypoxanthine phosphoribosyl transferase (Hprt),* and *hydroxylmethylbilane synthase (Hmbs).*

Analysis of prostaglandins using mass spectrometry

Isolated mouse HSCs were grown in a 12-well plate for 1 day or 7 days in normal medium containing 10 % FBS. To reduce the background levels of eicosanoids present in serum, the cells were washed with PBS and subsequently DMEM containing 0.5% FBS and 10 μM Ca^{2+} ionophore A23187 was added 1hr before harvesting. Eicosanoids secreted in the low serum medium were extracted and analyzed as described elsewhere with slight modifications [23]. Briefly, samples were recovered in a total volume of 1 mL of 15 % (v/v) methanol + 0.5 % glacial acetic acid in the presence of 10 pmol 16,16-dimethyl-PGF$_{2α}$ that served as an internal standard to determine the recovery of the compounds of interest. Samples were then centrifuged at 2,000 rpm at 24°C for 10 min. To isolate the compounds of interest, partial purification of samples was achieved through extraction on C18 solid-phase extraction columns. The eicosanoids were eluted with 2 x 0.35 mL ethyl acetate and evaporated to dryness under nitrogen. Evaporated samples were reconstituted with 50μL of 50% ethanol and subject to HPLC–MS analysis using the multiple reaction monitoring (MRM) mode as described previously [23]. Molecule specific transitions used for the detection of individual eicosanoids are described in Supplemental data, Table S3. For normalization of the data, the cells were scraped and protein was determined by the Pierce® BCA protein assay kit (Thermo scientific, Rockford, IL, USA) with BSA as standard.

RESULTS

HSCs change their eicosanoid secretion profile upon activation

In order to determine whether HSCs play a role in the production of eicosanoids during liver injury and repair, we compared the secretion of various eicosanoids in quiescent and activated mouse and rat HSCs. Isolated mouse and rat HSCs at day 1 after plating were shown to be in their quiescent state and to be activated at day 7 as determined by the expression of α-smooth muscle actin (α-SMA) [4, 6]. Microarray analysis of the mouse HSCs at day 1 and day 7 confirmed the upregulation of a number of activation markers like α-smooth muscle actin (Acta2; 76-fold upregulated), matrix metallopeptidase 3 and 10 (Mmp3 and Mmp10; 43- and 960-fold upregulated, respectively), and various collagens (Col1a1, Col5a2, Col 8a1, and Col12a1; 10-, 18-, 16-, and 30-fold upregulated, respectively).

As shown in Fig. 1, we could detect a number of different eicosanoids in the medium of the HSCs after stimulating the cells with Ca^{2+}-ionophore A23187. In the absence of Ca^{2+}-ionophore, the eicosanoid patterns were similar, but the levels were more than 10-fold lower (data not shown) [6]. Quiescent mouse and rat HSCs had a somewhat similar secretion pattern. In HSCs from both species, PGE$_2$ was the most secreted eicosanoid followed by PGD$_2$ (Figs 1 and 2). Activation of the HSCs revealed a more distinct eicosanoid secretion capacity of mouse and rat cells, although in
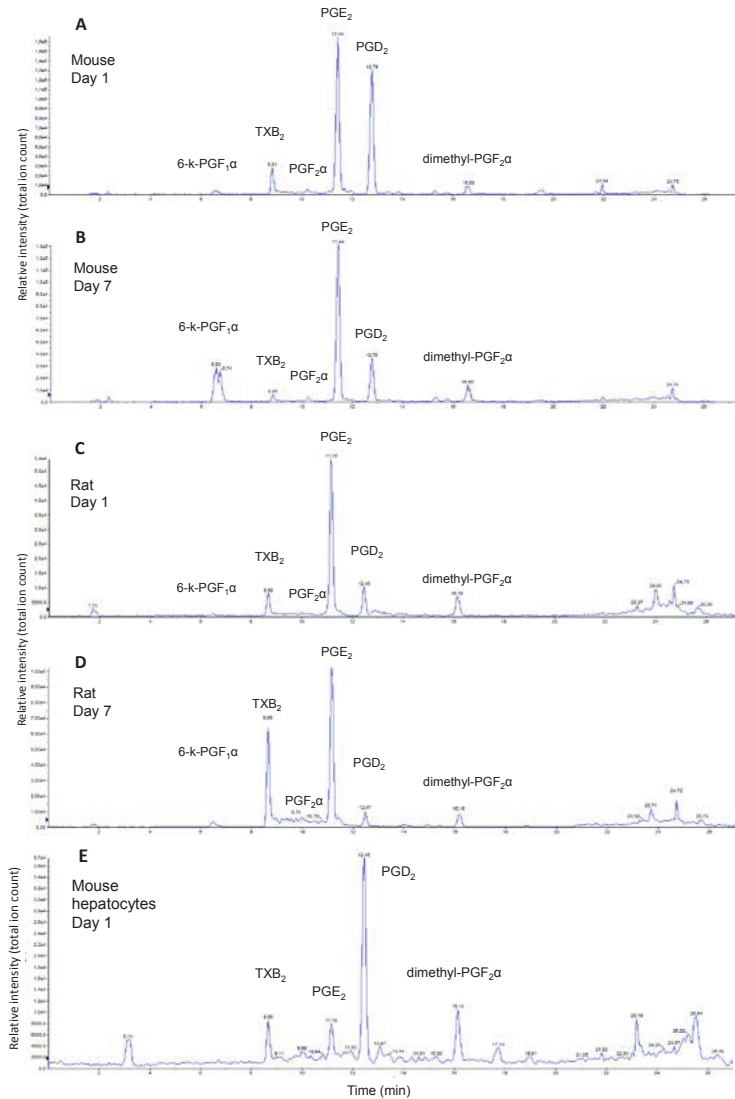
Figure 1. HSCs change their eicosanoid secretion profile upon activation. Primary mouse HSCs or hepatocytes and rat HSCs were grown for 1 day or 7 days in 12 well plates. Subsequently cells were incubated for 1 hr in 1 ml of DMEM with 0.5 % FBS and 10 μM Ca2+-ionophore A23187. Eicosanoids secreted in the medium were analyzed by HPLC-MS as described in the Methods section after addition of 10 pmol of 16,16-dimethyl PGF2α (dimethyl PGF2α) as internal standard. Representative chromatograms of A: mouse HSCs on day1; B: activated mouse HSC on day 7; C: rat HSCs on day1; D: activated rat HSC on day 7; E: mouse hepatocytes on day 1, notice that the amount of cellular protein is much higher in case of hepatocytes compared to HSCs and the maximum of the Y-axis is lower. 6-k-PGF1α = 6-keto-PGF1α

CHAPTER 5
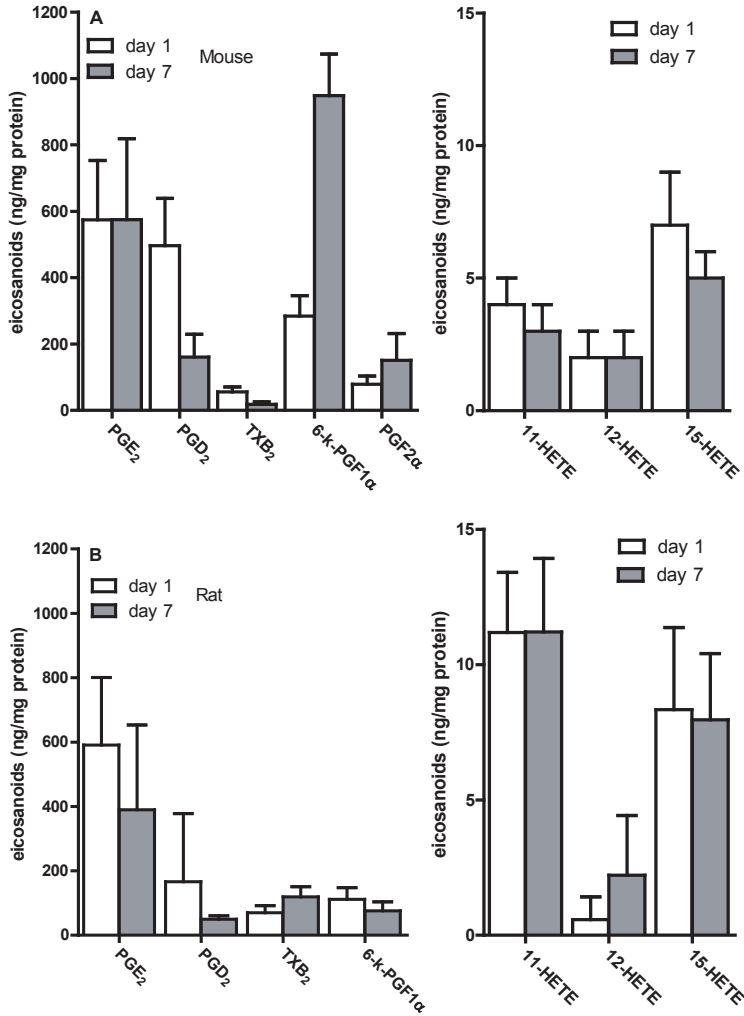
Figure 2. Quantitation of the main eicosanoids secreted by mice and rat HSCs. Primary HSCs from mouse (upper panels; A) or rat (lower panels; B) were grown for 1 day (white bars) or 7 days (grey bars) in 12 well plates. Subsequently cells were incubated for 1 hr in 1 ml of DMEM with 0.5 % FBS and 10 µM Ca2+-ionophore A23187. Eicosanoids secreted in the medium were analyzed by HPLC-MS after addition of 10 pmol of 16,16-dimethyl PGF2α as internal standard. Notice the different scale of the Y axis in case of HETEs. Shown are means and SD of 4 experiments. 6-k-PGF1α = 6-keto-PGF1α.

Table 1. Correlation between changes in eicosanoid secretion and eicosanoid-related gene expression upon activation of mouse and rat HSCs.

Primary mouse and rat HSCs were grown for 1 day or 7 days in culture. Eicosanoids secreted for 1 hr in medium with 0.5 % FBS and 10 μM Ca^{2+}-ionophore A23187 were determined by HPLC-MS. Gene expression was determined by microarray analysis in case of mouse cells and by qPCR in case of rat HSCs. Data are expressed as the means of the level at day 7 divided by the level at day 1 (fold up) of 3 experiments ± SD. nd = not detectable

				Microarray	qPCR
Eicosanoids	**Mouse**	Rat	**Gene Description**	**Mouse**	**Rat**
	Fold up	Fold up		Fold up	Fold up
			phospholipase A2, group IVA	6.20 ± 1.42	4,35 ± 2,83
total PGs	1.31 ± 0.12	0.7 ± 0.12	prostaglandin-endoperoxide synthase 1	0.85 ± 0.18	6,57 ± 4,06
11-HETE	0.91 ± 0.34	0.95 ± 0.28	prostaglandin-endoperoxide synthase 2	1.00 ± 0.37	0,08 ± 0,11
PGD_2	0.30 ± 0.13	0.52 ± 0.39	prostaglandin D2 synthase	0.41 ± 0.10	
PGE_2	0.95 ± 0.20	0.61 ± 0.26	prostaglandin E synthase	3.87 ± 0.83	0,29 ± 0,20
			prostaglandin E synthase 2	4.75 ± 0.89	0,30 ± 0,04
			prostaglandin E synthase 3	0.93 ± 0.08	0,38 ± 0,09
6-k-PGF1α	3.64 ± 1.06	0.89 ± 0.53	prostaglandin I2 (prostacyclin) synthase	7.48 ± 3.49	
TXB_2	0.29 ± 0.18	1.99 ± 0.93	thromboxane A synthase 1	0.22 ± 0.08	2,88 ± 0,79
5-HETE	nd	nd	arachidonate 5-lipoxygenase	0.87 ± 0.23	4,02 ± 2,51
12-HETE	1.27 ± 0.76	1.7 ± 1.6	arachidonate 12-lipoxygenase	0.04 ± 0.02	
15-HETE	0.82 ± 0.22	1.04 ± 0.5	arachidonate 15-lipoxygenase	0.41 ± 0.01	
LTB_4	nd	nd	leukotriene C4 synthase	0.17 ± 0.08	
			prostaglandin reductase 1	6.19 ± 1.34	
			prostaglandin reductase 2	2.33 ± 0.53	
			prostaglandin E receptor 1 (EP1)	1.48 ± 0.55	
			prostaglandin E receptor 2 (EP2)	0.95 ± 0.26	
			prostaglandin E receptor 3 (EP3)	2.24 ± 0.42	
			prostaglandin E receptor 4 (EP4)	0.28 ± 0.11	

CHAPTER 5

both cell types PGD_2 secretion was decreased. Activated mouse HSCs typically increased the secretion of 6-keto-$PGF_{1\alpha}$ almost 4-fold, making this the most highly secreted eicosanoid (Figs 1 and 2; Table 1). $PGF_{2\alpha}$ was also elevated in the medium of activated mouse HSCs, but not detectable in that of rat HSCs. Activated rat HSCs, on the other hand, specifically increased the secretion of thromboxane B_2 two-fold (Figs 1 and 2; Table 1).

The leukotrien LTB_4 and its precursor 5-HETE were not detectable in the medium from either quiescent and activated mouse and rat HSCs (Table 1). The most abundant HETEs, 11-HETE and 15-HETE, were secreted at much lower rates compared to the prostanoids. As these HETEs can be generated by pathways not involving lipoxygenases [24], they may not be directly related to leukotrien production.

To investigate whether HSCs may be a relevant source of eicosanoids in the liver, we compared the eicosanoid secretion by HSCs with that by hepatocytes. As shown in Figure 1A, mouse hepatocytes secreted less prostanoids after 1 hr stimulation with Ca^{2+}-ionophore as compared to mouse HSCs, although they were seeded at a higher density. Especially PGE_2, the highest secreted prostanoid by HSCs, was virtually absent in the hepatocyte medium.

HSCs change the expression of eicosanoid-related genes upon activation

As shown in Table 1, there was generally a good correlation between the changes in specific eicosanoid secretion rates in activated HSCs and the changes in expression of their respective synthases. For instance, the increase in 6-keto-$PGF_{1\alpha}$, the stable metabolite of PGI_2/prostacyclin, was accompanied by a large up-regulation of prostaglandin I_2/prostacyclin synthase in mouse HSCs. Whereas, the higher secretion of TXB_2, the stable metabolite of thromboxane A_2, was mirrored by upregulation of the mRNA for thromboxane A synthase 1 in activated rat HSCs. The changes in PGE_2 secretion (i.e no changes in mouse HSCs and a decrease in rat HSCs) were best correlated with the changes in expression of the PGE synthase 3 isoform (Table1). This isoform is also the highest expressed PGE synthase at the mRNA level in rat HSCs (Fig. 3A).

Surprisingly, we observed an isotype switch in mRNA expression of the first genes in the formation of prostanoids from Ptgs2 (COX-2) to Ptgs1 (COX-1) in rat HSC upon activation (table 1, Fig. 3A). However, the change in mRNA expression of COX-2 and COX-1 in rat HSCs was not reflected in expression of their respective enzymes, as the COX-2-specific inhibitor celecoxib was almost as potent in activated rat HSCs as it was in quiescent cells (Fig. 3B). The isotype switch in mRNA expression from COX-2 to COX-1 was not observed in mouse HSCs, and the IC_{50} for celecoxib and the general COX-inhibitor indomethacin were around 0.1 µM in both activated and quiescent mouse and rat HSCs (Fig. 3B).
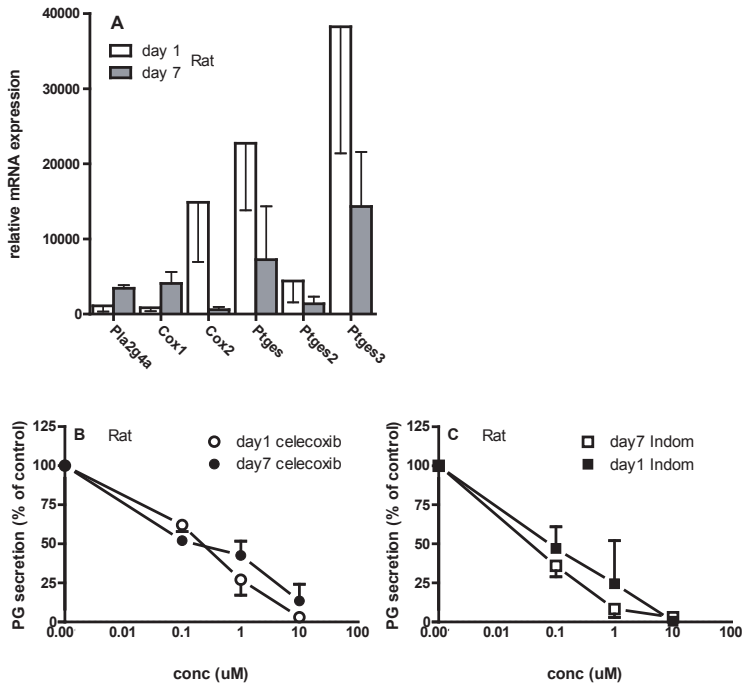
Figure 3. Expression of prostaglandin synthesizing genes in rat HSCs and sensitivity to COX inhibitors. Primary rat HSCs were grown for 1 day or 7 days in culture. A: Gene expression was determined by qPCR. B and C: Prostaglandins secreted for 1 hr in medium with 0.5 % FBS and 10 µM Ca2+-ionophore A23187 in the presence of different concentration of the Ptgs2/COX-2-selective inhibitor celecoxib (B), or the non-specific Ptgs/COX inhibitor indomethacin (C), were determined by HPLC-MS. Data are expressed as percentage of the total level of PGs secreted in the absence of inhibitors (control), and are the means of 3 experiments ± SD.

Effect of eicosanoids on HSC activation

To investigate whether the observed secretion of eicosanoids by HSCs has an autocrine/paracrine effect on HSC activation, we determined the effect of various inhibitors of eicosanoid secretion on the expression level of the HSC activation marker, α-SMA. The Ca^{2+}-dependent phospholipase A$_2$-inhibitor arachidonyl trifluoromethyl ketone (AACOCF3) caused a clear inhibition of α-SMA expression in both mouse and rat HSCs at µmolar concentrations (Fig. 4A and 4B). The COX-inhibitors celecoxib and indomethacin did also inhibit rat HSC activation, however, at concentrations that were more than 100-fold higher than required for inhibition of prostaglandin secretion (cf. Figs 3B and 4B). In mouse HSCs, a high concentration (100 µM) of celecoxib did inhibit α-SMA expression, but indomethacin did not affect activation (Fig 4A). This suggests that under our culture condi-
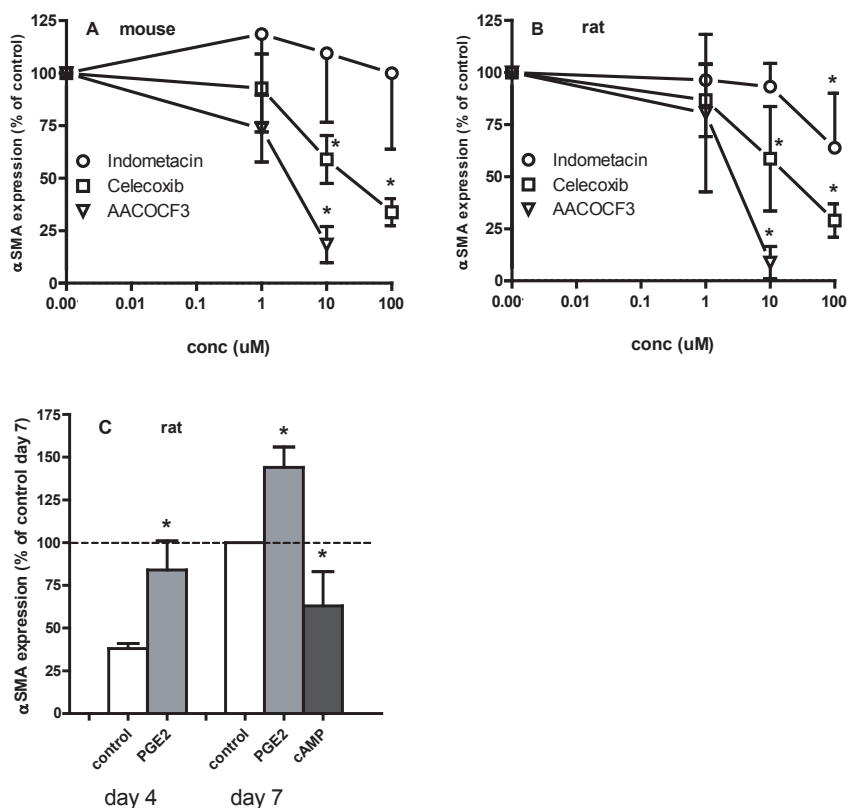
CHAPTER 5

127

Figure 4. Effects of COX- and cPLA2-inhibitors and PGE2 on HSC activation. Primary mouse (A) or rat (B) HSCs were incubated in the absence (control) or presence of various concentrations of the selective COX-2 inhibitor celecoxib, the COX-1 and COX-2-inhibitor indomethacin, or the cPLA2-inhibitor AACOCF3 from day 1 until day 7. At day 7, relative gene expression of αSMA (HSC activation marker) was measured by qPCR. C. Primary rat HSCs were grown for 3 days or 6 days in the presence of exogenous PGE2 (10nM), or vehicle (DMSO), or for 6 days in the presence of 100 μM of PK-A-specific the membrane permeable cAMP-analogs (cAMP), N6-Mono-tert.Butylcarbamoyladenosine-3′,5′-cyclic monophosphate and 5,6-Dichlorobenzimidazoleriboside-3′,5′-cyclic monophosphorothioate, Sp-isomer. Cells were harvested at either day 4 or day 7, and relative gene expression of αSMA was measured by qPCR. Shown are means ± SD of 3 experiments. * P< 0.05 t-test versus control.

tions , either para/autocrine prostaglandin secretion is unlikely to affect HSC activation, or that very low amounts of eicosanoids are sufficient for HSC activation.

To see whether prostaglandins can influence the activation process, we tested exogenous PGE_2 on HSC activation. As shown in Fig. 4C, incubation of rat HSCs with 10nM PGE_2 for 3 and 6 days had an approximately two-fold and a 1.5-fold higher expression of α-SMA as compared to vehicle treated cells, respectively, suggesting that PGE_2 can stimulate HSC activation. There are four types

of G-protein-coupled Prostaglandin E_2 receptors described, EP1-EP4 [25]. Two of them, i.e. EP2 and EP4, are known to raise the second messenger cAMP by activating an adenylyl cyclase-stimulating G-protein, G_s , whereas EP1 and EP3 are coupled to a Ca^{2+}-signaling pathway or an inhibitory G-protein, G_i, respectively [25]. We therefore investigated the effect of protein kinase A-site specific membrane permeable cAMP-analogs 6-MBC-cAMP and Sp-5,6-DCl-cBIMPS [26] on HSCs activation. As shown in Fig 4C, the cAMP-analogs inhibited α-SMA mRNA expression, suggesting that the stimulating effect of PGE_2 is mediated by an EP1 or EP3 receptor. Interestingly, both EP1 and EP3 were upregulated, and EP4 was down regulated in activated mouse HSCs (Table 1).

DISCUSSION

In this report, we show that mouse and rat HSCs can secrete substantial amounts of prostanoids, but almost no leukotrienes. The amount of prostanoids secreted by the HSCs (more than 1 μg/mg protein/hr) are comparable, if not higher, than the values reported for other cell types thought to be responsible for eicosanoid secretion in the liver i.e. sinusoidal endothelial cells and Kupffer cells [27, 28]. The hepatocytes themselves are not considered a large source of these bioactive lipids [28], as was also found by us in experiments with primary mouse hepatocytes treated under similar conditions as the HSCs. The total amount of secreted prostanoids did not change much upon activation. In mouse HSCs, this was in line with a minimal shift in the expression of the first enzymes of the prostanoid synthesis, PTGS/COX 1 and 2. In rat HSCs, however, we observed a shift in mRNA expression from the PTGS2/COX-2 isotype to the PTGS1/COX-1 isotype. This is unexpected as COX-1 is considered the 'constitutional' isoform, whereas COX-2 is found to be expressed in most cell types only after induction by certain inflammatory stimuli. Also in primary human HSCs, COX-2 was reported to be upregulated after 3 days in culture as compared to freshly isolated cells [13]. But in cultured rat HSCs COX-2 protein levels were reported to decrease from day 1 to day 7, in line with our mRNA data [29]. This demonstrates that HSCs from different species are not regulating enzymes from the eicosanoid pathways in a quantitatively similar way, not even in related animals such as rat and mice.

We also observed that activated rat and mouse HSCs upregulated different prostanoids. The TXA_2 secretion was increased in activated rat HSCs, whereas PGI_2/prostacyclin became the most secreted eicosanoid in activated mouse cells. The physiological relevance of these shifts are not immediately apparent as both PGI_2 and TXA_2 have multiple biological functions, which are mostly counteracting [8, 30]. A synthetic PGI_2/prostacyclin analog was shown to suppress liver fibrosis in mice by stimulating the secretion of HGF [31]. Furthermore, in a mice model with a genetic ablation of COX-2, both $PGE_{1/2}$ and PGI_2/prostacyclin agonists could decrease concanavalin A-induced liver injury [15]. This suggests that the upregulation of the PGI_2/prostacyclin by activated mouse HSCs

could serve as a feedback mechanism to dampen liver fibrosis. TXA_2, on the other hand, is reported to have profibrotic effects, as a thromboxane receptor (TP) agonist was found to stimulate collagen expression and proliferation in rat HSCs [32].

To investigate whether the eicosanoids secreted by the HSCs could affect the activation of the HSCs in an auto/paracrinic way, we tested the effect of inhibitors of eicosanoid secretion. The general COX-inhibitor, indomethacin, at concentrations that almost completely inhibited prostaglandin secretion, was unable to alter the expression of the HSC activation marker α-SMA. The inhibition of HSC activation by higher doses of the COX-2 specific inhibitor celecoxib and by the PLA_2-inhibitor AACOCF3 are therefore most likely mediated by mechanisms other than prostaglandin secretion. The PLA_2-inhibitor AACOCF3 was suggested to inhibit HSC activation by preventing the PLA_2 stimulation of the profibrotic transcription factor PPAR-β [29]. The lack of effect of COX-inhibitors at concentrations that inhibit eicosanoid secretion on HSC activation does not exclude the possibility that HSCs are affected by eicosanoids at concentrations that are higher than obtained under our culture conditions in the absence of stimuli like Ca^{2+}-ionophore. HSC activation was reported to be influenced by exogenous prostaglandins like the tromboxane receptor (TP) agonist, isoprostane [32], and a PGD_2 receptor agonist [33]. We also found an effect of PGE_2, the most abundantly secreted eicosanoid by mouse and rat HSCs, by mouse and rat HSCs upon activation.. The stimulatory effect of PGE_2 in our system is most likely mediated by an EP1 or EP3 receptor, as it was not mimicked by cAMP. Interestingly, the inhibitory effects of prostanoids like PGD_2 on HSC activation seems to be mediated via a cAMP pathway [33, 34], whereas the stimulatory effects are mediated by G-protein receptor coupled to G_q or Gi [30, 32].

In conclusion this study demonstrates that HSCs can both act as receivers, and as secretors of various prostanoids, when properly stimulated. Thus, depending on the circumstances/fibrotic stimuli, prostanoids may either stimulate or dampen the fibrotic process.

ACKNOWLEDGEMENTS

REFERENCES

1. Blaner, W. S. *et al*. (2009). Hepatic stellate cell lipid droplets: a specialized lipid droplet for retinoid storage. *Biochim. Biophys. Acta* **1791**, 467-473.

2. Friedman, S. L. (2008). Hepatic stellate cells: protean, multifunctional, and enigmatic cells of the liver. *Physiol. Rev.* **88**, 125-172.

3. Friedman, S. L., Sheppard, D., Duffield, J. S. & Violette, S. (2013). Therapy for fibrotic diseases: nearing the starting line. *Sci. Transl. Med.* **5**, 167sr1

4. Testerink, N. *et al*. (2012). Replacement of retinyl esters by polyunsaturated triacylglycerol species in lipid droplets of hepatic stellate cells during activation. *PLoS One* **7**, e34945.

5. Tuohetahuntila, M. *et al*. (2016). ATGL and DGAT1 are involved in the turnover of newly synthesized triacylglycerols in hepatic stellate cells. *J. Lipid Res.*

6. Tuohetahuntila, M. *et al*. (2015). Role of long-chain acyl-CoA synthetase 4 in formation of polyunsaturated lipid species in hepatic stellate cells. *Biochim. Biophys. Acta* **1851**, 220-230.

7. Pinot, M. *et al*. (2014). Lipid cell biology. Polyunsaturated phospholipids facilitate membrane deformation and fission by endocytic proteins. *Science* **345**, 693-697.

8. Ricciotti, E. & FitzGerald, G. A. (2011). Prostaglandins and inflammation. *Arterioscler. Thromb. Vasc. Biol.* **31**, 986-1000.

9. Bozza, P. T., Magalhaes, K. G. & Weller, P. F. (2009). Leukocyte lipid bodies - Biogenesis and functions in inflammation. *Biochim. Biophys. Acta* **1791**, 540-551.

10. Murakami, M. *et al*. (2011). Recent progress in phospholipase A(2) research: from cells to animals to humans. *Prog. Lipid Res.* **50**, 152-192.

11. Salvado, M. D., Alfranca, A., Haeggstrom, J. Z. & Redondo, J. M. (2012). Prostanoids in tumor angiogenesis: therapeutic intervention beyond COX-2. *Trends Mol. Med.* **18**, 233-243.

12. FitzGerald, G. A. & Patrono, C. (2001). The coxibs, selective inhibitors of cyclooxygenase-2. *N. Engl. J. Med.* **345**, 433-442.

13. Efsen, E. *et al*. (2001). Agonist-specific regulation of monocyte chemoattractant protein-1 expression by cyclooxygenase metabolites in hepatic stellate cells. *Hepatology* **33**, 713-721.

14. Haeggstrom, J. Z. & Funk, C. D. (2011). Lipoxygenase and leukotriene pathways: biochemistry, biology, and roles in disease. *Chem. Rev.* **111**, 5866-5898.

15. Yin, H., Cheng, L., Langenbach, R. & Ju, C. (2007). Prostaglandin I(2) and E(2) mediate the protective effects of cyclooxygenase-2 in a mouse model of immune-mediated liver injury. *Hepatology* **45**, 159-169.

16. Hui, A. Y. *et al*. (2006). Effect of celecoxib on experimental liver fibrosis in rat. *Liver Int.* **26**, 125-136.

17. Bahde, R., Kapoor, S. & Gupta, S. (2014). Nonselective inhibition of prostaglandin-endoperoxide synthases by naproxen ameliorates acute or chronic liver injury in animals. *Exp. Mol. Pathol.* **96**, 27-35.

18. Yu, J. *et al*. (2008). Elucidation of the role of COX-2 in liver fibrogenesis using transgenic mice. *Biochem. Biophys. Res. Commun.* **372**, 571-577.

19. Liu, H., Wei, W. & Li, X. (2009). Celecoxib exacerbates hepatic fibrosis and induces hepatocellular necrosis in rats treated with porcine serum. *Prostaglandins Other Lipid Mediat.* **88**, 63-67.

CHAPTER 5

20. Horrillo, R. *et al*. (2007). Comparative protection against liver inflammation and fibrosis by a selective cyclooxygenase-2 inhibitor and a nonredox-type 5-lipoxygenase inhibitor. *J. Pharmacol. Exp. Ther.* **323**, 778-786.

21. Titos, E. *et al*. (2010). Protection from hepatic lipid accumulation and inflammation by genetic ablation of 5-lipoxygenase. *Prostaglandins Other Lipid Mediat.* **92**, 54-61.

22. Sandberg, R. & Larsson, O. (2007). Improved precision and accuracy for microarrays using updated probe set definitions. *BMC Bioinformatics* **8**, 48.

23. de Grauw, J. C., van de Lest, C. H. & van Weeren, P. R. (2011). A targeted lipidomics approach to the study of eicosanoid release in synovial joints. *Arthritis Res. Ther.* **13**, R123.

24. Niknami, M., Dong, Q. & Witting, P. K. (2009). Pitfalls in the use of arachidonic acid oxidation products to assign lipoxygenase activity in cancer cells. *Free Radic. Res.* **43**, 951-956.

25. Sugimoto, Y. & Narumiya, S. (2007). Prostaglandin E receptors. *J. Biol. Chem.* **282**, 11613-11617.

26. Fricke, K., Heitland, A. & Maronde, E. (2004). Cooperative activation of lipolysis by protein kinase A and protein kinase C pathways in 3T3-L1 adipocytes. *Endocrinology* **145**, 4940-4947.

27. Hashimoto, N. *et al*. (1995). Prostanoid secretion by rat hepatic sinusoidal endothelial cells and its regulation by exogenous adenosine triphosphate. *Hepatology* **21**, 1713-1718.

28. Kuiper, J., Zijlstra, F. J., Kamps, J. A. & van Berkel, T. J. (1988). Identification of prostaglandin D2 as the major eicosanoid from liver endothelial and Kupffer cells. *Biochim. Biophys. Acta* **959**, 143-152.

29. Zhao, L., Gandhi, C. R. & Gao, Z. H. (2011). Involvement of cytosolic phospholipase A2 alpha signalling pathway in spontaneous and transforming growth factor-beta-induced activation of rat hepatic stellate cells. *Liver Int.* **31**, 1565-1573.

30. Hata, A. N. & Breyer, R. M. (2004). Pharmacology and signaling of prostaglandin receptors: multiple roles in inflammation and immune modulation. *Pharmacol. Ther.* **103**, 147-166.

31. Xu, Q. *et al*. (2013). Suppression of fibrogenic gene expression and liver fibrosis using a synthetic prostacyclin agonist. *Biomed. Res.* **34**, 241-250.

32. Acquaviva, A., Vecchio, D., Arezzini, B., Comporti, M. & Gardi, C. (2013). Signaling pathways involved in isoprostane-mediated fibrogenic effects in rat hepatic stellate cells. *Free Radic. Biol. Med.* **65**, 201-207.

33. Fujita, T. *et al*. (2016). Hepatic stellate cells relay inflammation signaling from sinusoids to parenchyma in mouse models of immune-mediated hepatitis. *Hepatology* **63**, 1325-1339.

34. Kawada, N., Kuroki, T., Kobayashi, K., Inoue, M. & Kaneda, K. (1996). Inhibition of myofibroblastic transformation of cultured rat hepatic stellate cells by methylxanthines and dibutyryl cAMP. *Dig. Dis. Sci.* **41**, 1022-1029.

Table S1. Rat primer sequence for the target and reference genes used in qPCR

Gene	Accession Number	Forward primer 5 → 3	Reverse primer 5 → 3	Tm
α-SMA	NM_031004	AGATGGCGTGACTCACAACGTG	AGGAATAGCCACGCTCAGTCAG	65ºC
Hprt	NM-012583	GTGTTGGATACAGGCCAGACTTTG	TCCACTTTCGCTGATGACACAAAC	60ºC
Hmbs	NM_013168	GCTTCGCTGCATTGCTGAAAGG	ACTCCACCAGTCAGGTACAGTTG	*60 ºC*
Ywhaz	NM_013011	ACATCTGCAACGACGTACTGTCTC	AGCAGCAACCTCAGCCAAGTAG	58ºC
Pla2g4a	NM_133551	AGCATGGCACTGTGTGATCAGG	AAATGGCCACCACAGGCACATC	64ºC
Ptgs1	NM_017043	CAACACTTCACCCACCAG	ACTGTCGTTCCAGACTATCTC	63ºC
Ptgs2	NM_017232	CTTGAACACGGACTTGCT	CTCTGCTCTGGTCAATGG	60.5ºC
Ptges	NM_021583	CAGGAGTGACCCAGATGTG	AAATGTATCCAGGCGATGAGAG	65ºC
Ptges2	NM_001107832	ATCATCACTTATTACCCACCC	CACTTCATCTCCTCCGTC	70ºC
Ptges3	NM_001130989	CTTAATTGGCTTAGTGTGGAC	CTGCTCCGTCTACTTCTG	63ºC
Tbxas1	NM_012687	GATTCTGCCCAATAAGAACCGA	TCAAAGGCTTCTACACCCAC	65ºC
Alox5	NM_012822	GATGCTAAATGCCACAAGGA	ATGAAGCGATTGATGAACAGG	63ºC

Table S2. Mouse primer sequence for the target and reference genes used in qPCR

Gene	Accession Number	Forward primer 5 → 3	Reverse primer 5 → 3	Tm
α-SMA	NM_007392	TCTTCCAGCCATCTTTCATTGGG	CCTGACAGGACGTTGTTAGCATAG	61ºC
Hprt	NM_013556	TCAGTCAACGGGGGACATAAA	GGGGCTGTACTGCTTAACCAG	64ºC
Hmbs	NM_001110251	ACTCTGCTTCGCTGCATTG	AGTTGCCCATCTTTCATCACTG	58 ºC
Ywhaz	NM_001253805	AACAGCTTTCGATGAAGCCAT	TGGGTATCCGATGTCCACAAT	64ºC

Table S3. MRM transitions of the main eicosanoids analyzed

Analyte	MRM (m/z)
PGE_1	353 → 317
PGE_2	351 → 271
PGD_2	351 → 271
TXB_2	369 → 195
6-keto-$PGF_1\alpha$	369 → 163
$PGF_2\alpha$	353 → 193
5-HETE	319 → 115
11-HETE	319 → 167
12-HETE	319 → 179
15-HETE	319 → 175
LTB_4	335 → 195
dimethyl $PGF_2\alpha$ (IS)	381 → 319

CHAPTER 5

Chapter

6

Summarizing Discussion

INTRODUCTION

Chronic liver diseases comprise a significant clinical problem. A critical step in the development of chronic liver disease is the transition from the so-called inflammatory stage to the fibrotic stage. As described in chapter **1**, an important role in this transition is played by hepatic stellate cells (HSCs). In a healthy liver, HSCs are involved in vitamin A (retinol) homeostasis as they are filled with large lipid droplets containing retinyl esters (REs), together with triacylglycerols (TAGs) and cholesterol esters (CEs). However, upon liver injury/inflammation, HSCs transdifferentiate into a myofibroblastic cell type. In this so called "activated" phenotype, HSCs have lost their lipid droplets and secrete fibrillar collagen and growth factors. The activated HSCs are thought to represent a dual edged sword in liver disease. On the one hand, they are believed to enhance liver repair as they secrete factors regulating the proliferation and differentiation of hepatocytes and liver progenitor cells (LPCs), respectively. In this respect HSC are thought to be a part of the liver "stem cell niche" responsible for liver regeneration after injury. However, the molecular mechanisms of interaction between the different cell types in the liver have so far not been clarified, but may comprise lipid mediators, like prostaglandins. On the other hand, HSCs are the major source of fibrillar collagens that are characteristic for liver fibrosis and subsequent cirrhosis. Regarding this latter aspect it is generally believed that prevention of HSC activation or conversion of activated HSC back to their quiescent/lipid droplet containing state would be desirable to attenuate liver fibrosis and subsequent cirrhosis.

One of the unresolved issues in the field of HSC research is whether the change in lipid metabolism is causally related to the activation process. In other words, can HSC activation be altered when formation or breakdown of lipid droplets is disturbed? In order to answer this question a more fundamental knowledge on the molecular mechanism of lipid droplet homeostasis in HSCs is required as this is currently lacking. The main objective of the experiments described in this thesis was to unravel the (retinoid)lipid-related pathways involved in the transformation of hepatic stellate cells into an activated state, and to investigate whether disruption of these lipid pathways prevents or reverses the activated state of hepatic stellate cells. As some lipids, e.g. polyunsaturated fatty acids (PUFAs), are precursors for the signaling molecules like eicosanoids, we also investigated the potential of HSCs to secrete these lipid mediators.

LIPID METABOLISM IN ACTIVATED HSCs

An overview of lipid metabolism in HSCs as derived from experiments described in this thesis and from other studies is depicted in Figure 1. In prior studies we established that the lipid composition of the HSC changes dramatically after activation *in vitro*. Activated rat HSCs gradually lose
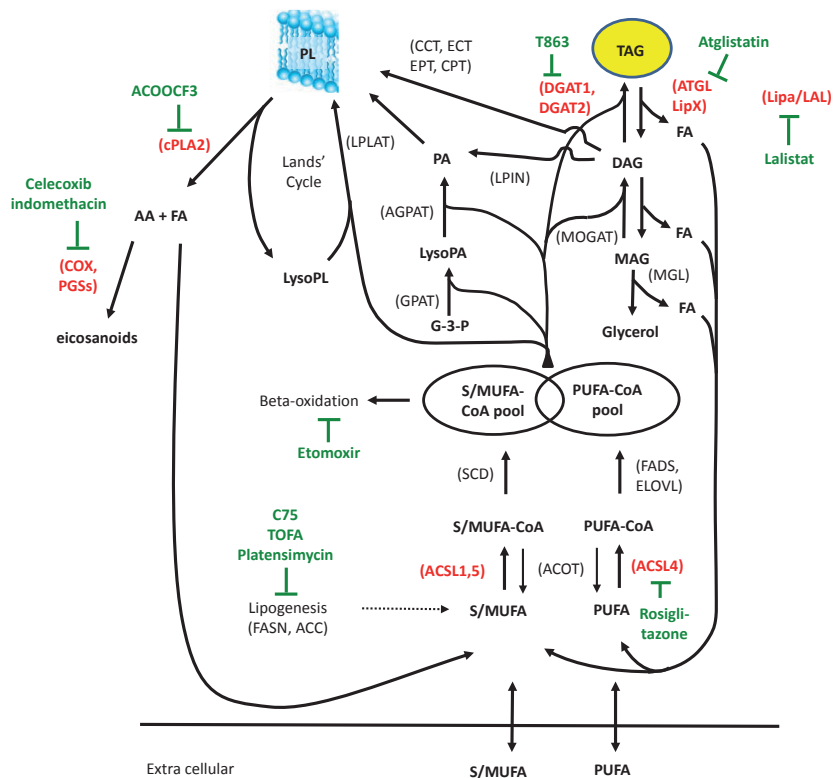
Figure 1. Lipid pathways in activated HSCs. Lipids and other metabolites are in bold and the abbreviations of gene families implicated in their formation/degradation are between parenthesis. In red are lipid enzymes described in this thesis, and in green the inhibitors used to delineate their function. This figure also shows possible connections between TAG and PL metabolism. S/MUFA = saturated and/or mono-unsaturated fatty acids. LipX = unidentified lipase. PA = phosphatidic acid. PGSs = various prostaglandin synthases. Other abbreviations are as in the main text of this thesis. Dashed arrows indicate minor or not existing pathways in HSCs.

their main retinoid species, and this decrease in retinoids is accompanied by an increase in CEs and PUFA-containing TAG species[1]. In chapter **2**, we described our studies on the mechanism responsible for the increase in PUFA-TAGs during the first phase of rat HSC activation. We found that an isotype switch in the fatty acid (FA)-CoA ligases of the ACSL family, from the non-specific type 1 to the PUFA-specific type 4, was largely responsible for the observed increase in PUFA-TAGs. In first instance the ACSL isotype switch will affect the composition of the acyl-CoA pool. In order to change the composition of the TAG pool, we must assume that the newly formed PUFA-enriched acyl-CoAs are rapidly incorporated in TAGs, replacing the existing TAGs. Such a relatively

fast remodeling of TAGs by a concerted action of TAG synthesis and lipolysis was indeed observed in rat HSCs in studies with deuterium labeled fatty acids (FAs) as described in chapter **3**. In mouse HSCs, we observed a similar switch from ACSL1 to ACSL4 upon activation as in rat cells, but no clear increase in PUFA-TAGs. Mouse HSCs were shown to have a lower rate of TAG synthesis, and only in the absence of the TAG-lipase, ATGL, the increase in PUFA-TAG formation was unmasked. These studies reveal the importance of both TAG synthesizing and degrading enzymes in the appearance in PUFA-TAGs.

A fast mobilization of the PUFA-TAG pool is also a requirement to serve as a storage site of PUFAs to protect the cells against a shortage of these essential FAs for eicosanoid secretion as proposed in chapter **2**. As shown in Figure 1, there are a number of connections between TAG metabolism and phospholipid (PL) metabolism, and from PL to eicosanoid formation. All these connections start with the lipolysis of TAG to DAG, releasing a PUFA, or a PUFA-containing DAG, which can be subsequently converted to PUFA-PLs. The changes in the expression of the various enzymes involved in the synthesis of eicosanoids by activated HSCs are described in detail in chapter **5**. We found that these changes were different in mouse and rat cells.

In activated mouse HSCs, prostaglandin I_2/prostacyclin synthase was upregulated. In activated rat HSCs, however, thromboxane A synthase was increased. In rat HSCs, but not in mice, we also observed a shift in mRNA expression from the PTGS2/COX-2 isotype to the PTGS1/COX-1 isotype. The precise function of the observed shifts in eicosanoid secretion capacity is as yet unknown, but they demonstrate that HSCs can be a source of prostaglandins during liver injury and repair.

In chapter **3**, we identified enzymes involved in the rapid TAG formation and breakdown. We found that DGAT type 1 was especially involved in the formation of TAG during activation. For the degradation of TAGs we observed a role for at least three lipases: ATGL, LAL/Lipa, and an as yet unidentified lipase (depicted as LipX in Figures 1 and 2). This unknown lipase was found to be sensitive to the presumed ATGL-specific inhibitor, Atglistatin, and might therefore resemble characteristics of ATGL. From studies with mice deficient in the ATGL-regulator, comparative gene identification-58 (CGI-58), it was also evident that there is at least one other TAG-lipase resembling ATGL in the way it is regulated [2], as the CGI-58 knock-out mice have a disturbed lipolysis in different places as compared to ATGL-deficient mice.

In rat and mouse HSCs we have strong evidence that the different lipases do not target the same LDs, but that HSCs have different pools of LDs as will be discussed in more detail in the next section.
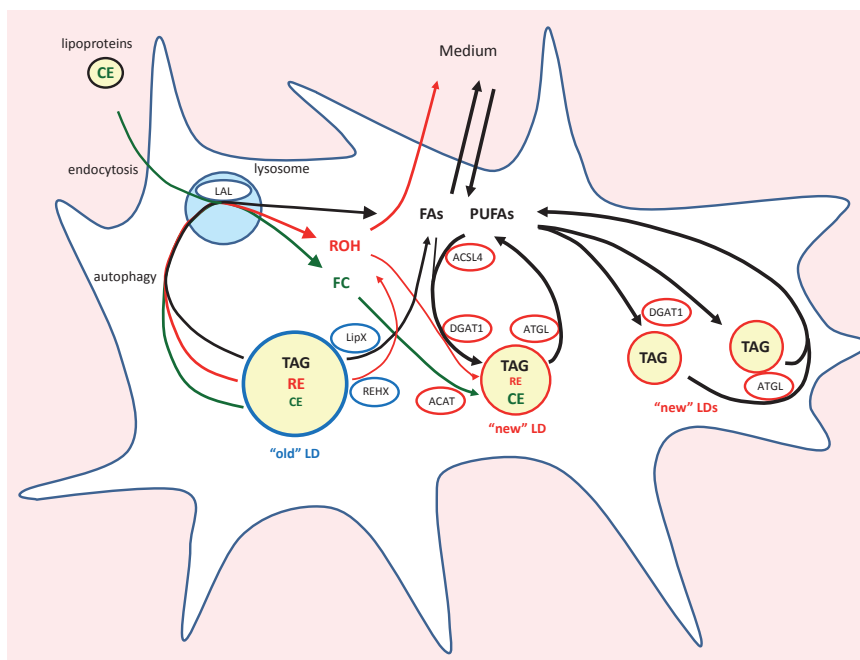
CHAPTER 6

Figure 2. Activated HSCs have two different metabolic pools of LDs. Pre-existing/"old" LDs and associated enzymes in blue, and "new" LDs and its synthesizing and degrading enzymes are in red. Black arrows show TAG metabolism, red arrows show retinoid flow, and green arrows show sterol flow.

ACTIVATED HSCs HAVE TWO DIFFERENT METABOLIC POOLS OF LDs

We have found evidence for metabolically different LD pools in HSCs from studies using deuterated FAs in combination with the different lipase inhibitors (lalistat, orlistat and atglistatin), the DGAT1 inhibitor T863, and from experiments in ATGL^{-/-} mice, as described in chapters **3** and **4**. We here propose that activated HSCs contain a pool of pre-existing/"old" LDs, and a relatively rapid recycling pool of "new" LDs. The "old" LDs, containing predominantly TAGs and REs, are localized around the nucleus, and are degraded with a half time of a few days, partly in the lysosome by LAL/Lipa, and partly by an unidentified lipase (LipX) and a cytosolic RE-esterase (REHX; Figure 2).

The TAGs in the "new" LDs are made at the periphery of the cells, preferential by DGAT1 in combination with ACSL4, and are thus enriched in PUFAs. The TAGs in the "new" LDs are degraded by ATGL, possibly in combination with LipX. Turnover of the newly-incorporated (deuterated) FAs from the new LDs is relatively fast. We observed half times of less than 8 hrs for the removal of the newly incorporated FAs from TAG (chapter **3**). Interestingly, in model cells also evidence for different pools of LDs was obtained. In these cells, DGAT1 has been associated with the formation

of small new LDs, whereas DGAT2 was involved in the enlargement of existing LDs [3], similarly to their here proposed role in HSCs. Furthermore, isolated HSCs from *Dgat1* [-/-] mice have larger and fewer LDs compared to their wild type controls [4].

From studies with both deuterium–labeled glucose and FAs, we observed that FAs were incorporated in "new" glycerol-backbones derived from glucose, but also in pre-existing glycerol-backbones, presumably as replacement of an acyl chain released by a lipase (M. Tuohetahuntila, unpublished observations). This latter mechanism can be used to remodel TAGs as it is very similar to the Lands' cycle, known to remodel PLs [5]. In this TAGs equivalent of the Lands' cycle, ATGL and DGAT1 fulfill similar roles as PLA_2 and LPLATs, respectively, in the original Lands' cycle (see Figure 1).

The above described two-pool model, depicted in Figure 2, explains also previous observations in activated HSCs, that LDs reduce in size, but increase in number and are localized in cellular extensions [1], without having to assume fission of the LDs and extensive migration to the periphery. The new model explains the apparent redistribution of LDs by a degradation of the lipid content (both TAGs and REs) of original LDs, concurrent with an rapid resynthesis of TAGs and REs in novel lipid droplets in the cell periphery. In the presence of an inhibitor of RE degradation, lalistat, we could actually observe by live-cell imaging two pools of LDs, one with RE in the center of the cell, and one without REs in the periphery (chapter **4**). The FAs and free retinol required for the synthesis of the new TAGs and REs are partly derived from the "old" lipids (recycling) but can also come from the external medium. The recycling pathway is especially important for the RE synthesis as external retinol concentrations are low. The recycling of retinol also explains our inability to observe the different pools of LDs in the absence of lalistat, and in previous studies using Raman imaging to visualize LDs [1].

We could not observe a contribution of *de novo* synthesized FAs by the lipogenic pathway (see Figure 1) to the newly formed TAGs in studies with deuterium-labeled glucose (M. Tuohetahuntila, unpublished observations).

Finally, it must be noted that the rapid and dynamic alteration in HSC lipid metabolism described above were observed in cell culture. Therefore, it remains to be established whether similar changes in lipid metabolism occur during stellate cell activation under various pathophysiological situations *in vivo*.

CHAPTER 6

EFFECT OF CHANGES IN LIPID METABOLISM ON HSC ACTIVATION

The identification of a number of important lipid metabolizing enzymes allowed us to investigate the role of lipid metabolism in the activation of HSCs, one of the major aims of this thesis research project. In table 1, the effects of various inhibitors on lipid levels are compared to their effects on HSC activation. In rat HSCs we found that all of the compounds that either inhibited lipid synthesis (rosiglitazone and T863) or inhibited lipid degradation (Atglistatin, lalistat, and orlistat), inhibited *in vitro* activation of the HSCs. Mice HSCs were more resistant to these treatments, as both the effects on lipid levels and on activation were lower or absent. The lower effect of the inhibitors in mice HSCs on lipid levels might be caused by the lower turnover of TAGs in mouse cells (chapter **3**). So in general there is a good correlation between the effect on lipid levels and the effect on activation, suggesting that a rather large disturbance in lipid metabolism is required to inhibit HSC activation. As inhibition of TAG and/or RE formation had the same effect as inhibiting their breakdown, HSCs seem to require a dynamic neutral lipid pool for optimal functioning. It was suggested that the TAG pool may act as a buffer for FAs required for energy [6], or synthesis

Table 1. Effect of inhibitors on lipid metabolism and HSC activation.
The roles of the various targets and their inhibitors in HSC lipid metabolism are depicted in Figure 1.

Inhibitor	Presumed target	Effect on lipid content/metabolism (at day 7)	Effect on activation (α-SMA expression at maximal dose)	Reference
Rosigli-tazone	ACSL4	~60% lower levels of TAG, ~80 % lower levels of PUFA-TAG, no effect on CE and RE (rat)	~50% Inhibition (rat)	Chap. 2
T863	DGAT1	~80% lower the levels of TAG, and CE, ~60% lower levels of RE (rat)	~30 % Inhibition (rat)	Chap. 3
		no effect total TAG, ~50% lower levels of PUFA-TAG, and CE (mouse)	no Inhibition (mouse)	
Atglistatin	ATGL LipX	~10-fold higher levels of TAG, no effect on CE and RE (Rat)	~30 % Inhibition (rat)	Chap. 3
		~3.5-fold higher levels of TAG, no effect on CE and RE (mouse)	no Inhibition (mouse)	
Lalistat	LAL/Lipa	3-4-fold higher levels of TAG, CE and RE (rat)	~30 % Inhibition (rat)	Chap. 4
		2-3-fold higher levels of TAG, and RE, ~8-fold higher levels of CE (mouse)	~30 % Inhibition (mouse)	
Orlistat	LAL/Lipa (partly) ATGL, LipX	~3.5-fold higher levels of TAG, ~2-fold higher levels of CE and RE (rat)	~70 % Inhibition (rat).	Chapt. 4
		~1.5-fold higher levels of TAG, ~3.5-fold higher levels of CE (mouse)	no Inhibition (mouse)	
Etomoxir	CPT1 (β-oxidation)	~2-fold higher levels of TAG (rat)	no Inhibition (rat)	Chapt. 4

of membranes or bioactive lipids, like prostanoids [7]. We found no evidence that the activation of rat HSCs requires either FAs for energy or prostanoid synthesis, as neither an inhibitor of the β-oxidation (etomoxir; table 1) nor of prostaglandin synthesis (low dose of indomethacin; chapter **5**) inhibited HSC activation. The requirement for HSCs during activation to make or degrade LDs, rather than a pre-existing pool of lipids, would not be in conflict with observations in mouse LRAT^{-/-} HSCs. These cells were shown to activate normally despite their initial lack of large LDs [8], as they have no defect in making LDs during *in vitro* activation (M.R. Molenaar, unpublished observations).

The use of pharmaceutical tools to delineate the role of specific pathways is almost always flawed by possible off-target effects and so it cannot provide an entirely conclusive answer regarding the role of lipid metabolism in HSC activation. Therefore, we also investigated the effects of genetic interventions in lipid metabolism. We observed normal activation in *atgl*-deficient mouse HSCs and in rat HSCs with siRNA-mediated knock-down of ATGL or DGAT1 (chapter **3**). Since the effects on lipid levels of these genetic models were rather small compared to the pharmaceutical interventions, these studies corroborate the notion that relatively small disturbances in lipid metabolism are without effect on HSC activation *in vitro*. However, these studies offer no insight in the effects of large disturbances.

Evidence that genetic manipulation of lipid metabolism can effect HSC activation are so far limited. One study reported the effects of forced expression of PPARγ in culture-activated rat HSCs. The expression of PPARγ itself was shown to be sufficient to reverse the morphology of activated HSC to the quiescent phenotype, including an accumulation of retinyl palmitate. As the ectopic expression of PPARγ in these cells induces a panel of (adipogenic) transcription factors, it is not clear whether the observed phenotypic reversal to quiescent HSC is caused directly by the change of lipid metabolism or that it is caused by changes in expression of other genes, more directly associated with HSC activation [9, 10]. Another study showed that knockdown of *Dgat*1 in rat liver *in vivo* inhibited activation of HSCs *in vitro* [11]. Interestingly, levels of LRAT and cellular retinol binding protein-1 were upregulated during the DGAT1 knockdown, so increased storage of REs might be involved in the protective action of the DGAT1 knockdown. On the other hand, deletion of *Dgat1* in mice had no effect on subsequent HSC activation in culture [4]. Interestingly, the latter study also indicated that a limited effect on HSC activation *in vitro*, does not preclude a significant effect on HSC activation *in vivo*, as the DGAT1-deficient mice were less sensitive to induction of liver fibrosis.

Extrapolation of the effects of drugs on HSC activation *in vitro* to their effects in whole animal models is also hampered by potential side effects on other cell types. The use of lipase inhibitors, for instance, may only be used for limited time periods as chronic treatments are expected to have

CHAPTER 6

serious side effects, since *Atgl*^{-/-} and *Lipa*^{-/-} mice develop severe pathologies [12] [13]. DGAT1-inhibitors are more likely to be tolerated in mice models as *Dgat1*^{−/−} mice are viable, lean, resistant to diet-induced obesity [14], and have an attenuated response to agents that induce liver fibrosis [4]. Due to their potential as treatment for obesity and diabetes type II, various DGAT1 inhibitors were already tested in human clinical settings. In these studies, problems with intestinal side effects like diarrhea were noted, which may be related to the inhibition of DGAT1-mediated lipid synthesis in the gut [15]. Finally, the ACSL4 inhibitor used in our study, rosiglitazone, was also tested in humans for its potential to treat metabolic disease by activating PPARγ. In patients with non-alcoholic steatohepatitis (NASH), it was found to improve ballooning degeneration, but not fibrosis [16]. However, the concentrations used were presumable too low to inhibit ACSL4 as rosiglitazone has a higher affinity for PPARγ (see chapter 2).

In conclusion, the here described studies provide ample evidence for a role of lipid metabolism in the activation of (rodent) HSCs *in vitro*. Therefore, investigations to the effects of lipid metabolism altering treatments on liver fibrosis in whole animal models are warranted, but will require careful titration as total neutral lipid levels nor the extend of accumulation/degradation is a good indicator for the effect on HSC activation. Rather interference with neutral lipid fluxes may be worth considering in future research.

REFERENCES

1. Testerink, N. *et al*. Replacement of retinyl esters by polyunsaturated triacylglycerol species in lipid droplets of hepatic stellate cells during activation. *PLoS One* **7**, e34945 (2012).

2. Radner, F. P. *et al*. Growth retardation, impaired triacylglycerol catabolism, hepatic steatosis, and lethal skin barrier defect in mice lacking comparative gene identification-58 (CGI-58). *J. Biol. Chem.* **285**, 7300-7311 (2010).

3. Wilfling, F. *et al*. Triacylglycerol synthesis enzymes mediate lipid droplet growth by relocalizing from the ER to lipid droplets. *Dev. Cell.* **24**, 384-399 (2013).

4. Yuen, J. J., Lee, S. A., Jiang, H., Brun, P. J. & Blaner, W. S. DGAT1-deficiency affects the cellular distribution of hepatic retinoid and attenuates the progression of CCl4-induced liver fibrosis. *Hepatobiliary. Surg. Nutr.* **4**, 184-196 (2015).

5. Shindou, H., Hishikawa, D., Harayama, T., Eto, M. & Shimizu, T. Generation of membrane diversity by lysophospholipid acyltransferases. *J. Biochem.* **154**, 21-28 (2013).

6. Hernandez-Gea, V. *et al*. Autophagy releases lipid that promotes fibrogenesis by activated hepatic stellate cells in mice and in human tissues. *Gastroenterology* **142**, 938-946 (2012).

7. Tuohetahuntila, M. *et al*. Role of long-chain acyl-CoA synthetase 4 in formation of polyunsaturated lipid species in hepatic stellate cells. *Biochim. Biophys. Acta* **1851**, 220-230 (2015).

8. Kluwe, J. *et al*. Absence of hepatic stellate cell retinoid lipid droplets does not enhance hepatic fibrosis but decreases hepatic carcinogenesis. *Gut* **60**, 1260-1268 (2011).

9. She, H., Xiong, S., Hazra, S. & Tsukamoto, H. Adipogenic transcriptional regulation of hepatic stellate cells. *J. Biol. Chem.* **280**, 4959-4967 (2005).

10. Hazra, S. *et al*. Peroxisome proliferator-activated receptor gamma induces a phenotypic switch from activated to quiescent hepatic stellate cells. *J. Biol. Chem.* **279**, 11392-11401 (2004).

11. Yamaguchi, K. *et al*. Diacylglycerol acyltranferase 1 anti-sense oligonucleotides reduce hepatic fibrosis in mice with nonalcoholic steatohepatitis. *Hepatology* **47**, 625-635 (2008).

12. Haemmerle, G. *et al*. Defective lipolysis and altered energy metabolism in mice lacking adipose triglyceride lipase. *Science* **312**, 734-737 (2006).

13. Du, H., Duanmu, M., Witte, D. & Grabowski, G. A. Targeted disruption of the mouse lysosomal acid lipase gene: long-term survival with massive cholesteryl ester and triglyceride storage. *Hum. Mol. Genet.* **7**, 1347-1354 (1998).

14. Smith, S. J. *et al*. Obesity resistance and multiple mechanisms of triglyceride synthesis in mice lacking Dgat. *Nat. Genet.* **25**, 87-90 (2000).

15. DeVita, R. J. & Pinto, S. Current status of the research and development of diacylglycerol O-acyltransferase 1 (DGAT1) inhibitors. *J. Med. Chem.* **56**, 9820-9825 (2013).

16. Singh, S., Khera, R., Allen, A. M., Murad, M. H. & Loomba, R. Comparative effectiveness of pharmacological interventions for nonalcoholic steatohepatitis: A systematic review and network meta-analysis. *Hepatology* **62**, 1417-1432 (2015).

CHAPTER 6

Nederlandse samenvatting

Identificatie van eiwitten die betrokken zijn bij de vetstofwisseling in hepatische stellaat cellen: mogelijke therapeutische aangrijpingspunten voor leverfibrose

INLEIDING

De lever speelt een belangrijke rol in het lichaam. Dit orgaan is onder andere betrokken bij de energievoorziening en bij het verwijderen van schadelijke stoffen. Lever fibrose, en zijn vervolg stadium levercirrose, zijn dan ook levensbedreigende aandoeningen. Leverfibrose wordt deels veroorzaakt door speciale levercellen die littekenweefsel vormen. Deze zogenaamde hepatische stellaatcellen (HSCs) zijn in een gezonde lever gevuld met vetdruppeltjes, waarin de reserve voorraad vitamine A zit. Vitamine A heet ook wel retinol en is nodig voor een aantal processen, bijvoorbeeld in het oog, om licht te kunnen waarnemen. De gezonde toestand van de stellaatcellen, waarin ze boordevol met vetdruppels zitten, noemen we de "rustende" staat. Maar na beschadiging of ontsteking van de lever verliezen de stellaatcellen hun vetdruppels met vitamine A en veranderen ze in bindweefsel cellen, die fibrose veroorzaken. We noemen deze overgang de "activering" van de hepatische stellaatcellen. Omdat de geactiveerde stellaatcellen verantwoordelijk zijn voor de voortschrijdende littekenvorming in de lever, wordt algemeen aangenomen dat het tegen gaan van het activeringsproces een belangrijke bijdrage kan leveren aan het voorkomen of herstellen van lever fibrose.

Het is onduidelijk of het verdwijnen van de vitamine A gevulde vetdruppels een oorzakelijke rol speelt in het activeringsproces. Anders gezegd, verloopt de activering anders wanneer wordt voorkomen dat de stellaatcellen hun vetdruppels verliezen? Om deze vraag te kunnen beantwoorden moeten we eerst weten welke eiwitten betrokken zijn bij de vorming en afbraak van de vetdruppels in de hepatische stellaat cellen.

Het belangrijkste doel van de onderzoeken beschreven in dit proefschrift is dan ook de identificatie van eiwitten die betrokken zijn bij de vetstofwisseling in hepatische stellaat cellen. Vervolgens is bestudeert of het remmen van die eiwitten leidt tot een vermindering van het activeringsproces. Door te bestuderen hoe de stellaatcellen precies hun vetdruppels verliezen hopen we aangrijpingspunten te vinden voor therapieën tegen leverfibrose.

Vetstofwisseling in geactiveerde hepatische stellaatcellen

Tot de vetten, ook wel lipiden genoemd, behoren een groot aantal verschillende stoffen, die gemeen hebben dat ze slecht oplossen in water. Lipiden worden gebruikt bij de energie voorziening van cellen (vnl. vetzuren), als bouwstenen voor celmembranen (vnl. fosfolipiden en cholesterol), maar ook voor specifieke zaken als het waarnemen van licht (de uit vitamine A gemaakte stof retinal) en communicatie tussen cellen (bijvoorbeeld de uit meervoudig-onverzadigde vetzuren gemaakte eicosanoiden en de uit vitamine A gemaakte stof retinolzuur). Een overschot aan lipiden kan worden opgeslagen in cellen in vetdruppels. Om te worden opgeslagen in vetdruppels moeten de lipiden maximaal waterafstotend zijn. Hiertoe worden retinol/vitamine A en

cholesterol aan vetzuren gebonden via een esterbinding tot respectievelijk retinylesters (REs) en cholesterylesters (CEs). De vetzuren zelf worden met zijn drieën aan een glycerol verestderd tot tri-acylglycerolen (TAGs). De eiwitten waarvan bekend is dat ze een rol spelen in de vorming en afbraak van de lipiden-esters zijn beschreven in hoofdstuk **1**.

Om het vetmetabolisme te bestuderen in hepatische stellaat cellen tijdens de activering, werden stellaat cellen geïsoleerd uit ratten of muizen levers. De cellen werden vervolgens buiten de lever gekweekt in plastic bakjes, waarin ze spontaan een proces ondergaan wat lijkt op de activering door leverschade. De hoeveelheid van de verschillende lipiden werd vervolgens bepaald met behulp van massaspectrometrie (MS) na scheiding van de lipiden met behulp van hogedruk vloeistof chromatografie (HPLC). Uit eerder onderzoek aan stellaatcellen was gebleken dat er in de eerste fase van de activering in de kweekbakjes een grote verschuiving in de samenstelling van de vetdruppels optreedt. De hoeveelheid retinylesters neemt af en de hoeveelheid van tri-acylglycerolen met meervoudig onverzadigde verzuren (PUFAs) neemt toe. Verder ontstaan er meer maar kleinere vetdruppels (proefschrift N. Testerink).

In hoofdstuk **2** beschrijven we dat de toename van meervoudig onverzadigde vetzuur bevat-tende tri-acylglycerolen veroorzaakt wordt door een verandering in de hoeveelheid van enzymen van de klasse van vetzuur-CoA synthases (ACSLs). Deze enzymen zorgen ervoor dat vetzuren ingebouwd kunnen worden in triacylglycerolen door aan de vetzuren een energierijke chemische molecuul (CoA) te plakken. Tijdens de activering verliezen de hepatische stellaatcellen ACSL1, die een voorkeur heeft voor verzadigde vetzuren, terwijl de hoeveelheid ACSL4, die een voorkeur heeft voor meervoudig onverzadigde vetzuren, juist toeneemt (zie figuur 1 uit hoofdstuk **6**). Een mogelijke rol voor de ophoping van meervoudig onverzadigde vetzuur bevattende tri-acylglycerolen is dat ze een buffer vormen voor meervoudig onverzadigde vetzuren die nodig zijn tijdens de activering. Arachidonzuur, een specifiek meervoudig onverzadigde vetzuur, is namelijk de uitgangsstof voor de synthese van een klasse van hormonen, de eicosanoiden. In hoofdstuk **2** laten we zien dat een remmer van ACSL4 de synthese door de stellaatcellen van deze vetzuur-afgeleide hormonen remt.

In hoofdstuk **3** wordt onderzoek beschreven met behulp van speciale vetzuren die gemarkeerd zijn met zware isotopen, zodat ze onderscheiden kunnen worden met massa spectrometrie. Hieruit bleek dat de tri-acylglycerolen zowel worden opgebouwd als afgebroken met een relatief grote snelheid. Met behulp van remmers van specifieke enzymen en met genetische manipulatie van de hoeveelheid van bepaalde enzymen vonden we dat de tri-acylglycerolen niet allemaal even snel worden afgebroken en opgebouwd, maar dat dat afhangt van de soort vetdruppels waarin de tri-acylglycerolen zitten. De oorspronkelijke grote vetdruppels waarin vooral tri-acylg-lycerolen en retinolesters zitten, worden relatief langzaam afgebroken door een nog onbekend

lipase (LipX in figuur 1 en 2 van hoofdstuk **6**) en door het lysosomale lipase (LAL). Stukjes van de originele vetdruppels worden afgesnoerd door een proces dat autofagie genoemd wordt en naar het lysosoom vervoerd voor afbraak door LAL. In hoofdstuk **4** wordt ook aangetoond dat het lysosomale lipase naast tri-acylglycerolen ook de retinolesters en cholesterolesters kan afbreken. Naast de afbraak van de originele "oude" vetdruppels vindt er een snelle opbouw van nieuwe vetdruppels plaats door het enzym DGAT1, die het derde vetzuur aan di-acylglycerol (DAG) koppelt zodat tri-acylglycerol ontstaat. Deze nieuwe vetdruppels worden specifiek afgebroken door de lipase ATGL (zie hoofdstuk **3**). De combinatie van de afbraak van de grote originele vetdruppels en de vorming en afbraak van steeds nieuwe vetdruppels in de stellaat cellen tijdens de activering zorgt er voor dat het totale aantal vetdruppels sterk toeneemt, maar dat de vetdruppels wel kleiner worden. Een model van het dynamische vetmetabolisme in de hepatische stellaatcellen is geschetst in figuur 2 van hoofdstuk **6**.

Effect van verstoringen in het lipide metabolisme op de activering van hepatische stellaatcellen

De identificatie van een aantal enzymen die betrokken zijn bij de aanmaak en afbraak van lipiden en de beschikbaarheid van remmers van die enzymen maakt het mogelijk om het effect van het lipide metabolisme op de activering van de stellaatcellen te bestuderen. We vonden dat alle stoffen die òf de aanmaak òf de afbraak van vetten remden, ook de activering van ratten stellaatcelen in het kweekbakje remden (zie tabel 1 in hoofdstuk **6**). De stellaatcellen uit muizenlevers werden echter minder of helemaal niet beïnvloed door deze remmers. In het algemeen lijkt er een goed verband te bestaan tussen de verandering in het lipide metabolisme en de mate van activering van de stellaatcellen. Ook bleek dat er relatief grote veranderingen in lipide metabolisme nodig zijn om de activering te remmen. Dit laatste werd bevestigd door proeven waarbij we de hoeveelheid van de lipide enzymen met behulp van genetische manipulatie lieten afnemen. Hierbij vonden we kleine effecten op het lipide metabolisme en geen effecten op de activering van de stellaatcellen (hoofdstukken **2**, **3** en **4**). De precieze reden dat stellaatcellen lipide druppels moeten kunnen maken voor hun activering is nog onduidelijk. Maar het kan zijn dat ze een buffer van (specifieke) vetzuren nodig hebben voor membraanopbouw, energie of voor de vorming van eicosanoide-hormonen.

In hoofdstuk **5** beschrijven we vervolgens welke specifieke eicosanoiden de stellaatcellen precies kunnen uitscheiden en hoe dat verandert na de activering. We vonden dat in geactiveerde muizen stellaatcellen de expressie van prostaglandine I2/prostacycline synthase omhoog was gegaan. In geactiveerde ratten stellaatcellen daarentegen was de hoeveelheid van een ander eicosanoide-vormend enzym, namelijk thromboxaan A synthase, verhoogd. De activering van stellaatcellen werd versneld als we de eicosanoide prostaglandine E_2 toevoegde aan het kweekmedium. De stellaatcellen scheiden zelf vermoedelijk te weinig eicosanoiden uit in de kweekbakjes om

zichzelf te activeren, want we vonden geen verschil in activering als we de eicosanoide secretie verhinderden met specifieke remmers.

Conclusie

Tijdens de activering van hepatische stellaatcellen in een kweekbakje vinden er grote veranderingen plaats in lipide metabolisme door een aantal specifieke enzymen. Remmers van die enzymen veroorzaakte een verminderde activering van de geïsoleerde stelaatcellen. Deze studies bieden daarom voldoende aanleiding voor het testen van dergelijke geneesmiddelen op leverfibrose in diermodellen.

Acknowledgements

Acknowledgements

First and foremost, my deepest gratitude is to my promoter Prof.dr. Bernd Helms for giving me the opportunity to do my PhD in the faculty of veterinary medicine and for his thoughtful guidance, critical comments, and correction of the thesis.

Immeasurable appreciation and a special thanks to my co-promoter Dr. Bas Vaandrager for his continuous support of my Ph.D study and research, for his patience, motivation, enthusiasm, and immense knowledge. He provided me with the ideal mix of freedom to pursue my research; support through times of success and failure; and wisdom when I needed him the most, even for personal matters. I am truly privileged to be a student of such very kind human being.

Many thanks to Dr. Martin Houweling for working together with me with rat and mice liver stellate cell isolation. Without his efforts my job would have undoubtedly been more difficult. I greatly benefited from his keen scientific insight, his knack for solving seemingly intractable practical difficulties.

Every result described in this thesis was accomplished with the help and support of fellow collaborators. I wish to express my sincere thanks to Dr.Jos Brouwers, Dr. Chris van de Lest and Jeroen Jansen for helping me with the lipidomic facilities. My sincere gratitude to Dr. Richard Wubbolts and Esther van 't Veld, at the Center of Cellular Imaging, for their endless help and assistance with the confocal and live cell images. I would like to extend my gratefulness to Dr. Bart Spee, at the Department of Clinical Sciences of Companion Animals, for the assistance with real time quantitative PCR.

I am fortunate to have a good friend Martijn Molenaar and thanks to his excellent technical assistance in the lab and willingness to help and giving his best suggestions. I also have to thank my friends Ruud Eerland (paranymph), Janneke Boere, Aike Jeucken and Dr. Nick Olrichs with whom I have shared highs and lows throughout my study and work. I also thank to my friend Nafiseh Sirati for accepting to be my paranymph. I also thank to all my colleagues in cell biology.

I would also like to thank Dr. Dora Kaloyanova, Petra Boon, Louise Kaaden, Rachid Amarouchi for being so kind and care and immediate help when needed. Thanks to Titia Stuut-Vriesema and Herwin Frijters who made all administration issues during my stay at UU very easy.

Finally, I take this opportunity to express the profound gratitude from my deep heart to my beloved parents and to my sister and brothers for their love and continuous support both spiritually and materially.

About the author

Curriculum Vitae

Maidina Tuohetahuntila was born on July 2,1979 in Xinjiang province of China. She obtained her bachelor degree in 'Information Technology' at Xinjiang University in 2002. Thereafter she worked as a consultant at the agency of Xinjiang Uyghur Autonomous Region, Department of Education till 2004. September 2004, she joined in a master program of 'Bioinformatics' at Chalmers University of Technology, Sweden and graduated in 2006. She also obtained her second master degree in 'Molecular biology' in 2007 from Gothenborg University, Sweden. After obtaining her master degrees, she worked as a research assistant in the College of Pharmacy at the University of Texas at Austin, USA from 2008 to 2010. In Jan 2010, she joined to Oregon Stem Cell Center, USA as a research assistant till June 2011. In July 2011, she started her PhD study at the department of Biochemistry and Cell Biology in the faculty of Veterinary Medicine, Utrecht University, The Netherlands.

List of publications

Journal Articles

Tuohetahuntila M, Molenaar MR, Spee B, Brouwers JF, Houweling M, Vaandrager AB, Helms JB. (2016). "ATGL and DGAT1 are involved in the turnover of newly synthesized triacylglycerols in hepatic stellate cells". *J. Lipid Res.*

Valtolina C, Vaandrager AB, Favier RP, Robben JH, **Tuohetahuntila M**, Kummeling A, Jeusette I, Rothuizen J. (2015). "No up-regulation of the phosphatidylethanolamine N-methyltransferase pathway and choline production by sex hormones in cats". *BMC Vet Res*.

Tuohetahuntila M, Spee B, Kruitwagen HS, Wubbolts R, Brouwers JF, van de Lest CH, Molenaar MR, Houweling M, Helms JB, Vaandrager AB. (2015). "Role of long-chain acyl-CoA synthetase 4 in formation of polyunsaturated lipid species in hepatic stellate cells". *Biochimica et Biophysica Acta.*

Kaoud TS, Yan C, Mitra S, Tseng CC, Jose J, Taliaferro JM, **Tuohetahuntila M**, Dalby KN. (2012). "From in Silico Discovery to intra-Cellular Activity: Targeting JNK-Protein Interactions with Small Molecules". *ACS Med Chem Lett.*

Journal Articles in preparation/submitted

Tuohetahuntila M, Martijn R. Molenaar, Bart Spee, Jos F. Brouwers, Richard Wubboltsa , Martin Houweling, Cong Yan , Hong Du, Arie B. Vaandrager, and J. Bernd Helms. "Lysosomal acid lipase inhibitor affects retinyl ester breakdown and hepatic stellate cell activation".

Tuohetahuntila M, Pawel W. Stachowiak, Chris H. van de Lest, Christian Wolfrum, Martin Houweling, Arie B. Vaandrager, and J. Bernd Helms. "Role of eicosanoid secretion in mouse and rat hepatic stellate cell activation".

Chiara Valtolina Arie B. Vaandrager, Robert P. Favier, **Tuohetahuntila M**, Jan Rothuizen, and Joris H. Robben. "Sex specific differences in hepatic and plasma lipid profiles in healthy cats pre and post spaying and neutering: relationship with feline hepatic lipidosis".

*You can never cross the ocean until you have the courage
to lose sight of the shore* – Christopher Columbus